THE UNIVERSITY
of EDINBURGH

Extracting morphological networks from individual grey matter MRI scans in healthy subjects and people at high risk for schizophrenia.

Betty M. Tijms

Doctor of Philosophy
University of Edinburgh
2011

Abstract

Recently graph theory has been successfully applied to magnetic resonance imaging data. However, it remains unclear as to what the nodes and edges in a network should represent. This problem is particularly difficult when extracting morphological networks (i.e., from grey matter segmentations). Existing morphological network studies have used anatomical regions as nodes that are connected by edges when these regions covary in thickness or volume across a sample of subjects. Covariance in cortical thickness or volume has been hypothesised to be caused by anatomical connectivity, experience driven plasticity and/or mutual trophic influences. A limitation of this approach is that it requires magnetic resonance imaging (MRI) scans to be warped into a standard template. These warping processes could filter out subtle structural differences that are of most interest in, for example, clinical studies.

The focus of the work in this thesis was to address these limitations by contributing a new method to extract morphological networks from individual cortices. Briefly, this method divides the cortex into small regions of interest that keep the three-dimensional structure intact, and edges are placed between any two regions that have a statistically similar grey matter structure. The method was developed in a sample of 14 healthy individuals, who were scanned at two different time points. For the first time individual grey matter networks based on intracortical similarity were studied. The topological organisation of intracortical similarities was significantly different from random topology. Additionally, the graph theoretical properties were reproducible over time supporting the robustness of the method. All network properties closely resembled those reported in other imaging studies.

The second study in this thesis focussed on the question whether extracting networks from individual scans would be more sensitive than traditional methods (that use warping procedures) to subtle grey matter differences in MRI data. In order to investigate this question, the method was applied to the first round of scans from the Edinburgh High Risk study of Schizophrenia (EHRS), before any of the subjects was diagnosed with (symptoms of) the disease. Where traditional methods failed to find differences at the whole

brain level between the high risk group and healthy controls, the new method did find subtle disruptions of global network topology between the groups. Finally, the diagnostic value of the networks was studied with exploratory analyses that found that, in comparison to healthy controls, people at high risk of schizophrenia showed more intracortical similarities in the left angular gyrus. Furthermore within the high risk group an increase of intracortical similarities could predict disease outcome up to 74% accuracy.

The main conclusion of this thesis was that the new method provides a robust and concise statistical description of the grey matter structure in individual cortices, that is of particular importance for the study of clinical populations when structural disruptions are subtle.

Acknowledgments

Declaration

I declare that this thesis was composed by myself, that the work contained herein is my own except where explicitly stated otherwise in the text, and that this work has not been submitted for any other degree or professional qualification except as specified.

(Betty Tijms)

Table of Abbreviations

2D	two dimensional
3D	three dimensional
AAL	automated anatomical labelling atlas
ANIMAL	nonlinear image matching and anatomical labelling package
ANOVA	analysis of variance
CT	computerised tomography
DSI	diffusion spectrum imaging
DTI	diffusion tensor imaging
EHRS	Edinburgh High Risk study of Schizophrenia
FD	fractal dimension
FDR	false discovery rate
FLASH	fast low angle shot
fMRI	functional magnetic resonance imaging
FOV	field of view
HO	Harvard Oxford atlas
HARDI	high angular resolution diffusion tensor imaging
HMRF	hidden Markov random field
ICC	intra class correlation coefficient
LONI, LPBA40	probabilistic atlas
MA	Massachusetts
MCI	minor cognitive impairment
mm	millimetre
MPRAGE	magnetisation prepared rapid acquisition gradient echo
MRI	magnetic resonance imaging
n	number of subjects
OOB	out of bag
PFC	prefrontal cortex
RISC	Rust Inventory for Schizotypal Cognitions
SD	standard deviation
sMRI	structural magnetic resonance imaging
SPHARM	spherical harmonics
SPM	Statistical Parameter Mapping
SVM	support vector machine
TE	echo time
TI	inversion time
TR	repetition time
USA	United States of America
VBM	voxel based morphometry
WFU	Wake Forest University

Table of Contents

1. Introduction

An important issue in neuroscience is the quantification of the morphology of individual cortices. This issue is of particular importance when studying connectivity patterns in neuropsychiatric disorders that show subtle disruptions in brain structure. Such subtle disruptions could be present in so-called 'high risk' studies, where healthy people with an increased risk for a certain disease are compared to healthy people lacking such risk. Differences between such populations might provide insight into developmental disruptions associated with that disease. Finding subtle differences in grey matter magnetic resonance imaging (MRI) data with traditional methods is difficult because these methods require the warping of the individual scans onto an average template. Such warping procedures have the potential to filter out subtle differences between individuals. This means that traditional methods might lose information that could be of importance for the development of diagnostic tools. Currently methods exist to quantify whole brain complexity in individual brains (e.g., Bullmore et al., 1994; Thompson et al., 1996), but these methods suffer from limitations such as how to map individuals to each other and how to map these quantifications with functional MRI.

In this thesis a new method to statistically quantify the morphology of individual cortices using tools from graph theory is presented. Briefly, any form of data can be represented as a graph (i.e., network), which can be described with graph theoretical properties. Nodes represent the data and edges are placed between nodes when a relationship between them exists. Recently graph theory has been successfully applied to describe MRI data in grey matter, white matter and functional MRI. An additional attractive feature of this framework is that it has the potential to map networks from different modalities in individual cortices. More background about graph theory is provided in the first Section of Chapter 2.

Methods exist to extract individual networks from functional and white matter MRI data. In functional networks, nodes are connected where a correlation between their time-series exist. In white matter MRI (involving diffusion tensor or diffusion spectrum imaging techniques), nodes are connected where a white matter tract exist. Until now, such methods do not exist for grey matter MRI data

(in this thesis also referred to as 'morphological' data, as a general term for several types of grey matter that can be extracted from structural MRI and that contribute to a description of cortical structure, such as for example cortical thickness and volume). Current methods that extract morphological networks usually divide the cortex into a number of anatomical regions and then connect these regions when they covary in either thickness (e.g., He, Chen et al., 2007) or volume across a group of subjects (e.g., Bassett et al., 2008). A drawback of these methods is that they require the registration of individual cortices into a standard space, potentially missing features that are of importance between groups. Also, no study has explored the relationship between morphological networks and functional networks, possibly because individual descriptions of morphological networks are lacking (but see Gong et al., 2011 for a recent study that investigated the relationship between group averaged white matter networks and cortical thickness networks).

The work in this thesis contributes to these important issues with the proposal of a new method to extract individual morphological networks. For the first time, the network properties of individual morphological networks from a sample of healthy people were studied and compared to random networks. Furthermore the biological meaning was investigated by extracting individual morphological networks from a sample at high risk of schizophrenia for the first time.

This thesis will be divided into two parts. In the first part relevant background material regarding graph theory and its application in MRI research so far will be discussed in Chapter 2, followed by a detailed presentation of the proposed method and a discussion of its results in Chapter 3. Briefly, this method extracts morphological networks from individual grey matter MRI data, where the nodes represent small cortical regions with their three-dimensional structure intact and edges connecting nodes that show a statistically similar structure. The main conclusions after extracting these networks from a healthy sample were that: I. networks based on intracortical similarities provide a robust and concise statistical description of the grey matter structure of individual cortices. II the resulting network properties were comparable with those from other imaging network studies.

The second part investigated whether the new method was more sensitive to subtle structural differences than traditional methods. In order to answer this question the new method was applied to the Edinburgh High Risk study of Schizophrenia (EHRS), where people were recruited with and without a family background of schizophrenia. People who have direct family members with schizophrenia have an increased risk of developing the disease themselves when compared to people without such a family background (McGue and Gottesman, 1989). Traditional methods to analyse cortical morphology have not found differences in this sample between people with and without an increased risk of schizophrenia in scans that were acquired when all subjects were clinically healthy. Chapter 4 will provide more background about schizophrenia and high risk studies of schizophrenia. In Chapter 5 the new method was applied to the EHRS. The main finding of this part was that while groups with and without a family history of schizophrenia did not differ in their global network organisation, only the high risk group showed subtle disruptions that were suggestive of a less efficient network organisation. Within the high risk group it was found that the group who later became ill demonstrated more disruptions of network topology than those who remained well. These results indicate that the proposed method is indeed more sensitive than traditional approaches to subtle morphological differences between groups. In addition, they validate the method and give it biological relevance. Finally, exploratory analyses suggested that the degree (i.e., number of connections) of the networks could be of important diagnostic value, because up to 74% of the subjects could be correctly classified using both the average network degree and the degree of the right angular gyrus.

The last Chapter of this thesis will discuss the implications and limitations of this work and will also present suggestions for future research.

2. Quantifying cortical morphology in individual MRI scans

This Chapter provides the background necessary to understand the new method that was developed for this thesis. The first Section will introduce why it is an important, but also a difficult issue to describe the connectivity architecture of the human brain and the role of graph theory in this type of research (2.1). Section 2.2 will discuss the importance of studying individual cortical morphology, followed by a review of existing methods to quantify individual cortical morphology in Section 2.3. Then Section 2.4 will introduce the new method to quantify individual cortical morphology that was developed for this thesis. Finally, Section 2.5 provides a general introduction to graph theory and a detailed explanation of the graph theoretical measurements that were used throughout this thesis.

2.1 Networks extracted from cortical morphological data

The precise connectivity architecture of the human brain remains unknown, because it is complex and difficult to extract (e.g., Rykhlevskaia, 1998; Sporns and Zwi, 2004; Sporns et al., 2004; Sporns, Tononi and Kötter 2005; Bassett and Bullmore, 2006; Sporns, Honey and Kötter, 2007; Sporns, 2006, 2009, 2010, 2011; Bullmore, Barnes, et al., 2009; Bullmore and Sporns, 2009; Honey, Thivierge and Sporns, 2010; Bullmore and Basset, 2011). The size of the skull imposes an important constraint on the morphology of the brain. However, brain size does not necessarily scale with the complexity of the cortical surface (e.g., Murre and Sturdy, 1995). Additionally, evidence has been found that the arrangement of cortical areas present in the brain minimises the volume of axons required to connect them (Murre and Sturdy, 1995; Klyachko and Stevens, 2003; Chklovskii, 2004; Chkovskii et al., 2004; Chklovskii, 2004; Stepanyants and Chklovskii; 2005; Jehee and Murre, 2008; Stepanyants et al., 2009). Furthermore, the anatomical structure of the brain poses physical constraints on the function of the brain: neurons can only communicate (either electrically or chemically) when they are physically near each other. It is possible to describe the connectivity architecture of the brain in terms of a network where nodes (e.g., neurons or groups of neurons) can transfer information when a link exists between them

(Rykhlevskaia et al., 2008). Graph theory offers simple tools to quantify the human brain in a concise manner, providing summary measures that indicate how efficient the topological organisation of networks is in terms of wiring length, while at the same time also providing local measures for each node in the network. These characteristics make networks an attractive tool to study the organisation of the human brain. Since 2005 many studies have tried to quantify imaging data with the tools of graph theory and many reviews have been published in a brief period of time speculating about the meaning of the 'small world' organisation of the brain (Chialvo, 2004; Reijneveld et al., 2007; Evans et al., 2008; McIntosh et al., 2008; Sporns, 2009; Bullmore and Sporns, 2009; Bullmore et al., 2009; Bassett et al., 2009; He et al., 2009; Cho et al., 2010; Stam, 2010; Gerloff et al., 2010, Wang, 2010; He and Evans, 2010; Rubinov et al., 2010; Power et al., 2010; Wen et al., 2011; Wig et al., 2011; Sporns, 2011; Kaiser, 2011; Gong et al., 2011; Bullmore et al., 2011; Bassett et al., 2011; Petrella, 2011; Prettejohn et al., 2011; see Table 1 for a selection of neuroimaging studies that have used graph theory and Section 2.6 for a detailed explanation).

Given that graph theory can be applied to many types of data, it offers a framework that is particularly suited for multi-modality research, because potentially nodes of grey matter could be mapped to corresponding nodes containing functional MRI (fMRI) data. Just a few studies have addressed this attractive characteristic of graph theory (Zemanova et al., 2006; Honey et al., 2007; 2008; Alstott et al., 2009; Binzegger et al., 2009; Honey et al., 2009; Rubinov et al., 2009). Another appealing feature of graph theory is its diagnostic potential, because in principle networks can be described for individuals. While methods exist to extract networks from individual white matter and functional MRI data (e.g., Eguíluz et al., 2005; Hagmann et al., 2007; den Heuvel et al., 2008), such methods do not exist for grey matter MRI. To bridge this gap, it was my idea to develop a new method that describes the morphology of an individual cortex as a network. The next Section will discuss why it is important to have a network description of grey matter.

In MRI studies nodes usually represent anatomical areas or individual voxels. In functional MRI, the nodes are connected where a temporal correlation in their functional signal exists, and in white matter MRI nodes are connected

where a white matter tract exists. However, the choice of connectivity for grey matter (or morphological) MRI is less straightforward. Studies have demonstrated that it is possible to construct morphological networks by assessing covariation of cortical thickness of volume between cortical areas across people (He, Chen et al., 2007; Bassett et al., 2008; Chen et al., 2008; He et al., 2008). Such covariances have been reported to be sensitive enough to distinguish between (clinical) groups of people (e.g., Wright et al., 1999; McAlonan et al., 2005; Mechelli et al., 2005; Mitelman et al., 2005; Lerch et al., 2006; He, Chen et al., 2007; Bassett et al., 2008; Colibazzi et al., 2008; He et al., 2008; Bernhardt et al., 2009; Modinos et al., 2009; Lv et al., 2010; Yao et al., 2010; Zhu et al., 2010; Bernhardt et al., 2011; Fan et al., 2011; Hänggi et al., 2011; Wu et al., 2011).

Interregional covariation in cortical volume or thickness has been suggested to be caused by mutual trophic information (Pezawas et al., 2004), by genetic influences (Schmitt et al., 2008), or mutual experience dependent plasticity (Draganski et al., 2004; Mechelli et al., 2004). Mechelli et al. (2005) proposed that if brain areas would develop independently, one would not be able to find covariation between them. Usually studies using interregional covariation in cortical thickness or volume across people imply that these correlations have a neuronal basis. In other words, if two regions covary in thickness or volume across people, they must be connected by axons. Lerch et al. (2006) showed qualitatively that structures known to be connected by the arcuate fasciculus (a white matter structure that connects prefrontal areas with posterior parietal and temporal areas) correlate in thickness. Recently Gong et al. (2011) have demonstrated that about 40% white matter connections correspond to cortical thickness covariation. However, it remains unknown how such morphological covariation translates to individual cortices.

Furthermore, caution must be taken when comparing the different studies, as prior models must be used to parcellate the brain into regions of interest, while no standard method or model to achieve this exists. This is mainly caused by the difficulty to ensure a concise mapping of individual brains on atlases and templates. Extraction of exactly the same anatomical region from every individual brain is extremely difficult due to the high degree of variability between people in

their cortical morphology. Even so, procedures to achieve an approximate mapping of an individual brain into a standard space exist and these are usually referred to as 'warping procedures'. A disadvantage of these procedures is that they can potentially filter out subtle structural differences that are of particular interest in clinical populations. Therefore it is important to study grey matter networks derived from individual cortices, however such methods did not exist at the start of this thesis.

To summarise this Section: graph theory has been successfully applied to functional, white matter and grey matter MRI data from in vivo human cortices. While functional and white matter networks can be described for individual cortices, such approaches do not exist in grey matter MRI. Furthermore, although no justification exists to interpret morphological covariation over people as indicative of connectivity within a brain, such implications have been suggested by current morphological studies. It remains unclear as to what the causes of morphological covariation are. In addition, methods that require warping of anatomical data onto a standard space lose morphological information. This becomes more important when differences between groups are subtle. The next Section will describe the extent of individual variability in cortical morphology to further emphasise the need for an individual-based network description of cortical morphology.

2.2 Morphology of individual cortices

The importance of neuronal morphology for function has been acknowledged since the pioneering work of Ramon-Y-Cajal and Brodmann around the start of the 20th century. Later in 1981, Wässle and his colleagues found that the on/off alpha cells in the cat retina correlated with the specific morphology of their dendrites. However, the study of neuronal morphology and cognitive function is a hard problem, and has only recently been more thoroughly explored with computational neuroscience (e.g., Murre and Sturdy, 1995; Mainen and Sejnowski, 1996; Fernandez and Jelinek, 2001; van Ooyen et al., 2002; da Fontoura Costa and Manoel, 2003; da Fontoura Costa et al., 2003; Chklovskii, 2004; Muir and Douglas, 2010). For example, van Mainen and Sejnowski (1996)

demonstrated with a simulation model that the firing pattern of a neuron, when it is stimulated in the soma, varies widely according to the specific morphology of its dendrites (when keeping all other morphological properties constant). This illustrates that the study of structure-function relationships in the brain is already difficult at the cell level, and it remains largely unknown how interconnectedness between neurons of similar or different morphology gives rise to cortical structure at a macro-scale that is measured with MRI.

At the macro level of MRI, great inter-subject variability in cortical morphology exists (e.g., Brodman, 1909 (Translated version of 1994); Zilles et al., 1988; Kennedy et al., 1998; Thompson et al., 2002). For example, Kennedy et al. (1998) investigated inter-individual cortical variation by measuring topographic variations in grey matter volume at three different levels of the cortex: total volume, the gyri and of subdivision of the gyri. They concluded that variability of most cortical regions is not a simple function of overall brain size: about 70% of cortical variability could be accounted for by grey matter volume from smaller regions of interest and only 10% could be accounted for by the total volume of the cortex. Based on these findings, Kennedy et al. (1998) concluded that the anatomical representation of function probably gets lost when a standard template is used to parcellate the cortex into anatomical regions. These findings were supported by Geyer et al. (1999), who used postmortem brains to demonstrate that cytoarchitectonic areas 3a, 3b and 1 of the human primary somatosensory cortex cannot be delineated with just macrostructural landmarks, suggesting that individual analyses of these areas would be better.

To explain how cortical gyrification patterns (and thus morphological variability) develop, van Essen (1997) has proposed the axonal tension hypothesis. Briefly, this hypothesis states that cortical areas that are connected by axons are pulled together forming gyri, whereas areas that are not connected drift apart and form sulci. Individual variation in cortical morphological patterns might be the result of variations in the interconnectedness of the areas. Van Essen hypothesised that environmental factors must play a role in establishing individual variation in morphological patterns. Indeed it has been shown that while some gyri have a genetic component, that are present in every individual (and even across species) such as the precentral gyrus, variability of the so called 'tertiary'

gyri can mostly be explained by environmental factors (Bartley et al., 1997; Baare et al., 2001). This means that gyri and/or sulci can exist in some people while they are absent in others. For example, Paus et al. (1996) studied the variability of the central and paracingulate sulcus, and showed in a sample of 247 subjects that a small percentage of them did not have a paracingulate sulcus in either the left (8%) or right (15%) hemisphere. In addition, he found that the central sulcus, present in all subjects, showed considerable variability in its branching morphology.

The fact that neuronal morphology affects signal processing, combined with the high degree of inter-individual variability in cortical morphology, poses the question whether the variability in cortical morphology is related to cognitive function. The recent rise of plasticity studies using MRI has been an important first step toward understanding the relationship between cortical morphology and cognitive function in humans. These studies investigate whether changes in behaviour due to learning a certain task correlate to changes in cortical structure in areas known to be involved in such a task (Draganski et al., 2004; Bohbot et al., 2007). In a natural setting it was shown that the posterior part of the hippocampus of London taxi-drivers was larger than non-experienced taxi-drivers (Maguire et al., 2000), and this difference was associated with spatial memory. Experienced pianists showed different correlations in right and left grey matter volume of sensorimotor areas than healthy controls (Lv et al., 2008). Such studies have suggested that these differences between experienced and amateur groups are caused by the difference in training in that particular subject.

Draganski et al. (2004) were the first to show such an effect in a controlled experiment, where one group was trained in juggling, while a second group did not receive such training. Brain scans before and after the training period showed a difference in grey matter volume that was correlated to learning task. Since then, other studies have shown similar effects (Draganski et al., 2004; Mechelli et al., 2004; Pan et al., 2007; Hyde et al., 2009). Pan et al., (2007) demonstrated in a sample of people who were blind from an early age that grey matter atrophy occurred in regions that lost functional connections. Such studies raise questions that are important for clinical groups as well, because they might provide a basis for non pharmacological treatment- and prevention programmes (e.g.,

improvement of cognition in minor cognitive impairment (MCI) patients by training, see: Belleville et al., 2011). Another study directly measured the relationship between cognitive function and grey matter volume, where they found that people who had less grey matter in their primary visual cortex had a stronger experience of two visual illusions (Schwarzkopf et al., 2010). These results all illustrate that function seems to be directly related to cortical morphology.

Nevertheless, in contradiction to the above studies, Thomas et al. (2009) failed to find structural changes while they did find functional changes after training in a mirror task (following a randomly moving white dot with a joystick where the left-right axis was reversed). This could be due to the simpleness of the task, however it cannot be ruled out that subtle changes did occur. When using a group based analysis technique, such as voxel-based morphometry to test effects of a certain task (as all these studies have used), such subtle effects could be filtered out when warping procedures are applied to compare averaged group brains in a standard space. When an effect is strong enough (i.e. it occurs in most subjects at approximately the same location that is less variable between subjects), this will be stronger due to filtering the noise. However, when an effect is more subtle, it will become weaker when warped. When studying function-structure relationships in patient data, this is of even more importance, since focal structural abnormalities could be of the most interest (e.g. for finding baseline differences in high risk studies), and these have the highest risk to be filtered out in group-based analyses. From these studies, it is clear that a method is needed to quantify individual variation. The next Section will discuss two of such approaches: the gyrification index and the fractal dimension (FD).

2.3 Existing methods to quantify morphology in individual cortices

At the start of this project, just a few methods existed to quantify morphology in individual cortices, among which were the gyrification index and the fractal dimension. The gyrification index gives an indication of the complexity of the cortical surface by comparing the contour of the total brain (a line that traces all the gyri and sulci) with the contour of the outer-surface of the brain (Zilles et al., 1988). A higher gyrification index indicates a more complex surface, as the total

contour is longer, indicating the presence of more gyri and sulci in comparison with a shorter total contour. Traditionally the gyrification index was measured manually (e.g., Armstrong et al., 1995; Harris et al., 2004), but automated procedures exist as well (Moorhead et al., 2006; Bonnici et al., 2007). However, a disadvantage of the gyrification index is that it is measured in a coronal plane, which dismisses the three-dimensional information in cortical morphology (however some global (Thompson et al., 2003), or region of interest approaches including three-dimensional (3D) information exist as well (Rettmann et al., 2005)). In addition, the gyrification index has no local specificity, it only gives one number for a cortical slice. To overcome these problems, Schaer et al. (2008) proposed a method to quantify local gyrification, based on extracted cortical surfaces. Briefly, the method determines for each vertex the ratio of the surface of the grey/white matter boundary in a sphere centring around this vertex and the pail surface. How the local gyrification method relates to traditional two-dimensional (2D) measurements of gyrification remains to be investigated. Also, although this method provides locally specific measurements of gyrification, it fails to address the issue of how to map individual cortices for comparison. Thompson et al. (2003) proposed a method to generate maps where the individual convolutions are mapped in reference to each other, but, this method cannot be applied in a single individual.

Another measurement which does not require warping procedures and that can be assessed in an individual brain is the fractal dimension. The fractal dimension describes the relationship of a quantity of an object over different spatial resolutions, giving an indication of self-similarity (Mandlebrot, 1967; 1985). Many objects in nature, including the morphology of the cortex, can be described as a fractal (Chuang et al., 1991; Bullmore et al., 1994; Cook et al., 1995; Free et al., 1996; Kiselev et al., 2003; Im et al., 2006; Zhang et al., 2008; Esteban et al., 2009). Kiselev et al. (2003) pointed out that self-similarity of the cortex would mean that the statistical properties of the folding pattern of small cortical structures would be similar to those of larger cortical structures. As the cortex becomes more complex, for example, due to an additional gyrus or sulcus, the fractal dimension changes (Jiang et al., 2008). Since the fractal dimension captures the complexity of the brain with one number, it is considered to be a

compact measure. Despite its compactness, the fractal dimension is sensitive enough to show differences between clinical groups and healthy controls (Bullmore et al., 1994; Cook et al., 1995; Ha et al., 2005; Pan et al., 2006; Sandu et al., 2008; Esteban et al., 2009; King et al., 2009). Variability in the fractal dimension between individuals has been related to cortical thickness and folding (Im et al., 2006). Further, Im et al. (2006) speculated that folding patterns and the frequency of folding are related to each other in many cortical areas. Since cortical thickness is measured at the finest spatial scale, and can account for much of the variance found in the fractal dimension together with folding area, perhaps similarities of cortical thickness and folding within the cortex could be found within a spatial scale.

These findings raise the question as to what causes the fractal dimension of the brain. The fractal dimension might result from complex processes according to which the cortical surface develops that comprises a specific architecture including processes like: cell-migration, neuronal differentiation and dendrogenesis, cortical lamination and development of thalamo-cortical and cortico-cortical connections. The axonal tension theory of van Essen discussed earlier could also explain the fractal dimension. Similarly, da Fontoura-Costa (2005) proposed that morphologically complex networks, such as the brain, might be determined by connectivity patterns of individual morphological structures. Such connectivity patterns of individual morphological structures can be described as graphs or networks (Da Fontoura-Costa, 2005).

Barbas (1986) studied cortical covariation within an individual cortex using axonal tracers in Rhesus monkeys and found that cortico-cortical connectivity patterns could be predicted by cortical structure: axons of lower-level areas terminated in the lower layers of higher level areas, whereas axons of higher-level areas terminated in the upper layers of lower-level areas (Barbas, 1986; Barbas & Rempel-Clower, 1997). In a follow-up study in 2001, Drombowski et al. could relate neuronal density and cortical thickness of the individual areas to the different architectonic types for each area. This study and a later study (Hilgetag and Barbas, 2005) imply that cortical areas that are connected can be described by a similarity in thickness and folding. These studies support the idea that areas that project to each other have a similar structure.

Finally, during the development and publication of the method presented in Chapter 3 three other methods were proposed to describe individual morphological networks that were all based on the distance between average cortical thickness of any two anatomical areas (Raj et al., 2010; Dai et al., 2011; Zhou et al., 2011; note the last two studies were published around the same time as the work from Chapter 3). These developments support the need for individual network descriptions for morphological data. However these methods differ from the current work and also suffer from limitations that the present work tried to solve. The method proposed by Raj et al. (2010) is still dependent on group averaged data. Also, all these methods depended on anatomical parcellation schemes, thus these methods could still suffer from warping procedures (Raj et al., 2010; Dai et al., 2011; Zhou et al., 2011). Furthermore, these studies did not quantify network properties (Dai et al., 2011; Zhou et al., 2011) or did not quantify whole brain structural networks (Raj et al., 2010). Because it is not clear whether these descriptions differ from random networks, it is difficult to understand the biological meaning of these networks.

To summarise this Section, both the gyrification index and the fractal dimension measure the complexity of cortical morphology. While the gyrification index can be measured locally, problems associated with matching individual cortices remain. In addition, these methods do not quantify complex morphological interrelationships between anatomical areas. The fractal dimension can be computed within individual brains, but because it is just one number it lacks specificity. The work in this thesis further extends these studies with the development of a new method that uses graph theory to quantify these complex morphological interrelations within individual cortices. The advantage of the new method (Chapter 3) is that it does not require warping procedures to match individual cortices, and also includes local and global quantifications of networks. By describing cortical morphology as a graph it is possible to compare the network properties of individuals, but also the distribution of such property values between groups. The following Section provides an introduction to the new method (more details will be described in Chapter 3).

2.4 Graph theory and cortical morphology: a new method

The main work in this thesis focussed on resolving the issues posed by current methods that extract morphological networks by proposing a new method to construct networks from individual cortices, based on intracortical similarities in grey matter morphology. The nodes of the networks extracted by the new method represent small regions of grey matter, with their three-dimensional structure intact, and edges are placed between regions that show statistical similarity. Intracortical similarities could be caused by mutually trophic influences (Pezawas et al., 2004) or experience driven plasticity (e.g., Andrews et al., 1997; Draganski et al., 2004; Mechelli et al., 2004). As discussed above, animal tracer studies have found that cortical thickness, folding and neuronal density can predict anatomical connectivity (Barbas, 1986; Barbas and Rempel-Clower, 1997; Dombrowski et al., 2001). These studies suggest that similarity in thickness and folding might be an indication of connectivity between cortical areas.

Only a few studies have tried to quantify patterns of intracortical similarity in specific parts of the human brain (Andrews et al., 1997; Kennedy et al., 1998). For example, Andrews et al. (1997) found within individual brains that the grey matter of the lateral geniculate nucleus, the optical tract and the primary visual cortex covary in volume.

The work in this thesis extends these studies. In two different studies, the graph theoretical properties of the derived networks were investigated and mapped for the first time. The study discussed in Chapter 3 extracted networks from a healthy sample, which was scanned at two different time points. Here it was hypothesised that if connectivity can be assessed by measuring statistical similarity of structure within the cortex, then the associative areas are expected to have more connections than, for example, primary sensory areas, resulting in a spatially non-uniform connectivity distribution. Such spatially non-uniform connectivity distributions have been found in studies that derived morphological networks from group data (Lerch et al., 2006; He, Chen et al., 2007; Bassett et al., 2008). Furthermore, this study compared the results with previous research that reported network property values from group morphological, functional and white matter magnetic resonance imaging (MRI) data. Finally, the robustness of the

method was assessed by measuring the stability of the network statistics between two scanning sessions.

The study in Chapter 5 compared the extracted network property values between different clinical groups, in order to investigate whether the new method would be more sensitive to subtle structural disruptions between groups than traditional group based methods. Before, we proceed to those studies, first graph theory will be explained and an overview of its measurements is given.

2.5 Graph theory

Graph theory is a field of mathematics that is used to describe relationships between objects from a certain collection (see e.g., Watts and Strogatz, 1998; Albert and Barabási, 2002; Newman, 2003). Once it has been established what the nodes in a graph (i.e. network) represent they are connected according to rules that determine their relationships. For example, social relationships can be described as a graph where the nodes represent people and an edge is placed between people who are acquainted with each other. How nodes are connected impacts the amount of edges (i.e. wiring length) needed, and when wiring length is expensive this naturally imposes restrictions on the organisation (i.e. topology) of a network. Returning to the social network example, it would be expensive to provide a separate and direct physical telephone line connection between every individual. Apart from costs that wiring length brings, wiring can also take up space. However, the time and/or effort needed to exchange information between any two nodes in a graph can dramatically increase when connections are missing. These examples illustrate that the wiring scheme of a network gives information about its efficiency. A continuum can be defined to categorise networks, based on the structure of their wiring scheme, with at one end a regular wiring scheme in which nodes are fully connected (e.g., a lattice) and on the other end of the continuum a random wiring scheme (i.e., there is no apparent rule to connect one node with another; Erdős and Rényi, 1960). It has been shown that a regular network uses the most wiring in this continuum to connect every node, but can process information in great detail because nodes operate in a cluster (e.g., Chklovskii et al, 2004). A random network on the other hand uses minimal wiring to connect all nodes, but due to lack of structure in the wiring scheme information

exchange might not be optimal (e.g., Chklovskii et al., 2004). However, many networks have a wiring scheme that is somewhere in between regular and random networks. Such networks are said to be 'small world', a term coined by Millgram (1967) who estimated that across the world everyone is connected to each other through six people ('six degrees of separation'). Watts and Strogatz (1998) suggested that many social and biological networks (such as axonal wiring in C. elegans, but also relationships between film actors) are 'small world' and proposed to quantify this property by comparing network properties of wiring length and clustering (i.e., the amount of connections that exist between neighbours of a given node) with those of randomised networks.

The (human) brain has been thought to consist of separate modules that process specific information (e.g., the occipital lobe is mostly concerned with visual information), and these modules can rapidly exchange information via long range connections (e.g., the parietal lobe is also known as the 'associative' cortex, in other words, it associates information from different brain regions), suggestive of a small world organisation. The following Sections will give a detailed overview of the basic network properties in graph theory, which were used for the work in this thesis.

2.5.1 Graph metrics

A network can be described with local properties, that are assessed for every node in a network (e.g., the number of connections it has with other nodes), but also with global properties (e.g., its size). This Section describes in detail the following properties: nodes, edges, size, sparsity, degree, minimum path length, clustering coefficient, the small world property and the betweenness centrality.

Node (v)

A node (*v)* is the fundamental building block of a network. It represents a unit of data and is sometimes also called a 'vertex' (physics; Newman, 2003).

Edge

An edge can connect any two nodes, signifying a relationship between them such as, for example, whether two people are acquainted to each other (Millgram,

1967) or whether two neurons are physically connected (C. elegans, Watts and Strogatz, 1998). An edge can be weighted or unweighted. A graph containing unweighted edges is said to be 'binary', and from such a graph only basic network properties can be assessed. When a graph is 'weighted' more information is present in the network. For example in white matter MRI the weight of a connection could represent the number of white matter tracts found between two nodes, corresponding to the probability whether two nodes are actually connected. Furthermore, edges can be 'directed' or 'undirected', referring to the direction of the relationship between two nodes. When this direction is unknown, undirected edges are used. However, for example in transportation, directed edges could be used to indicate a one-way street. In this thesis 'connection' and 'edge' were used interchangeably, and only undirected and unweighted edges were used in the studies described in Chapter 3 and 5.

Size (V)

The size (*V*) of the network is equal to the number of nodes.

Sparsity (S)

Sparsity (*S*) is the connectivity density in an unweighted network, which is the proportion of connections that are present to the total number of connections possible between all nodes in the network ($V * (V - 1)$). Both size and sparsity have a strong influence on other network properties (e.g., van Wijk et al., 2010).

Degree (k)

The degree (*k*) is simply the number of connections each node v_i has with any other node v_j in the network. Some nodes have many connections and these are regarded as *hubs*. The distribution of the degree over all the nodes in a network depends on the type of network: in a regular network this distribution would be a delta-function, as all nodes have exactly the same amount of connections (Albert and Barabási, 2002). Such a network does not contain hubs. However, in other wiring configurations the degree distribution might change its shape, because the nodes do not have the same chance of being connected. This is the case in, for example, scale-free networks that are characterised by a skewed distribution that

follows a power-law (i.e., if one would take the logarithm of the distribution one could draw a straight line through it; Albert and Barabási, 2002). Such networks have many nodes with a low degree and a few hub nodes with a high degree. The internet is an example of a scale-free network, and this property has been related to resiliency to random attacks (i.e., random removal of nodes, Cohen et al., 2000).

Minimum and average path length

The shortest (or minimum) path length $L_{i,j}$ between two nodes v_i and v_j is the minimum number of edges that needs to be travelled to go from a node v_i to node v_j. The average shortest path length of a node v_i is the average of its shortest path lengths to all other nodes V (Dijkstra et al., 1959; Watts and Strogatz, 1998):

$$L_i = \frac{\sum_{j=1, j \neq i}^{V} L_{i,j}}{V}. \tag{1}$$

When wiring length is expensive (e.g., in the brain longer and more axons take up more space and also bring costs in terms of energy needed for signal transmission) then a network that tries to minimise the number of edges to be traversed between any two nodes will be more optimal in terms of wiring cost. It has been shown (e.g., Watts and Strogatz, 1998) that a regular network can reduce its average path length by adding or rewiring random long range connections, because these introduce shortcuts in a network, connecting nodes or clusters of a network that were previously far apart from each other.

The average minimum path length L of a network is the average of L_i over all V nodes (Dijkstra et al., 1959; Watts and Strogatz, 1998):

$$L = \frac{\sum_{i=1}^{V} L_i}{V}. \tag{2}$$

Clustering C: the clustering coefficient c_i of a node v_i is defined as the number of edges k_j between its direct neighbours (denoted by subgraph g_i) divided by the total number of all possible edges k_{g_i} in g_i (Luce and Perry, 1949; Watts and Strogatz, 1998):

$$c_i = \frac{\sum_{k_j \in g_i} k_j}{k_{g_i}(k_{g_i}-1)/2}. \tag{3}$$

When the clustering coefficient is 1, all the neighbours of node v_i are connected with each other and form a fully connected cluster. When the clustering coefficient is 0, the node v_i is not part of a cluster. Nodes in random networks usually show zero to little clustering, because the nodes are wired randomly. Nodes in regular networks show high clustering because nodes and their neighbours are all connected to each other. Clusters can efficiently exchange information between nodes, and are therefore regarded as specialised units in a network. This property is desirable when information needs to be processed in detail. The clustering coefficient $C_{network}$ of the network is the average clustering coefficient c_i over all N nodes:

$$C_{network} = \frac{\sum_{i=1}^{V} c_i}{V}. \tag{4}$$

Small world (σ)

A network is defined as having the small world property (σ) when it shows more clustering than a random network, its average minimum path length remaining similar to that of a random graph (Watts and Strogatz, 1998; Humphries et al., 2006). There are several ways to randomise a network. Networks can be compared to fully random graphs (Erdős and Rényi, 1960). However fully random networks might show a dependence between clustering coefficient and size and/or degree of the network (van Wijk et al., 2010). This relationship is avoided when the degree distribution is kept intact during random reorganisation of the network (Maslov and Sneppen, 2002). Finally, networks can also be compared to regular networks (e.g., a lattice). A network can be compared to just one or several

random versions of itself to compute the small world property. The advantage of computing several h random networks is that the resulting network property will be more stable. The small world property is then computed with the average of the clustering coefficient and average minimum path length over all the random networks ($\overline{C}_{random}$ and $\overline{L}_{random}$ computed as: $\overline{C}_{random} = 1/h \sum_{i=1}^{h} C_{random_i}$ and $\overline{L}_{random} = 1/h \sum_{i=1}^{h} L_{random_i}$). Some studies recommend generating a hundred random networks, because different randomised networks might give different network property values. However, this depends on the size of the network under investigation: larger networks have less fluctuating graph property values than smaller graphs. For the study in Chapter 3, which studied large graphs (i.e. > 1000 nodes), it was found that 20 random graphs provide stable results as indicated by the low variation of the mean clustering coefficient over the random networks (measured in 20 random networks from 14 healthy people (280 random networks in total, mean size = 6977 nodes) with method proposed in Chapter 3: average random clustering coefficient mean = 0.39; min sd = 5.63 x 10^{-5}; max SD = 0.0001; average random minimum path length: mean = 1.77; min sd = 1.79 x 10^{-6}; max SD = 2.44 x 10^{-5}).

The ratio of $C_{network}$ to $\overline{C}_{random}$ is denoted by γ (Watts and Strogatz, 1998; Humphries et al., 2006):

$$\gamma = \frac{C_{network}}{\overline{C}_{random}}.$$

(5)

For a network to contain the small world property it is required that γ is larger than 1, which indicates that the network has more clustering than a random network.

The ratio of $L_{network}$ to $\overline{L}_{random}$ is denoted by λ (Watts and Strogatz, 1998; Humphries et al., 2006):

$$\lambda = \frac{L_{network}}{\overline{L}_{random}}.$$

(6)

For a network to contain the small world property it is required that λ is approximately equal to 1. This indicates that the average minimum path length of a network is comparable to that of a random network, and therefore it is easier for two nodes that are separated by other nodes to exchange information than in a regular network. The small world property (σ) is defined as the ratio of γ to λ (Humphries et al., 2006):

$$\sigma = \tfrac{\gamma}{\lambda}. \tag{7}$$

When the small world property (σ) of a network is larger than 1, it indicates that its topology lies between that of a completely regular (i.e., a lattice) and a completely random network. Such architecture is efficient because clusters can be highly specialised units of nodes that are densely connected and information can be exchanged between clusters via their long range connections (Milgram, 1967; Watts and Strogatz, 1998; Albert and Barabási, 2002; Newman, 2003; Sporns et al., 2004; 2005). Several studies have shown that networks extracted from imaging data contain the small world property (e.g., Achard et al., 2006; Bassett and Bullmore, 2006; He et al., 2007; van den Heuvel et al., 2008; Gong et al., 2009). The anatomical architecture of the macaque and cat cortex based on tracer studies is also small world (Sporns and Zwi, 2004). Table 1 summarises all neuroimaging studies that have found a small world architecture in the human brain (see Section 2.6 for a detailed explanation of this Table).

Betweenness centrality (BC)
The betweenness centrality (BC_i) of a node v_i quantifies the fraction of shortest paths $s_{j,m}$ between nodes v_j and v_m that run through node v_i in the total network G (Freeman, 1997):

$$BC_i = \sum_{i \neq j \neq minG} \tfrac{s_{j,m}(i)}{s_{j,m}}. \tag{8}$$

The betweenness centrality (BC) of a graph is the average over all nodes:

31

$$BC = 1/V \sum_i BC_i. \qquad\qquad (9)$$

A node through which many shortest paths run has a high betweenness centrality. Besides the number of connections a node has, it can also be defined as a hub when it has a high betweenness centrality.

The network properties described in this Section are the most basic properties to characterise a network. Many more (and more complicated) properties exist (see e.g., Albert and Barabási, 2002; Newman, 2005; Rubinov et al., 2010) that all describe some topological aspect. Furthermore, some studies chose to report the local and global *efficiency* instead of, or in addition to, the properties described in this Section (Latora and Marchiori, 2001). These properties are inversely related to the average minimum path length of a network. These measures are recently being used more often, because they are also applicable in the case of weighted networks. However, because most studies have reported the original network measures and because the work in this thesis focuses on unweighted networks, this measure was not investigated in the present work.

2.6 Graph theory applied to neuroimaging data

Since 2005, many studies have used graph theory to investigate the topology of the human brain in neuroimaging data. Most of these studies have demonstrated in healthy samples a non-trivial topology that was significantly different from random networks. Because the next Chapter discusses a new method to extract single subject grey matter networks, a literature search was performed to investigate the range of small world values that have been reported previously in healthy subjects.

The literature search was carried out in Pubmed, Web of Science and Google Scholar using (combinations of) the following key words: MRI, network, graph theory, small world, functional, structural, morphological, white matter, grey matter, DTI (i.e., diffusion tensor imaging), DSI (i.e., diffusion spectrum imaging).

To facilitate comparability, studies were selected according to the following criteria: networks were constructed based on whole brain data from healthy subjects, were unweighted and undirected. Furthermore, the size and connectivity density (sparsity level) needed to be reported. Finally, the small world coefficient must be reported. These criteria excluded the following studies: Wang. Li et al., 2010; Wang, Yu et al., 2010; Liao et al., 2011; Iturria-Medina et al., 2008; Gong et al., 2009; Lo et al., 2010; Iturria-Medina et al., 2011; Schwarz and McGonigle 2011 (note this is the only paper that investigated networks build from negative correlations); Yan et al., 2011; Dosenbach et al., 2007; Astolfi et al., 2007; Deshpande et al., 2009; Fair et al., 2009; Zhang, Cai, et al., 2010; Zhang, Wang, et al., 2011; Yu et al., 2011 ; van den Heuvel, Stam, Kahn et al., 2009; van den Heuvel et al., 2010 Raj et al., 2010; Yuan et al., 2010; Fransson et al., 2011; Archard and Bullmore, 2007; Cecchi et al., 2007; Hagmann et al., 2008; Gong, Rosa-Neto et al., 2009; He, Wang, Wang et al., 2009; Ferrarini et al., 2009; Valencia et al., 2009; Wang et al., 2009; Sepulcre et al., 2010; Wang, Metzak et al., 2010; Ginestet and Simmons 2010; Burdette et al., 2010; Chanraud et al., 2010; Sheppard et al., 2011; Shu et al., 2011; He et al., 2009; Lv et al., 2010; Telesford et al. 2010; Fan et al., 2011; Wu, Taki, Sato, Kinomura et al., 2011; Wu, Taki, Sato, Sassa et al, 2011).

The details of the healthy samples from the selected studies are summarised in Table 1. The studies were further categorised based on the imaging modality as functional (using fMRI), white matter (using data from DTI or DSI) and grey matter (using either cortical thickness or volume from grey matter segmentations of structural MRI).

Figure 1 gives an overview of the sparsity levels that the studies have investigated, with the corresponding maximum and minimum small world values. The largest variation of small world values (between 1.90 and 111.38) can be seen at sparsity levels between 0 and 10% existing connections. This might be due to differences in network size across studies. On the other hand the variability might reflect that network topologies become more unstable when more edges are removed (e.g., because nodes get disconnected).

For sparsity levels > 40% connections, small world values converge to 1. For intermediate sparsity levels between about 10% and 40% connections, the

small world value varies between 3 and 1.10. This Figure suggests that for these intermediate sparsity levels the small world property is stable across studies of different modalities and different sizes, suggesting that network topologies are most robust in this sparsity range.

Table 1
Overview of neuroimaging network studies, categorised in functional, white and grey matter MRI.

Study	Subjects (F)	age +/- SD or [range]	Network Size	Atlas	additional info
functional MRI					
1. Eguíluz et al., 2005.	7 (nr)	nr	4891 - 31503	Voxel wise 3 x 3.5 x 3.5 mm^3	Finger tapping task
2. Salvador et al., 2005.	12 (5)	30 ([23 - 48])	45	AAL	Resting state
3. Achard et al., 2006.	5 (3)	nr [25-35]	90	AAL	Resting state
4. Liu et al., 2008.	31 (15)	26+/-4	90	AAL	Resting state
5. Supekar et al., 2008.	18 (11)	62.84 [37 - 77]	90	AAL	Resting state
6. van den Heuvel et al., 2008.	28 (14)	25.1 +/-7.1	≈ 10000	Voxel wise 4 mm^3	Resting state
7. Nakamura et al., 2009.	8 (3)	[19 - 51]	56	nr	Resting state
8. Zhang et al., 2009.	1 (nr)	nr	1397	Voxel wise 6 mm^3	Finger tapping task
9. Wang, Wang, Zang et al., 2009.	18 (9)	[21 - 25]	20 - 90	AAL, ANIMAL	Resting state
10. Supekar et al., 2009.	22 (11)	20.4 [19 - 22]	90	AAL	Resting state
11. Sanz-A. et al., 2010.	21 (13)	70.7 +/- 6	90	AAL	Resting state
12. Zhang et al., 2010.	4 (nr)	nr	2255	Voxel wise, 6 mm^3	Finger tapping task
13. Liao et al., 2010.	27 (8)	24.1 (17- 51)	90	AAL	Resting state
14. Fornito, 2010.	30 (11)	26.77 +/- 10.30	84 - 4329	AAL and custom ROI	Resting state
15. Spoormaker et al., 2010.	25 (12)	24.7 +/- 3	90	AAL	Resting state
16. Lynall et al., 2010.	15 (1)	33.3 +/- 9.2	90	AAL	Resting state
17. Alexander-Block et al., 2010.	19 (10)	19 +/- 4	100	HO	Resting state
18. Hayasaka et al., 2010.	10 (5)	27.7 +/- 4.7	90 &16000	AAL & voxel wise, 4x4x5 mm^3	Resting state
19. Tian et al., 2011.	86 (48)	20.8 +/- 1.7	45	AAL	Resting state
20. Ferrarini et al., 2011.	20 (0)	23.95 +/- 2.52	21954	Voxel wise , 4mm^3	Resting state
21. Whitlow et al., 2011.	30 (15)	21.3 ([18 - 25])	116	AAL	Resting state
White matter					

Table 1

Overview of neuroimaging network studies, categorised in functional, white and grey matter MRI.

Study	Subjects (F)	age +/- SD or [range]	Network Size	Atlas	additional info
22. Hagmann et al., 2007.	2 (nr)	nr	956 & 1013	Custom	DSI
23. Gong, He, et al., 2009.	80 (42)	nr [18 - 31]	78	AAL	DTI
24. Li et al., 2009.	79 (35)	23.8 [17 -33]	90	AAL	DTI
25. Shu et al., 2009.	17 (7)	23 -19 - 28]	90	AAL	DTI
26. Vaessen et al., 2010.	6 (1)	nr [23 -28]	111	WFUpickatlas	DTI
27. Zalesky, et al., 2010.	3 (1)	26.67 +/- 4.73	82 - 4000	AAL and custom ROI	DTI & HARDI
28. Li et al., 2011.	5 (nr)	nr	68	MNI atlas	DTI
29. Wen et al., 2011.	342 (184)	79.7 +/- 4.55	68	Freesurfer atlas	DTI
30. Bassett et al., 2011.	7 (nr)	nr	54 - 880	AAL, HO, LPBA40	DSI & DTI
31. Zalesky, et al., 2011.	32 (17)	33 +/- 13	82	AAL	DTI
Morphological networks					
32. He, Chen and Evans, 2007.	124 (53)	24.38 +/- 4.25	45	ANIMAL	Cortical thickness
33. He et al., 2008.	97 (71)	75.93 +/- 9.03	54	ANIMAL	Cortical thickness
34. Schmitt et al., 2008.	600 (268)	11.08 +/- 3.43	54	ANIMAL	Cortical thickness
35. Bassett et al., 2008	259 (nr)	nr	104	BA with WFUPickatlas	Cortical volume
36. Sanabria-Diaz et al., 2010.	186 (66)	32.58 +/- 9.50	82 & 56	AAL & Jacob surface	Cortical surfce descriptors & thickness
37. Zhu et al., 2010.	428 (231) & 374 (170)	46.7 +/- 1.4 & 66.6 +/- 1.4	90	AAL	Cortical volume
38. Yao et al., 2010.	98 (49)	77.27 +/- 4.66	90	AAL	Cortical volume
39. Bernhardt et al., 2011.	47 (24)	32 +/- 12	52	ANIMAL	Cortical thickness
40. Hänggi et al., 2011.	24 (healthy)	27.3 +/- 10.1	154 & 2366	Freesurfer & custom	Cortical thickness
41. Tijms et al., 2011.	14 (5)	34.80 +/- 8.32	6982	Custom	Intracortical similarity

Table 1

Overview of neuroimaging network studies, categorised in functional, white and grey matter MRI.

Study	Subjects (F) [range]	age +/- SD or Network Size Atlas	additional info

F is female, SD is standard deviation, fMRI is functional magnetic resonance imaging, DSI is diffusion spectrum imaging, DTI is diffusion tensor imaging; HARDI is high angular resolution diffusion tensor imaging; AAL is Automated Anatomical Labeling atlas (Tzourio-Mazoyer et al., 2002), HO is Harvard-Oxford atlas, LPBA40 is LONI probabilistic atlas (Shattuck et al., 2008).
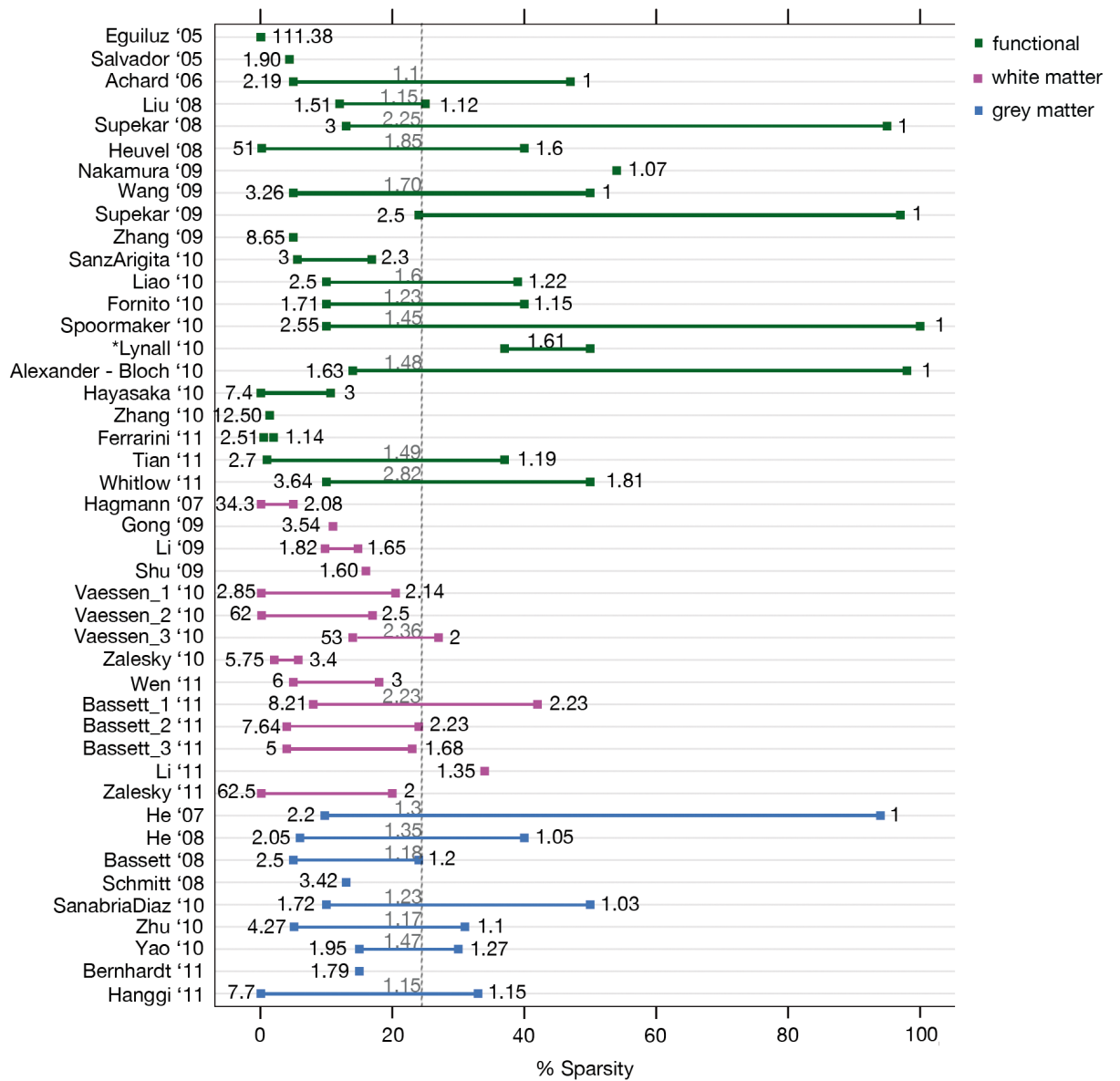
Figure 1. An overview of the sparsity levels that studies have used to investigate small world values in binarised networks of functional, white and grey matter MRI. White matter involves diffusion techniques such as DTI and DSI, while grey matter refers to grey matter segmentations of structural MRI. For each minimum and maximum sparsity value the corresponding small world value is indicated. The grey dotted line indicates the 23% sparsity level, that was investigated in the study in Chapter 3. The grey values along this line were reported by the corresponding studies for a sparsity level of 23%. * this study only reported the average small world value over the explored sparsity range.

3. Study I: Extracting networks based on intracortical similarities from individual grey matter segmentations in a healthy population

This Section presents a contribution to the important issue of characterising cortical morphology in individual grey matter scans. The main question under investigation was whether a statistical description of grey matter structure of individual cortices could be derived from intracortical similarities. Here the method will be introduced and explained in detail. Then results will be discussed, after application of the method to a healthy sample. The work in this Chapter has been published in Tijms et al. (2011).

3.1 Introduction

The work in this Chapter investigated whether graph theory could be used to quantify the morphology in individual brains, based on intracortical similarities. Up to now, morphological networks describe covariation between anatomical areas across people, representing group averaged data (e.g., He, Chen et al., 2007; Bassett et al., 2008). As described in the previous Chapter, animal tracer studies have found that morphological measures such as cortical thickness, folding and neuronal density can predict anatomical connectivity (Barbas, 1986; Barbas and Rempel-Clower, 1997; Dombrowski et al., 2001). These studies suggest that similarity in thickness and folding might be an indication of connectivity between cortical areas. Furthermore, the study from Andrews et al. (1997) was one of the few that have quantified the relationship between covariation of cortical morphology and anatomical connectivity in individual brains. Investigating the the lateral geniculate nucleus, the optical tract and the primary visual cortex, they found that all these structures covaried in grey matter volume.

Here the current work further extended these studies by proposing a new method that extracts networks from individual grey matter MRI segmentations. In these networks the nodes represent small cortical regions with their three-dimensional structure intact, that are connected when they show structural similarity. The method was applied to a sample of 14 healthy subjects, who where scanned at two different time points in previous work (Moorhead et al., 2009;

Gountouna et al., 2010). For the first time, the graph theoretical properties of these networks were studied and compared to the results from previous studies that constructed networks from group morphological, functional and white matter magnetic resonance imaging (MRI) data. It was proposed that if intracortical similarities are related to anatomical connectivity, then the associative areas were expected to show more intracortical similarities than, for example, primary sensory areas, resulting in a spatially non-uniform connectivity distribution. Such spatially non-uniform connectivity distributions have been found in studies that derived morphological networks from group data (Lerch et al., 2006; He, Chen et al., 2007; Bassett et al., 2008). Finally the robustness of the method was assessed by measuring the stability of the network statistics between two scanning sessions.

3.2 Method description

Figure 2 shows a schematic overview of the method that is completely automated and data-driven, and thus requires no a priori hypotheses about the regions of interest. Here a detailed description of the method in its final form is given. Details about scan acquisition and preprocessing can be found in Section 3.3. The current Section will conclude with an overview of methodological considerations during the development of the method.

The method starts with dividing the grey matter segmentation of an individual brain into 3 x 3 x 3 voxel cubes commencing from the first non-empty voxel, in a manner similar to methods that match scans from different modalities (Borgefors et al., 1997; Ourselin et al., 2000). Using cubes kept the three-dimensional structure of the cortex intact thereby spatial information from the MRI scan is used in combination with the grey matter partial volume values in the voxels. By keeping the spatial information intact, the cubes contain a quantity that reflects the local thickness and folding structure of the cortex. In contrast, cortical volume measures only the number of voxels at a location and thus does not include information concerning the spatial relationship between voxels. Similarly, cortical thickness measures do not contain information about the three-dimensional folding structure of the cortex. The size of the cubes was constrained by two factors: (i) The minimum spatial resolution that still captures cortical

folding has been shown to be 3 mm (Kiselev et al., 2003); (ii) Practical computational limitations exist with large matrices. Therefore we used a cube size of 3 x 3 x 3 voxels, corresponding to 6 x 6 x 6 mm^3. Each cube is represented by a different node v in the network. A network contained on average 6977 nodes (std = 783.92, over both subjects and runs). The next Section will explain in detail how the networks were constructed.
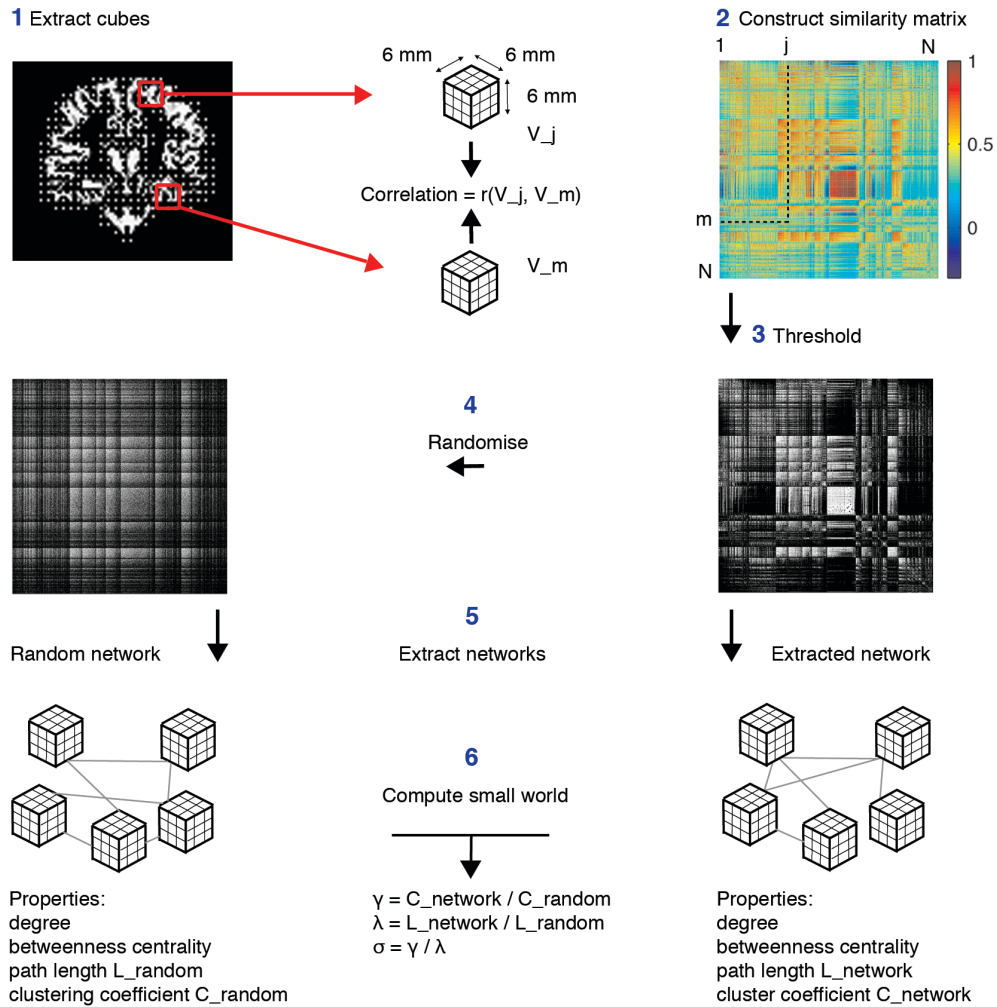
Figure 2. General pipeline of the extraction of individual networks. After preprocessing the grey matter was divided into 3 x 3 x 3 voxel cubes, visualised by a white voxel in the centre of each cube (1). The red arrows point to two example cubes v_j and v_m (note that the cubes were magnified for illustration purposes). The similarity between all V cubes within a scan was computed with the correlation coefficient, storing the result in a matrix with 1 to V rows and columns (2). In 3) the similarity matrix was binarised, with a threshold that ensured a 5% chance of spurious connections for all individuals (corresponding to a significance level of $p = 0.05$ corrected for multiple comparisons by the false discovery rate technique using an empirical null distribution). Twenty random matrices that kept intact the spatial degree distribution were generated for each binarised similarity matrix (4). Finally the networks were constructed and the degree, betweenness centrality, the path length, clustering coefficient and small world property were calculated from the extracted and randomised networks (6).

42

3.2.1 Intracortical similarity

To construct a network, two nodes v_j and v_m were connected when their similarity metric exceeded a certain threshold. After explorations of several similarity metrics (see Section 3.2.4), the correlation coefficient was chosen to quantify the structural similarity between two cubes because it is simple to understand and implement, while at the same time fast to compute (Lewis, 1995; Nikou et al., 1999; Weese et al., 1999; van Court et al., 2005; Penney et al., 2008). Additionally, the correlation coefficient does not require centering of the data, because it is normalised by the standard deviation of the cubes. The numerator of the correlation coefficient r_{jm} between cubes v_j and v_m calculates the sum over the product of the differences between the cubes' values at each voxel location i = 1, 2, ... n for n voxels (after subtraction of the cubes' average values, respectively $\overline{v}_j$ and $\overline{v}_m$). The denominator of the correlation coefficient is the product of the cubes' standard deviations:

$$r_{jm} = \frac{\sum_{i=1}^{n}(v_{ji}-\overline{v}_j)(v_{mi}-\overline{v}_m)}{\sqrt{\sum_{i=1}^{n}(v_{ji}-\overline{v}_j)^2}\sqrt{\sum_{i=1}^{n}(v_{mi}-\overline{v}_m)^2}}. \qquad (10)$$

Cubes with zero variance were excluded (average < 0.01%). Given that the cortex is a curved object, two similar cubes could be located at an angle from each other, which could decrease their similarity value. As the cubes were constructed from discrete MRI data, each seed cube v_j was rotated by an angle θ with multiples of 45° and reflections over all axes to find the maximum correlation value with target cube v_m:

$$r_{jm}^{max} = \underset{\theta}{\text{argmax}} \left(\frac{\sum_{i=1}^{n}(v_{ji}(\theta)-\overline{v}_j)(v_{mi}-\overline{v}_m)}{\sqrt{\sum_{i=1}^{n}(v_{ji}(\theta)-\overline{v}_j)^2}\sqrt{\sum_{i=1}^{n}(v_{mi}-\overline{v}_m)^2}} \right). \qquad (11)$$

In theory, other angles could be chosen as well. However, then interpolation between voxels would be necessary, which adds noise to the data and entails computational difficulties. In the next Section the influence of rotation on the value of the similarity metric was investigated by means of a simulation study, using a simplified model for the structural MRI data. Briefly, it was found that

using angles with multiples of 45° recovered 99% of the similarities, suggesting that these angles are sufficient to correct for rotation.

Using a simpler metric of similarity, namely the mean absolute difference, it further investigated whether the correlation coefficient could adequately detect structural similarity between two cubes. Figure 3 contains a plot of the mean absolute difference in voxel intensities between a thousand randomly selected cubes and all other cubes of a randomly selected network, confirming that the more similar two cubes were (as measured by the absolute difference in their voxel intensities) the higher the similarity coefficient. Because the correlation coefficient normalises the data in each cube, it was preferred over the simpler absolute difference metric.
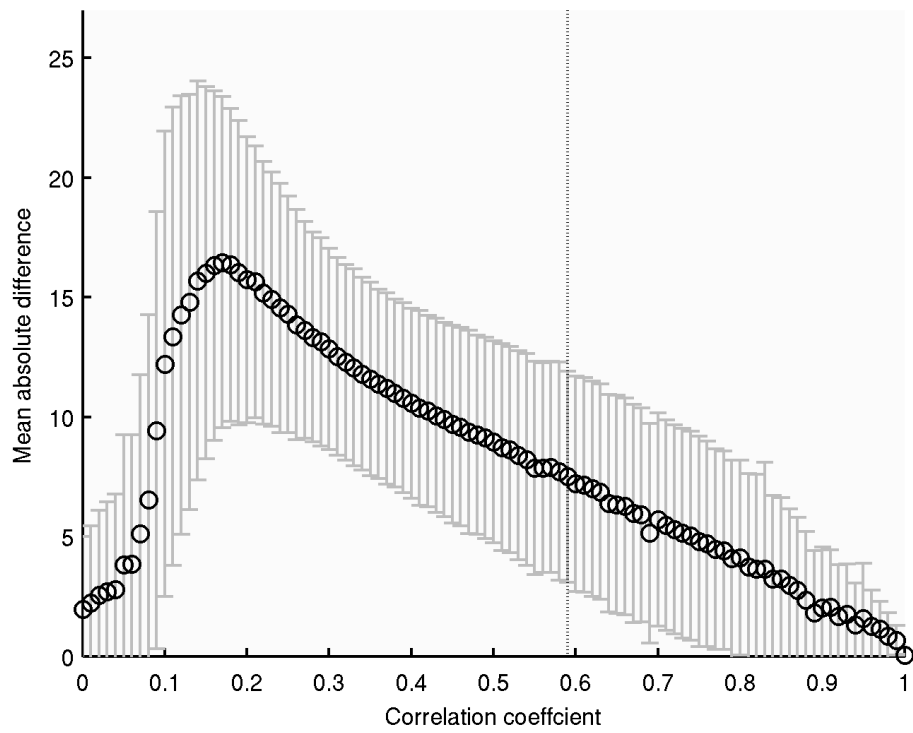
Figure 3. Structural similarity between cubes (measured as the mean absolute difference between corresponding voxel values of two cubes) as a function of the correlation coefficient. The more similar two cubes are, the lower the mean absolute difference between them and the higher the correlation coefficient. The vertical grey line indicates the threshold value for this specific network (edges were only placed between cubes when their correlation value exceeded this threshold).

3.2.2 Influence of rotation on the similarity metric: a simulation.

The correlation coefficient was computed for different rotation angles to extract similarities between cortical patterns that might be located at an angle from each other due to the curved nature of the cortex. Here a simulation study was performed to investigate the effect of such rotations on the correlation coefficient and the minimum number of angles that need to be taken into account to correct for these effects. Squares with simulated data were used instead of cubes, because squares need to be rotated around only one axis and therefore require less computational resources. A simple model was constructed by filling squares with random grey scale values between 0 and 1, where the value represents grey matter intensity at the centre of the pixel. Then the data was smoothed to add spatial relationships to the squares as follows: the pixel values were averaged with those from neighbouring pixel values. To ensure variation, interpolation started at randomly chosen pixels and with randomly chosen direct neighbours. The linear interpolation between neighbouring pixels was intended to mimic spatial relationships between observed voxels in MRI. It must be noted that this is an oversimplification of the cortical geometry that is observed in structural MRI and is merely intended to investigate the influence of rotation on cube matching. More sophisticated MRI simulations models exist such as Brainweb (http://mouldy.bic.mni.mcgill.ca/brainweb), and in the future such models should be used to further investigate the influence of rotation on the value of the similarity metric.

The influence of rotation on the correlation coefficient was assessed by comparing each of a 1000 different squares while rotating them for every degree between 0° and 360°. Two squares were considered to be similar when their correlation coefficient value exceeded the significance level of $p_{corrected} < 0.05$ (threshold determined with an empirical null distribution to correct for multiple comparisons as in the main Section). Figure 4a shows how, for a thousand squares and their copies, the correlation coefficient decreased with increasing angles up to 180° and that only 33% of all tests reached significance, which confirmed the necessity to correct for rotation.

The minimum number of angles necessary to correct for rotation was determined by computing the correlation coefficient after rotating the stationary cube by

multiples of either 90° (0°, 90°, 180° and 270°) or 45° (0°, 45°, 90°, 135°, 180°, 225°, 270°, 315°). In theory, other angles could be chosen as well. However, for other angles interpolation between voxels would be necessary, which brings computational difficulties and also adds noise to the original data. Figure 4b shows that correcting for rotation with angles at multiples of 90° recovered of 66% of the similarities, but missed all the rotations in the range with multiples of 30° to 60°. Adding angles with multiples of 45° recovered 99% of the similarities. Just 1% of the patterns, only occurring in the range with multiples of 25° to 35°, did not reach the significance threshold, suggesting that using angles with multiples of 45° is sufficient to correct for rotation. To explore the influence of these two different sets of angles to correct for rotation on the network property values, both extractions were compared to each other and these results will be discussed in Section 3.4.2.
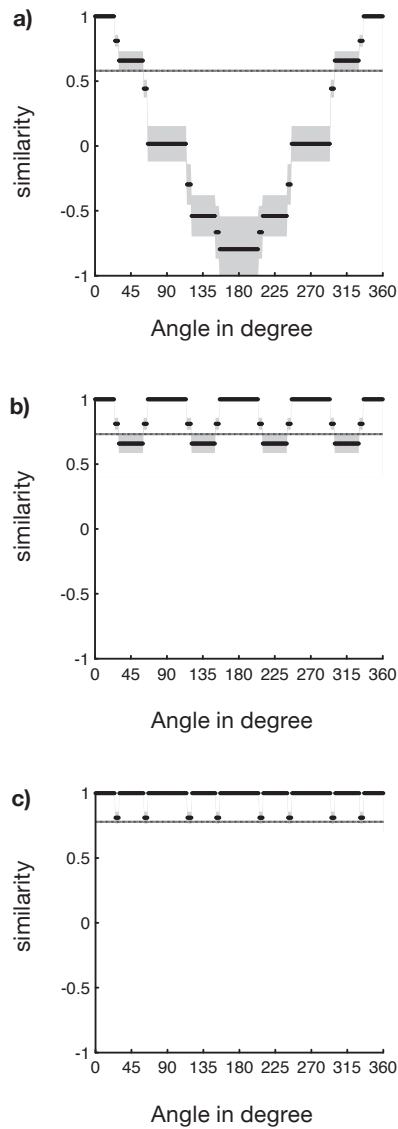
Figure 4. Simulation of the influence of rotation on the similarity measure without correction (a), correcting with multiples of 90° angles (b) and with multiples of 45° angles (c). All plots show for the average correlation value and the corresponding 95% confidence interval for a thousand randomly generated squares and their rotated identical copies for 0° to 360° degrees with steps of 1°. As in the main text, two patterns were considered to be identical when their correlation coefficient reached $p < 0.05$ significance, corresponding to the following thresholds with correlation values higher than 0.58 (a), 0.73 (b) and 0.78 (c; all thresholds determined with false discovery rate using an empirical null distribution). When not corrected for rotation only 33% of the similarities were found. This percentage increased to 66% when corrected with multiples of 90° angles and 99% when corrected with multiples of 45° angles.

3.2.3 Binarisation of the networks

The similarity matrices were binarised to construct undirected and unweighted graphs. The graphs were undirected because it is not feasible to infer causality from correlations. Although continuous weights would contain the most information (Barrat et al., 2004), the present study assessed only the basic network topology and therefore the networks were binarised.

To binarise the networks, a threshold was determined for each individual based on the significance of the correlations. Because correlations were computed between on average (over subjects in the first run) 6982 nodes and maximised for rotation and reflection, it was necessary to correct for multiple comparisons when determining the threshold. The false discovery rate (FDR) technique with the use of an empirical null model was employed to correct for multiple comparisons (Benjamini and Hochberg, 1995; Benjamini and Yekutieli, 2001; Noble, 2009). The false discovery rate is the proportion of false positives within a set of significant scores. This proportion corresponds to the area greater than a threshold value in the null model score distribution. An advantage of this approach is that all individuals will have the same 5% chance of spurious correlations. In the current study, similarities between small regions of grey matter were determined by the spatial organisation of grey matter voxels. Therefore, empirical null models were constructed by randomly permuting the locations of all voxels from the original data, and so removing the spatial information from the original scan while keeping all other information constant (mean and standard deviation of the intensity value distribution). A score distribution was compiled by computing the similarities between all cubes extracted from the randomised scan. Next, the threshold was set such that the area to the right of that score represented the probability that this score was observed with a p-value of 0.05. After the threshold was determined, it was used to binarise the networks where the presence of an edge was indicated by 1 (a correlation greater than the threshold) and absence of an edge indicated by 0 (a correlation lower than the threshold). In this study the word 'connection' refers to these edges, as they connect the nodes in our networks. These connections should not be confused with anatomical connections and indicate whether any two cubes have statistically similar grey matter

morphology. The sparsity of the networks was defined as the connectivity density within a matrix. This is simply the percentage number of existing edges compared to the maximum number of edges possible (*V * (V-1)*, where *V* is the number of nodes). The binarised networks had an average sparsity of 23% (SD = 1%, over both subject and runs).

3.2.4 Methodological considerations during method development

During the early stages of the method development, a great amount of time was invested to investigate the most optimal way of extracting the cubes from the grey matter segmentations. Previous versions of the method used a fixed template approach, in which all the indices where hand-coded. Briefly, the indices for each cube in a voxel were coded for the first 'slice' of cubes, and these were copied for the complete brain volume. This approach corresponds to a rigid grid, which can start at an arbitrary point in the MRI volume, and could not be easily adapted to change, for example, the size of the cubes. Also, depending on the start of the cube extraction (the first non-empty voxel), the total number of cubes extracted can vary slightly when moving the grid one or two voxels over any axis. Comparison of the properties from differently extracted networks within the same individual showed that these were highly stable for different extractions, but not identical (all properties correlated with r > 0.9). Therefore, the final version of the method was fully automated to easily change the dimensions of the cubes and also to extract the minimum number of cubes to make sure that the extracted network was maximally comparable between scans of the same subject.

Furthermore, during the development of the method computational resource issues were encountered, due to the large size of the similarity matrices. One solution was to sample the voxel resolution to 2mm isotropic voxels, because the use of smaller voxel resolutions led to matrices that were too large for matrix computations. Another solution was to optimise the code: first runs of the code took about 9 hours per scan to construct the similarity matrix and an additional 10 hours to compute the graph properties. The final version of the method takes just a few minutes to compute the similarity matrix, and in total 15 minutes to compute the graph theoretical properties (including those from the twenty random networks). Solutions to speed up computations included changes to data types that

take less memory than the standard double precision numbers in Matlab, but also precomputing parts of equations that remain constant. For example, the computation time of the correlation coefficient between all cubes within a scan was dramatically reduced by using a fast procedure as described by Lewis (1995).

Another issue that took time was the investigation of the most suitable metric to quantify the structural similarity between two cubes. Although the correlation coefficient is simple to compute, it might not be ideal for grey matter data as its values are bounded between 0 - 1 and therefore violate the assumption of normality. Future research is aimed at investigating the use of non-parametric tests of association like Spearman's ϱ. Other, simpler metrics than the correlation coefficient such as the absolute difference between corresponding voxels in cubes, the Dice coefficient (Dice, 1945) and variations on the Dice coefficient (e.g.,Jaccard index, Hamming distance) have also been studied and it was found that these suffer from limitations. For example, the mean absolute difference underestimates structural similarity between cubes that differ only slightly in intensity value as a result of spatial inhomogeneities in the data (i.e., a smooth spatial distortion in MRI data). The Dice coefficient (and similar measures) on the other hand give an index of the binary overlap in structure between cubes, not taking into account information about their voxel values. During this study, attempts were made to adjust the Dice coefficient to include voxel intensity values, however, this resulted in a less elegant measure than the correlation coefficient. A more complicated metric than correlation was also explored, namely mutual information (based on Russakoff et al., 2004). However, this measure proved to be too computationally expensive for the number of cubes that needed to be compared. From these tests the results from the mean absolute difference comparisons between cubes were used to assess the performance of the correlation coefficient in Chapter 3.

Another complex issue concerned the correction for rotation. Because MRI data is discrete it is not straightforward to rotate the cubes for arbitrary degrees, because doing so would entail interpolation of the voxels within the cubes. First attempts of implementing rotation demonstrated that interpolation dramatically changed the voxel intensities from their original values. Additionally, it became unclear how to match corresponding voxels between two cubes,

because rotation at some angles shifts voxel values outside the boundary of the cube. Therefore it was decided to rotate cubes with multiples of 90°. It was complicated and not straightforward to determine whether this approach of correcting for rotation with only four angles over all axes would be sufficient to recover existing similarities. To study whether correcting for multiples of 90° would be sufficient, attempts were made to generate MRI data with a known the spatial structure. However, these attempts did not led to convincing models of brain structure and it was decided to simulate the structure in cubes as described in Section 3.2.2. The simulation study showed that angle multiples 45° recovered more similarities than angle multiples of 90°, and these rotations could be achieved by nearest neighbour interpolation (that did not distort the voxel values).

All routines to extract graph theoretical properties were implemented in Matlab and optimised to run as fast as possible. The outcome of these measurements were compared to those extracted with the publicly available 'brain connectivity toolbox' (Rubinov et al., 2010). After adjusting the scripts from the brain connectivity toolbox, to enable it to run with the large matrices from the current work, the network property values were found to give identical results supporting that the graph theoretical properties were correctly implemented.

This Section has summarised just a selection of issues encountered, and it serves to illustrate the variety of problems that need to be solved when a new method is developed. The next Sections will describe the details of the subjects and scans that were used for this specific project.

3.3 Subjects and scan information

In this Section details are given about the sample to which method was applied, as well as details concerning the acquisition and preprocessing of the scans and a summary of the measures that were assessed in the networks.

3.3.1 Subjects

The data used here was previously collected for the CaliBrain study (Moorhead et al., 2009; Gountouna et al., 2010). Fourteen healthy volunteers (nine male, mean age at first scan 34.80 years, std = 8.23) participated in CaliBrain. All participants were native English speakers, right handed (self reported), had no history of

substance abuse, nor a history of diagnosed neurological disorder, major psychiatric disorder or treatment with psychotropic medication. All participants provided written informed consent and the study was approved by the appropriate research ethics committee.

3.3.2 Data acquisition

The scans were acquired at the University of Edinburgh (The Division of Psychiatry and the Scottish Funding Council Brain Imaging Research Centre within the Centre for Clinical Brain Sciences). The scanner was manufactured by General Electric (GE Healthcare, Milwaukee, Wisconsin) with a field strength of 1.5T and standard quadrature head coil (for more details see Moorhead et al., 2009). The subjects were scanned twice within a six month period. At each visit a high resolution T1-weighted scan was acquired using a 3D inversion recovery-prepared fast gradient echo volume sequence with a coronal orientation and the following parameters: repetition time (TR) of 8.2 ms; echo time (TE) of 3.3 ms; inversion time (TI) of 600 ms; flip angle of 15°; matrix size of 256 x 256; field of view (FOV) of 220 mm^2; 128 slices with 1.7 mm thickness without a gap, resulting in voxels with size 0.86 x 1.7 x 0.86 mm^3.

3.3.3 Preprocessing and segmentation

Twenty-eight T1-weighted scans were preprocessed using Statistical Parametric Mapping version 5 (SPM5, Wellcome Department of Cognitive Neurology and collaborators, Institute of Neurology, London, UK: http://www.fil.ion.ucl.ac.uk/ spm/software/spm5) with Matlab version 7.3.0.298 R2006b (Mathworks, Natick, MA, USA), on a Dell Precision 690 workstation with RedHat Enterprise Linux workstation WS version 4. First, the origin of all scans was manually set to the anterior commissure. Next, the scans were segmented with the Voxel Based Morphometry toolbox version 5 (VBM5, University of Jena, Department of Cognitive Neurology, C. Gaser: http://dbm.neuro.uni-jena.de/vbm) using a Hidden Markov Random Field (HMRF), without SPM priors, including bias correction and the option 'lightly cleaned' (as defined by VBM5) into grey matter, white matter and cerebrospinal fluid in native space. The HMRF used spatial constraints based on neighbouring voxels in a 3 x 3 x 3 voxel cube, increasing the accuracy of

segmentation. Note that this also introduces smoothing of the data. No further smoothing was applied during segmentation. After segmentation the data was resliced to 2 x 2 x 2 mm³ voxels. All further data analyses were implemented in Matlab version 7.3.0.298 R2006b (unless specified otherwise).

3.3.4. Statistical analyses

In all networks the clustering coefficient, the shortest path length, the betweenness coefficient were determined for all nodes in each network, as well as their network averages. The small world coefficient was also measured, using the average clustering coefficient and average shortest path length from 20 randomised versions per network and averaging over these networks. These metrics were described in detail in Section 2.3.2, and were implemented in Matlab. Correlations between the metrics were assessed in Matlab. Anderson-Darling tests supported that all graph properties were approximately normally distributed (all $p > 0.05$), and therefore parametric tests were used in subsequent analyses. One sided paired t tests were performed in R version 2.10 (http://cran.r-project.org), to test whether the clustering coefficient of the individual networks was larger than the average clustering coefficient from 20 randomised versions of the networks. Two sided paired t tests were performed to test the difference between the extracted and random average minimum path lengths. Furthermore, the intraclass correlation coefficient (ICC) was used to estimate the reproducibility of all graph theoretic measures over two time points. McGraw and Wong (1996) defined the ICC as the ratio of the variance between subjects ($\sigma^2_{between}$) to the total variance in test scores ($\sigma^2_{between} + \sigma^2_{within}$):

$$ICC = \sigma^2_{between} / \left(\sigma^2_{between} + \sigma^2_{within} \right).$$
(12)

The within-subject variance (σ^2_{within}) gives an indication of measurement error between repeated measurements. The ICC is close to 1 if the measurements of two repeated scans are consistent for each subject in the sample. Computation of the

ICC was performed in R version 2.10 (http://cran.r-project.org, using the 'irr' package).

3.4 Results

3.4.1 Influence of rotation on the network property values

The values of the properties were compared between networks that were extracted with a rotation correction with angle multiples of 90° and 45°, to investigate the influence of different correction schemes on network topology.

Using the same threshold of $p_{corrected} < 0.05$ to binarise the networks (determined with an empirical null model that was explained in Section 3.2.3), the new networks were more densely connected (23% connections) in comparison with the original networks (21% connections). This means that more connections were added to the networks when correcting the correlation coefficient with multiples of 45°. Note that although the amount of comparisons was doubled in comparison with the rotation correction with 90° the number of additional similarities only increased with 2%. This increase in number of connections was accompanied by a slight increase of the clustering coefficient from 0.50 to 0.53 and a decrease of the small world coefficient from 1.34 to 1.28. The average minimum path length was similar ($L_{old} = 1.85$ vs. $L_{new} = 1.86$).

The increased number of connections in the networks extracted with angle multiples of 45° appeared to be uniformly distributed over the network and not specific to certain nodes, as > 90% of the hubs (i.e., nodes with a degree higher than one standard deviation above the mean degree) remained stable in the individual networks. This was further supported by the finding of a highly stable spatial distribution of the clustering coefficient and degree values of the nodes (measured with the correlation coefficient within individuals, respective average r = 0.94, $p < 0.01$ and r = 0.91, $p < 0.01$). The stability of the spatial distribution of the nodal values suggests that the network property values are stable with regard to correction of rotation. All the following results discussed were extracted using angle multiples of 45°, because the rotation simulation study in Section 3.2.2. showed these angles recovered 99% of the similarities.

3.4.3 Graph properties of the individual networks

For the first time, this method permitted the investigation of morphological networks extracted from individual brains. Initially, to assess whether the extracted networks were small world, their average clustering coefficient and average minimum path length were compared to those from random networks. Figure 5a shows that the individual clustering coefficients of the extracted networks were higher than those from the randomised networks (one-sided paired t-tests, range of t values: min = 55.78; max = 147.92; all $p < 2.2$ x 10^{-16}). Figure 5b shows that the individual average minimum path lengths were significantly higher than those from the random networks (two-sided paired t test, t values range: min = 56.11; max = 88.57; all $p < 2.2$ x 10^{-16}). In addition, because the ratio of the average path lengths of the extracted and random networks was close to 1 (range λ: min = 1.04; max = 1.06) all networks had the small world property. To demonstrate that individual measures can be combined into a single group measure, the clustering coefficient and minimum path length averaged over all individuals are shown in Figure 5c and 5d. Similar to the individual cases, the clustering coefficient averaged over subjects was higher than the random clustering coefficients (one-sided paired t test: $t(13) = 15.73$, $p = 3.83$ x 10^{-10}). The minimum path length averaged over subjects was also higher than the random path length (two-sided paired t test: $t(13) = 30.73$, $p = 1.60$ x 10^{-13}). However the ratio was close to 1 (mean $\lambda = 1.05$, SD = 0.01) thus demonstrating that the networks were small world.
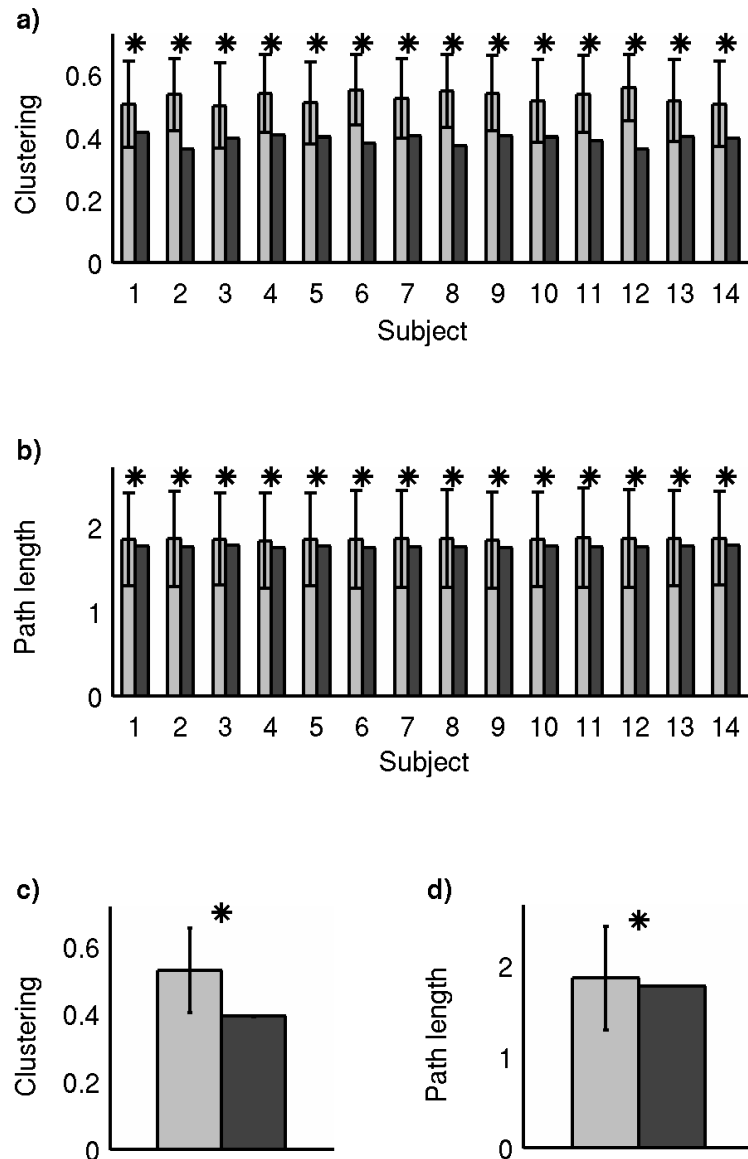
Figure 5. A network contains the small world property when its clustering coefficient is higher than random networks, while its path length is similar. Here plots are shown for the average clustering coefficient (a) and minimum path length (b) of the individually extracted networks (grey) and their randomised versions (black). The stars indicate a significant difference of $p < 0.05$ tested with a paired t-test between a network and the average nodal values of its corresponding random network. Next, we plotted the average clustering coefficient and minimum path length averaged over all networks (c) and their randomised versions (d). All networks had the small world property. The stars indicate a significant difference with $p < 0.001$ tested with paired t-tests between the average network values and their random networks.

3.4.2 Correlations between the network property values

Because the current analysis was performed in native space, all networks differed in size. Previous studies have shown that network properties can be dependent on the number of nodes, the degree and the sparsity of a network (e.g., He, Chen et al., 2007; Bassett et al., 2008; He et al., 2008; Bassett et al., 2010; Fornito et al., 2010; van Wijk et al., 2010; Zalesky et al., 2010). To investigate such relationships, pairwise correlations were computed between all network measures. The interrelationships were complex and are summarised in Table 2. The number of nodes had a strong positive relationship with the degree (r = 0.96, p = 4.12 x 10^{-8}). This correlation is in disagreement with diffusion tensor imaging (DTI) studies that have found a negative relationship between the number of nodes and the average degree (Bassett et al., 2010; Zalesky et al., 2010). For connectivity studies in DTI it is evident that increasing the parcellation resolution of grey matter leads to a decrease in the number of tracts that end in any given node. However, the current method computed similarities in grey matter that can exist without a direct white matter tract between them. The average minimum path length negatively correlated with the degree (r = -0.64, p = 0.01) and the number of nodes (r = -0.59, p = 0.03). This means that networks that had more nodes, had a higher average degree (i.e. more connections per node) and a shorter average minimum path length. The average betweenness coefficient showed a positive relationship with the degree (r = 0.95, p = 1.95 x 10^{-6}) and the number of nodes (r ≈ 1, p = 2.37 x 10^{-14}). However, no significant correlation was found between the betweenness coefficient and the minimum path length. The number of nodes did not show any significant associations with the other network properties.

Sparsity was strongly related to the clustering coefficient (r = 0.91, p = 5.75 x 10^{-6}) and to the small world coefficient σ (r = 0.61, p = 0.02). Furthermore, the clustering coefficient had a positive association with σ (r = 0.82, p = 0.0003) confirming that the small world coefficient depends on the extent of clustering in the original network. Similarly as with the number of nodes and the average degree, this means that when a network had more connections, it showed higher average clustering with a decreased average path length (also demonstrated in previous studies, see e.g.: He et al. 2008). No relationship was found between sparsity and network size.

Table 2
Pairwise correlations between the values of all computed graph properties over subjects at baseline.

	degree	nodes	L	C	σ	BC	S
degree	1	0.96***	-0.64*	0.40	0.30	0.95***	0.43
nodes		1	-0.59*	0.17	0.14	≈1***	0.17
L			1	-0.09	0.14	-0.52	-0.31
C				1	0.87***	0.17	0.91***
σ					1	0.17	0.61*
BC						1	0.14
S							1

Significance levels: *** $p<0.001$,** $p<0.01$, * $p<0.05$.
L is the average minimum path length, *C* the average clustering coefficient, σ the small world coefficient, *BC* the average betweenness coefficient and *S* the sparsity.

3.4.4 Comparison with other networks extracted from MRI data

Table 3 summarises morphological studies that reported network properties in healthy individuals (He, Chen et al., 2007; He et al., 2008; Bassett et al., 2008; Sanabria-Diaz et al., 2010; Yao et al., 2010; Zhu et al., 2010; Hänggi et al., 2011) for a sparsity similar to that found in the current study (23%), for comparison with the present networks. As all morphological studies (apart from Hänggi et al., 2011) reported smaller network sizes than the present study, only the clustering and small world coefficients can be compared directly with the present networks since these measures were significantly related to the sparsity and not to the size of the networks. In addition, studies were included that extracted networks of a comparable size to the present study from functional (Eguluíz et al., 2005; van den Heuvel et al., 2008; Zhang et al., 2009; Fornito et al., 2010; Hayasaka and Laurienti, 2010; Zhang et al., 2010) and white matter MRI (Hagmann et al., 2007; Zalesky et al., 2010). Their network properties were summarised for a sparsity of approximately 23% when this level was available and otherwise for the maximum sparsity.

In Table 3 one morphological network (Hänggi et al., 2011) and two resting state functional MRI networks were comparable to the present study in both size and sparsity (van den Heuvel et al., 2008; Fornito et al., 2010). All reported network property values were highly similar to the present study. The correspondence of network property values between the current study and the high resolution morphological network study suggest that possibly intracortical similarities within individuals contribute to covariance found in a group between anatomical regions. Furthermore, intracortical morphological correlations might reflect the organisation of correlations in resting state fMRI.

When comparing the present study with other morphometric studies, its clustering coefficient (0.53) was slightly higher than previously reported values (min = 0.25; max = 0.49). The value of the small world property of the present networks (1.28) fell within a small range of previously reported values (min = 1.17; max = 1.47), again suggesting that intracortical similarities might be organised similarly to correlations in thickness or volume between cortical areas assessed over subjects.

The present small world property was strikingly lower than the remaining functional studies (Eguíluz et al., 2005; Zhang et al., 2009; Hayasaka and Laurienti, 2010; Zhang et al., 2010) and two white matter studies (Hagmann et al., 2007; Zalesky et al., 2010). Finally, Table 3 shows that the property values of morphological networks varied within a narrow range, while those from functional and white matter MRI varied over a wider range (e.g., the small world values ranged between 1.28 and 168.54). In particular, the value of γ in those studies was one to a hundred times higher than in the present study (min = 1.28; max = 168.54), resulting in higher values for σ. This variation might be explained by differences in procedures used to construct random networks, but also by the low sparsity of these networks (min = 0.08%, max = 0.79%) in comparison with the present study (23%). Since the functional and white matter networks are comparable in size, this leaves an interesting question as to whether keeping sparsity constant would give rise to more similar networks across different scanning modalities.

Finally, Figure 1 shows the small world value at the 23% sparsity level of other fMRI, DTI and DSI studies that investigated networks of smaller size than the current study. Interestingly, these values vary within a narrow range of at most 2.85 and 1.1 with a mean of 1.62 and standard deviation of 0.51. The value of the present study of 1.28 is less than a standard deviation away of the mean value from the studies of Figure 1.

Study	V	C	L	γ	λ	σ	S
Morphological							
Present Study (n = 14)	6982	0.53	1.86	1.35	1.05	1.28	23%
He, Chen et al. 2007 (n = 124) cortical thickness	52	nr	nr	≈ 1.5	≈ 1.15	≈ 1.3	≈ 23%
He et al. 2008 (n = 97) cortical thickness	54	≈ 0.3	≈ 1.6	≈1.35	≈ 1	≈ 1.35	23%
Bassett et al. 2008 (n = 259) grey matter volume	104	≈ 0.25	nr	nr	nr	≈ 1.18	23%
	82 AAL- Area	≈ 0.3	≈ 1.81	nr	nr	≈ 1.28	22%
	56 Jacob - Area	≈ 0.28	≈ 1.84	nr	nr	≈ 1.23	22%
Sanabria-Diaz et al. 2010 (n = 186) comparison of cortical thickness and cortical surface descriptor networks.	82 AAL - Thickness	≈ 0.29	≈ 1.81	nr	nr	≈ 1.23	22%
	56 Jacob - Thickness	≈ 0.27	≈ 1.84	nr	nr	≈ 1.18	22%
Yao et al. 2010 (n = 98) grey matter volume	90	≈ 0.49	≈ 1.89	≈ 1.62	≈ 1.1	≈ 1.47	23%
Zhu et al. 2010 (n = 428) grey matter volume	90 (AAL)	≈ 0.26	nr	≈1.20	≈ 1.03	≈ 1.17	23%
Bernhardt et al. 2011 (n = 47) cortical thickness	52 (ANIMAL)	nr	nr	≈ 1.3	≈ 1.01	≈ 1.29	≈ 23%
Hänggi et al. 2011 (n = 24) cortical thickness	2366	≈ 0.49	≈ 1.15	≈ 1.3	≈ 1.13	≈ 1.15	≈ 33%

MRI studies that analysed networks with N > 1000

Study	V	C	L	γ	λ	σ	S
Functional							
Eguíluz 2005 (n = 7) averaged values over 2 tasks finger tapping task listening to music	4891	0.15	6.0	168.54	1	168.54	0.08%
van den Heuvel et al. 2008 (n = 28), resting state fMRI 0.01-0.09 Hz	10 000	≈ 0.52	≈ 1.75	≈ 1.9	≈ 1.03	≈ 1.85	20%

Table 3

Graph measures of our study and other morphological, functional and white matter MRI network studies for comparison.

Study	V	C	L	γ	λ	σ	S
Zhang et al. 2009 (n= 1), finger movement task	1397	0.54	2.59	11.25	1.3	8.65	4.80%
Fornito et al. 2010 (n = 30) resting state fMRI 0.04-0.08 Hz	4320	≈ 0.62	≈ 1.9	≈ 1.35	≈ 1.06	≈ 1.28	20%
Hayasaka & Laurienti 2010 (n = 10), resting state fMRI 0.009-0.08 Hz	16 000	0.24	3	≈ 7	≈ 1.22	6	0.79%
Zhang et al. 2010 (n = 4), finger movement task	2255	0.46	5.39	26.74	2.14	12.50	1.44%
White matter							
Hagmann et al. 2007, (n = 1) DSI	4052	≈ 0.30	≈ 3	≈ 20	≈ 1	≈ 20	≈ 0.61%
	4000 DTI	≈ 0.28	≈ 8.85	111.7	1.8	62.05	≈ 0.13%
Zalesky et al. 2010, (n = 3) comparison of DTI and HARDI.	4000 HARDI	≈ 0.24	≈ 6.15	77.5	1.4	55.36	≈ 0.16%

V is the number of nodes in the networks, *C* the average cluster coefficient, *L* the average minimum path length, γ the ratio of the networks cluster coefficient and that of its randomised version, λ the ratio of the average minimum path length of the network and that of its randomised version, σ is the small world coefficient (γ / λ) and finally *s* denotes the sparsity of the network in percentage connections. *nr* is 'not reported'. Network property values were measured for a sparsity level that corresponded to that of the present study (23%), but if this was not possible they were measured for the maximum sparsity available. The studies by van den Heuvel et al. (2009), Telesford et al. (2010) and Fransson et al., (2011), which also investigated network sizes of >1000, were not included because they did not report network sparsity or network property values.

3.4.5 Spatial distribution of the degrees in the networks

Next it was tested how the spatial distribution of the number of connections (i.e. degree) of the nodes in a network compared to the distribution reported in a previous study that derived cortical thickness correlations between anatomical areas in groups (Lerch et al., 2006). In that study the associative cortices were found to have the highest correlations in thickness with other regions of the brain. Figure 6a shows for each of the 14 subjects a slice from the medial right hemisphere with the standardised degree for all cubes resulting in a spatial distribution of the degree values. Each square is a side of a cube, with warmer colours indicating a higher degree. The figure shows that all individuals had a unique spatial distribution of the degree values. To demonstrate that it is possible to combine these networks into a single group network, the average of the individual patterns was plotted after warping these to a standard space and averaging standardised degree values over subjects (Figure 6b). Finally, with the use of the SPM tool SurfRend the group result was plotted on an inflated surface (Figure 6c, thresholded for computational reasons to include just the hubs, i.e. nodes with a degree higher than one standard deviation above the mean). Furthermore the individual spatial degree patterns were quantified by assessing the spatial distribution of hubs over 26 distinct anatomical areas per hemisphere extracted with an anatomical mask (constructed with the Wake Forest University (WFU) Pick-Atlas, http://www.fmri.wfubmc.edu, Advanced Neuroscience Imaging Research Core. See Table 4 for list of the anatomical areas, their abbreviations and sizes). The anatomical mask incorporated approximately the same regions as used in previous studies that extracted morphological networks using cortical thickness (He, Chen et al., 2007; Chen et al., 2008; He et al., 2008). The mask was warped to the individual native spaces, using the inverted parameter matrices from normalisation of the scans to standard space. Next for each subject the degree hubs (nodes with a degree higher than one standard deviation above the mean, within a subject) were identified and the percentage of hubs was calculated for each anatomical area. The bar plot in Figure 6d confirms that on average 77% of the hubs were located in the prefrontal (superior, medial, middle and inferior frontal gyri, precentral gyrus), the cingulate, posterior regions (postcentral gyrus, precuneus) the insula and temporal areas (superior, transverse

and middle temporal gyri). For comparison with other studies, the spatial distribution of the hubs for betweenness centrality were also plotted in Figure 6e (hubs defined as having a betweenness centrality value that is higher than one standard deviation above the mean betweenness centrality) which resulted in a similar spatial distribution with 77% of the hubs in the same areas as Figure 6d. In Table 5 these areas are summarised with their corresponding average degree and betweenness centrality. Table 5 also indicates other studies that found the same areas with structural MRI using cortical volume (Bassett et al., 2008) or cortical thickness (He, Chen et al., 2007; Chen et al., 2008), white matter (Iturria-Medina et al., 2008; Gong et al., 2009) and functional MRI (Achard et al., 2006; Buckner et al., 2009). The current hub areas have all been reported by at least one of the studies above. However, a strong relationship existed between the percentage of hubs and the region size in both hemispheres (left hemisphere: Spearman's $\varrho = 0.96$, $p = 5.84$ x 10^{-7}; and right hemisphere: Spearman's $\varrho = 0.97$, $p = 4.57$ x 10^{-07}), that might explain why these areas were also reported as hubs in other studies (also see: Bassett et al., 2010).
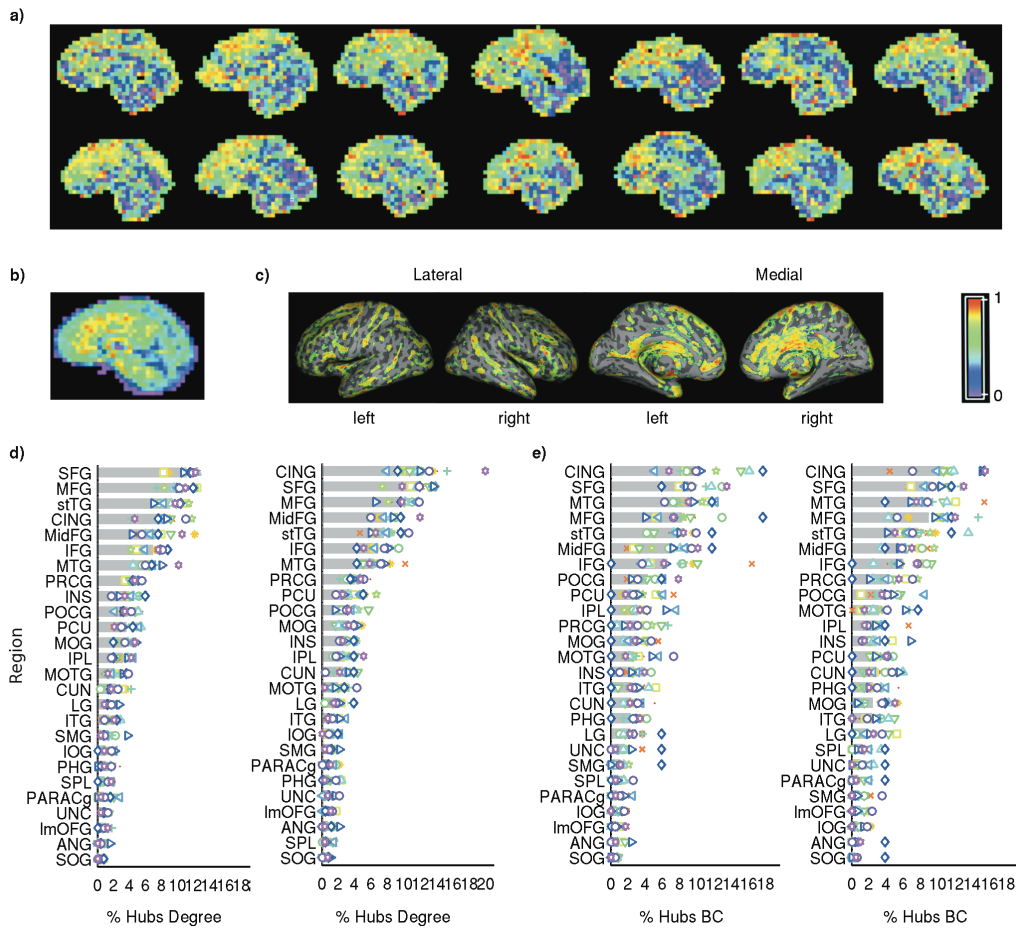
Figure 6. a) A plot of the degree of all cubes for one slice (right medial hemisphere) from each individual subject. The degrees were standardised by their maximal value. Warmer colours indicate that a cube has more structural similarities with other cubes in the brain than cubes with cooler colours. b) Shows the group average of the degree patterns after warping to standard MNI space, which supports the fact that most subjects have hubs along the right medial surface of the brain. c) Shows the spatial distribution of hubs (nodes with a degree higher than one standard deviation above the mean) averaged over all 14 subjects and plotted on a surface. To quantify the spatial degree distribution, we plotted the average percentage of hubs for both hemispheres based on the degree (d), and on the betweenness centrality (e) for 26 anatomical areas. Each symbol and colour combination in all bar plots represents an individual percentage of hubs in that area.

Table 4

The abbreviations (Abbrev.) of the cortical areas used in this study and the mean number of nodes it covers (standard deviation, SD, in brackets).

Abbrev.	Cortical area	Mean number of nodes (SD)		Abbrev.	Cortical area	Mean number of nodes (SD)	
		Left	Right			Left	Right
SFG	Superior frontal gyrus	155.71 (22.68)	165.79 (20.29)	stTG	superior and transverse temporal gyrus	137.86 (17.66)	137.36 (19.61)
MFG	Middle frontal gyrus	182.50 (28.57)	182.14 (26.56)	MTG	Middle temporal gyrus	126 (17.07)	126.29 (18.45)
IFG	Inferior frontal gyrus	119 (17.10)	123.36 (16.54)	ITG	Inferior temporal gyrus	29.21 (4.81)	30.21 (4.85)
MedFG	Medial frontal gyrus	123.21 (21.45)	127.64 (21.87)	UNC	Uncus	16.21 (2.86)	13.93 (2.23)
PARACg	Paracentral lobule	19.36 (4.58)	24.50 (4.55)	MOTG	Medial occipito-temporal gyrus	41 (5.78)	40.93 (2.23)
PRCG	Precentral gyrus	109.64 (15.51)	110.71 (16.07)	PHG	Para-hippocampal gyrus	54.93 (8.19)	54.14 (7.76)
lmOFG	lateral and medial Orbital frontal gyrus	8.93 (1.64)	10.97 (2.70)	SOG	Suprior occipital gyrus	5.21 (1.25)	5.29 (1.27)
SPL	Superior parietal lobule	21.36 (4.56)	21.29 (4.45)	MOG	Middle occipital gyrus	66.14 (11.15)	67.36 (12.67)
IPL	Inferior parietal lobule	77.86 (11.31)	77.43 (13.51)	IOG	Inferior occipital gyrus	18.71 (2.61)	18.07 (3.32)
SMG	Supramarginal gyrus	20.64 (3.24)	22.21 (3.09)	CUN	Cuneus	79.93 (14.40)	81 (14.63)
ANG	Angular gyrus	9.57 (3.25)	11 (20.04)	LG	Lingual gyrus	59.79 (10.91)	58.57 (7.76)
PCU	Precuneus	104.43 (16.56)	102.71 (18.18)	CING	Cingulate areas	159.36 (26.02)	175.07 (22.42)
POCG	Postcentral gyrus	90.93 (11.54)	92.29 (14.90)	INS	Insula	59.29 (9.55)	60.14 (8.39)

Table 5

Hub regions found based on betweenness centrality and comparison to previous studies.

Area	av. % hubs	av.BC x10^{-4}	av. deg x10^{-3}	Other studies
CINGr	11.98	1.99	2.76	b2, c2
SFGr	11.76	1.8	2.75	a1, b1, b2, c1,c2, c3
SFGl	11.23	1.77	2.74	a1, b1, b2, c3
MFGl	10.41	2.19	2.74	a1, a2, b2
MFGr	9.89	1.84	2.73	a1, a2, b1, b2, c2
stTGl	9.18	2.05	2.74	a1, b2
CINGl	8.49	1.96	2.73	a2, c2
MidFGr	8.1	2.14	2.74	a1, a2, c2, c3
stTGr	7.7	1.93	2.74	a1, c1,b3
MidFGl	7.28	1.74	2.75	a1, a2, b2, c2, c3
IFGl	7.06	1.55	2.73	a1, a2, c1, c2, c3
IFGr	6.96	1.59	2.74	a1, c2, c3
MTGl	6.84	1.9	2.72	a1, a2, b2, c3
MTGr	6.5	1.94	2.75	a1, a2, b2, c1, c2, c3
PRcGl	4.78	1.48	2.74	a1, b2, c1, c2, c3
PRcGr	4.16	1.51	2.75	a1, b2, c1, c2, c3
INSl	4.06	1.75	2.73	b1
POcGl	3.9	2.42	2.73	a1, b2, c3
PCUr	3.81	1.52	2.75	a1, a2, b1, b2
PCUl	3.77	1.59	2.74	a1, a2, b1, b2

Av. denotes average, BC the betweenness centrality and deg. the degree. We compared our results to: *a1* Functional study: Achard et al. (2006), a2 Functional study: Buckner et al. (2009), *b1* DTI study: Gong et al. (2009), *b2* DTI study: Iturria-Medina et al. (2008), *c1* Morphological study: Chen et al. (2008), *c2* Morphological study: Bassett et al. (2008), *c3* Morphological study: He, Chen et al. (2007).

3.4.6 Reproducibility of the measures

Finally, the robustness of the method was assessed by comparing the network metrics within individuals at two time points (plotted in Figure 7). The number of nodes was highly stable (ICC = 0.98, p = 3.48 x 10^{-11}, Figure 7a), as was the mean degree (ICC = 0.92, p = 2.11 x 10^{-7}, Figure 7b) and the betweenness centrality (ICC = 0.98, p = 4.97 x 10^{-9}, Figure 7f). The mean path length (ICC = 0.77, p = 2.47 x 10^{-4}, Figure 7c), mean clustering coefficient (ICC = 0.59, p = 8.33 x 10^{-3}, Figure 7d) and the small world property (ICC = 0.60, p = 0.007, Figure 7e) were also reproducible, supporting the robustness of the method for the number of nodes, the mean degree and the betweenness centrality and demonstrating moderate reliability for the mean path length, mean clustering coefficient and the small world property. The reproducibility of the degree, average minimum path length and the betweenness coefficient might reflect their relationship with the number of nodes.
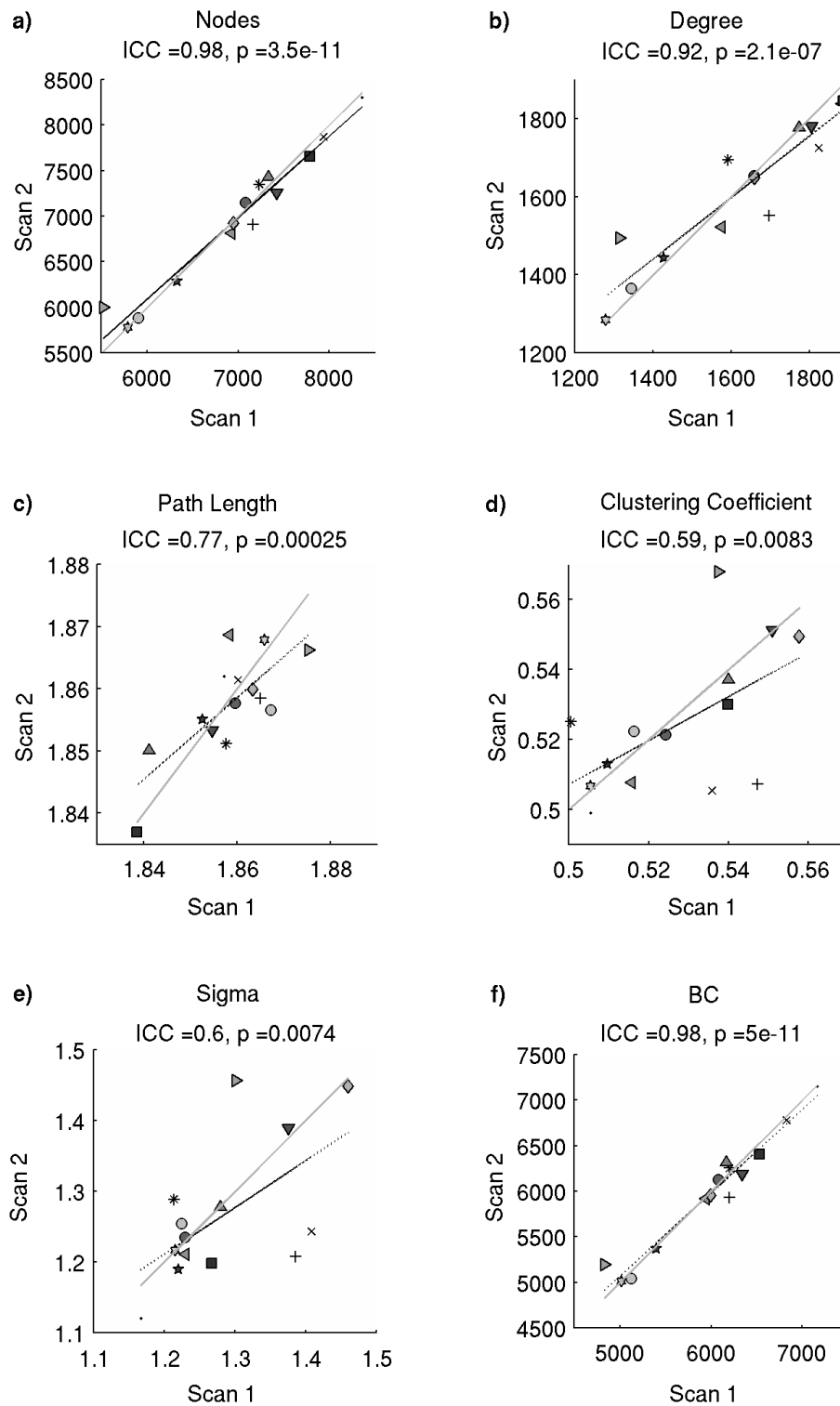
Figure 7. Reproducibility plotted for two scans of each subject, represented by an unique symbol and grey shade combination, for all the measures: a) the number of nodes, b) the mean degree, c) mean shortest path length, d) mean clustering coefficient, e) the small world property (sigma) and f) the betweenness centrality. The black line is fitted on the data, the grey line is the identity line which represent a perfect fit. The value of the intraclass correlation coefficient is indicated above each plot, with its corresponding p-value. All the measures were reproducible for a $p < 0.05$, indicating that the method is robust.

3.5 Conclusions

This Chapter presented a new method to statistically describe grey matter from individual T1-weighted MRI scans. The method was used to construct networks for individual cortices, where the nodes represented small three-dimensional areas that were connected by computing intracortical similarities in grey matter morphology. With the use of simple statistics from graph theory all networks were characterised as being 'small world', because they had a higher clustering coefficient and a similar minimum path length in comparison with random networks. All individual networks showed inter-subject variability that was most evident in the spatial distributions of the degree values. All network property values were highly similar to a group derived morphological network (Hänggi et al., 2011) and two resting-state functional MRI networks that were of comparable size and sparsity (van den Heuvel et al., 2008; Fornito et al., 2010). The values of the clustering and small world coefficients were also similar to other morphological networks measured at a comparable sparsity level (He et al., 2007; 2008; Bassett et al., 2008; Sanabria-Diaz et al., 2010; Yao et al. 2010). However, in comparison with the other functional (Eguíluz et al., 2005; Zhang et al., 2009; Hayasaka and Laurienti, 2010; Zhang et al., 2010) and white matter MRI studies (Hagmann et al., 2007; Zalesky et al., 2010), all the property values (apart from the clustering coefficient) were lower in the present networks. Finally, the graph theoretical properties were reproducible, supporting the robustness of the method. This Section will briefly discuss explanations for the spatial distribution of the hubs that was found, followed by methodological issues concerning this specific project. A general discussion about the mechanisms underlying intracortical similarities and issues that apply to other work in this thesis can be found in Chapter 6.

3.5.1 Spatial distribution of hubs

The spatial distribution of hubs (nodes with a high degree) in the current networks showed a striking similarity with the spatial distribution of correlations in cortical thickness (Lerch et al., 2006). It is important to note that the pattern reported here reveals the spatial distribution of the degree values for each node within individuals, while the cortical thickness study computed correlations between

71

areas using observations from different people. Possibly, the similarity of grey matter morphology within an individual brain could contribute to cortical thickness covariances found in group data. In the present study, the hubs were mostly located along the cortical midline. This spatial distribution has a remarkable overlap with the default mode network of brain function (Raichle et al., 2001; Greicius et al., 2003; Franco et al., 2009), that includes dorsal medial frontal regions (BAs 8, 9, 10, and 32), superior and middle frontal gyri (BAs 8, 9, and 10), medial posterior cingulate (BAs 30 and 31), the precuneus (BA 7), paracentral lobule (BA 5), inferior parietal regions (BAs 40, 39, and 7), the angular gyri (BAs 19 and 39) and the inferior frontal cortices (BAs 10, 47). These regions have shown decreased activation during attention related tasks, but show tonic activation during rest. Recently, Greicius et al. (2009) found structural connections between some of these regions using diffusion tensor imaging, which also supports the idea that functional connectivity might reflect structural connectivity (see also Honey et al., 2009). The present networks showed similar network properties compared to two resting-state functional MRI network studies of similar size and sparsity (van den Heuvel et al., 2008; Fornito et al., 2010), further supporting the idea that there might be overlap between the organisation of intracortical similarities and functional correlations in the brain. It would be interesting to investigate how similarities in grey matter morphology might be related to functional coactivation within individuals.

3.5.2 Methodological issues specific for this study

The subjects were scanned twice within a six month period and the results indicated that network property values were stable over that period. This result was interpreted as an indication of the robustness of the method, since it was assumed that the structure of subjects' brains would be stable over such a period. However, some studies have shown that grey matter volume can change over time as a result of training or experience (Andrews et al., 1997; Draganski et al., 2004; Mechelli et al., 2004; Hyde et al., 2009; but also see Thomas et al., 2009). Even though the present study did not include any learning or training tasks, such effects still might have influenced the results. It would be interesting to investigate

whether the proposed method could find such subtle differences with a controlled experiment.

To conclude, networks based on intracortical similarities contain interesting information that shows a significantly different topological organisation than random networks. Furthermore, the network property values were comparable with those reported by previous network studies of structural and functional MRI. Therefore, even if intracortical similarities do not have a clear direct relationship with anatomical connectivity, the new method does provide a concise statistical description of the grey matter structure of individual cortices.

The main question of the second project of this thesis was whether this method will be more sensitive to subtle structural disruptions than traditional group based methods. This question was investigated by examining individual graphs extracted from a sample of people at high genetic risk for schizophrenia. The next Chapter will give an introduction to schizophrenia and an overview of results from structural high risk of schizophrenia studies, followed by Chapter 5 were networks from people at high genetic risk of schizophrenia were studied for the first time.

4. Cortical morphology and high risk of schizophrenia

This Chapter provides a literature review about schizophrenia and high risk of schizophrenia studies, to provide relevant background for the work that will be presented in the next Chapter, where structural MRI scans were analysed with the new method to compare people at high genetic risk for schizophrenia with people lacking such risk.

4.1 Introduction

"The visions are extremely vivid. Paving stones transform into demonic faces, shattering in front of my petrified eyes. When I am in contact with people, they can become grotesquely deformed, their skin peeling away to reveal decomposing inner muscles and organs. Buildings and rooms spin and weave and their walls close in as I look on, paralysed by fear. ... The voices either ramble in alien tongues or scream orders to carry out violent acts. They also persecute me by way of unwavering commentary and ridicule to deceive, derange, and force me into a world of crippling paranoia."

--Robert Bayley, a schizophrenia sufferer (Schizophrenia Bulletin, 1996).

Robert Bayley is one of the many sufferers of schizophrenia, a disorder that disrupts the lives of about 1% of the population (Jablensky et al., 1995). Patients can experience visual and auditory hallucinations (positive symptoms) or lack of emotion, speech or motivation (negative symptoms) (Harrison, 1999). Given the disabling nature of schizophrenia, it is important to understand its causes in order to develop interventions. Schizophrenia is regarded as a developmental disorder, as its onset often occurs during adolescence (Häfner et al., 1993). Also, as early as 1911, Rosanoff and Orr reported that schizophrenia contains a strong genetic component: depending on the degree of familial relationship (from first cousin to both parents affected with schizophrenia) people with relatives suffering from schizophrenia have a 1.6% to 36.6% increased risk of developing the illness themselves than people without family history of schizophrenia (McGue and Gottesman, 1989). However, monozygotic twin studies have signified the

importance of environmental influences, because even though monozygotic twins share a 100% of their DNA, the risk that twins of patients with schizophrenia develops the disease themselves is 'just' 44% (McGue and Gottesman, 1989; Vogeley et al., 2001; Cannon et al., 2002). The complex interaction of genes and environment seems to set up a subtle disturbance in the usual balance of functional activation patterns and structural connections, that might only require normal maturational events to lead on to psychosis during adolescence.

4.2. Theories of schizophrenia

The precise causes of schizophrenia are still unknown, but are thought to involve complex interactions of different factors. A hundred years ago, Bleuler coined the term 'schizophrenia', which is derived from ancient Greek and roughly translates as 'split-mind', referring to the fragmented thinking of patients with schizophrenia (see Moskowitz and Heim (2011) for an overview of the impact of Bleuler work over the last 100 years:). The idea of a split in the faculties of the mind formed the basis for subsequent theories of 'disconnectivity' that try to explain schizophrenia by a disruption of connectivity between brain areas. How this disconnectivity arises is at the core of many theories of schizophrenia. Two popular theories that focus on disconnectivity are the abnormal pruning theory (Feinberg, 1983) and the disconnectivity theory (Friston & Frith, 1995; Friston, 1998). Feinberg proposed in 1983 that disconnectivity between brain areas in schizophrenia might arise from abnormal synaptic pruning, when either too many, too few or the wrong synapses are deleted during adolescence. He thought that the prefrontal cortex (PFC) should be affected in particular, since this cortical region develops well into adolescence (Martin & Rubenstein, 2003; Sur et al., 2005; Dumontheil, Burgess & Blakemore, 2008; Sowell et al., 2003, 2004). Feinberg hypothesised that abnormal pruning leads to the development of abnormal connections between brain areas that subsequently give rise to schizophrenia.

This concept was further examined in the disconnectivity theory, which focuses on disturbed connectivity between the PFC and the rest of the brain. Friston and Frith (1995) emphasised that disturbances in connectivity mostly occur locally, as opposed to long-range connections. They posited that subtle abnormalities at the synapse level can lead to erroneous integration of functional

signals from other brain areas. For example, auditory hallucinations that some patients experience might be explained by a disruption between the frontal and the temporal cortices. This has led to most research focussing on such connections, although the parietal lobe has also been suggested to play an important part in schizophrenia (Torrey, 1997). It is important to note that the disconnectivity theory in schizophrenia is based on disruptions of functional MRI correlations that can occur without morphological disruptions.

Research focussing on the disconnectivity theory in schizophrenia has mostly studied functional and structural MRI separately. Whether and how disturbances in the morphology of the brain interact with disturbed function in schizophrenia is largely unknown and important to study. The new method proposed in Chapter 3 could contribute to this kind of research by studying morphological and functional methods within the same individuals. However, it is important to first study individual morphological networks in schizophrenia. Therefore the following Sections will give on overview abnormalities found in grey matter MRI in relation to high genetic risk of schizophrenia and established schizophrenia.

4.3 Grey matter findings in established schizophrenia

Since Johnstone et al. (1976) found that schizophrenia patients had enlarged lateral and third ventricles in computerised tomography (CT) scans, it was clear that schizophrenia has a strong biological component. This finding triggered an enormous cascade of brain imaging research on schizophrenia. The theories of schizophrenia discussed in the previous Section emphasise the local nature of neuronal network disturbances, that might be manifest in regional grey matter volume differences between patients and healthy controls. But before discussing what can go wrong, it is important to understand how the cortex usually develops.

During healthy development, grey matter volume follows an inverted U-shape of growth and decline. Prefrontal cortical volume peaks at approximately 11-12 years, after which grey matter volume decreases (Jernigan et al., 1991; Giedd et al., 1999; Sowell et al., 2003; Paus et al., 2005). Synaptic density follows the grey matter course of development. It has been hypothesised that during adolescence synaptic pruning peaks, possibly due to synaptic competition

(Weinberger et al., 1992; Sowell et al., 2003). The most replicated finding in imaging research, but also in post-mortem studies is the enlargement of third and lateral ventricles in schizophrenia patients (e.g., Johnstone et al., 1976; Weinberger 1979; Keshavan et al., 1997; Staal et al., 2000; but see also: DeLisi et al., 2006). Enlargement of ventricles could indicate loss of surrounding grey and/ or white matter. It is clear that grey matter volume is reduced in schizophrenia (e.g., Wright et al., 2000; Wood et al., 2001; Ho, 2007; for reviews and meta-analyses see for example: Shenton et al., 2001; Lawrie et al., 2007; Correll et al., 2010; Fusar-Poli et al., 2010; Jung et al., 2010), but it remains unclear whether these reductions are generalised or (multi-)focal. The precise locations where grey matter volume differs between healthy controls and schizophrenia patients is hard to establish, due to inconsistencies between studies in methods and subject samples (Lawrie & Abukmeil, 1998; DeLisi, 2008; Shenton et al., 2001).

Besides grey matter volume, differences between people with and without schizophrenia have also been reported in other grey matter descriptors such as cortical folding patterns and cortical thickness. Some studies measure cortical folding patterns with the gyrification index, which is the ratio of the entire contour of the brain to the superficially exposed contour of the brain (Zilles et al., 1988). A higher gyrification index signifies a more complex cortical folding pattern. Findings of gyrification patterns vary, as some studies include only first episode schizophrenia patients while other studies have more mixed samples. Some studies have reported an overall lower gyrification index (Kulynych et al., 1997; Penttila et al., 2008), while others have found an overall higher gyrification index (White et al., 2003; Falkai et al., 2007). Gender differences have also been reported with male first episode schizophrenia patients showing a higher gyrification index in the right superior frontal cortex than female patients (Narr et al., 2004). Other studies have reported a lower gyrification index in the left hemisphere in schizophrenia (Sallet et al., 2003 ;Harris, Yates et al., 2004 (first episode study); Jou et al., 2005). And one study by Wiegand et al. (2005) failed to find differences using a measure related to gyrification (cortical complexity).

Finally, cortical thickness also seems to be affected in established schizophrenia. Sowell et al. (2004) studied how cortical thickness changes over a time span of two years in healthy children aged 7-11 years. They found that

cortical thickness varies between 1.5 to 5.5 mm. Grey matter thinning is most prominent in prefrontal and parietal areas in children around 12-13 years old. These areas may be subject to the greatest change in brains of people at high risk that developed schizophrenia. Sowell et al. (2004) also found that left prefrontal cortical thinning was related to a better general verbal intellectual performance. Kuperberg et al. (2003) were the first to apply Fischl and Dale's (2000) method to measure cortical thickness in schizophrenia patients. Patients had on average a thinner prefrontal cortex than healthy controls. This finding was replicated in later studies (White et al., 2003; Nesvag et al., 2008). However, Narr et al. (2004) only found a thinner prefrontal cortex in patients after covarying for sex. A subsequent study by Narr et al. (2005) showed that female patients showed thinner cortex in the prefrontal poles. Venkatasubramanian et al. (2008) found that only the orbitofrontal cortex of schizophrenia patients was thinner. However, some studies failed to find differences in prefrontal cortical thickness between patients and healthy controls (Goghari et al., 2006, 2007).

To conclude, some findings in established schizophrenia are widely replicated (such as enlarged third ventricle, globally decreased grey matter and some focal structural differences), while other findings show inconsistencies. The search for morphological factors associated with schizophrenia is even harder in studies that investigate people who have an increased risk to developing schizophrenia because they have a first degree relative with the disease (also called 'genetic high risk'). Longitudinal studies to assess the developmental trajectory of schizophrenia, are difficult to do and therefore fewer in number. However, this type of research is crucial to gain more understanding of a developmental disorder like schizophrenia. The next Sections will review grey matter findings in genetic high risk studies so far, starting with an overview of grey matter findings in the Edinburgh High Risk study of Schizophrenia (EHRS, that will further analysed in the next Chapter).

4.5 The Edinburgh High Risk study of Schizophrenia

Schizophrenia is usually triggered during adolescence, when people are between 16-25 years of age (Häfner et al., 1993). During the earliest stages of the disease some structural abnormalities found in people with established schizophrenia are

not present, and this led to the neurodevelopmental hypothesis of schizophrenia (Murray and Lewis; 1987; Weinberger, 1987). In order to investigate the neurodevelopmental hypothesis, studies have been developed that focus on people at high genetic risk for the disease because they have relatives diagnosed with schizophrenia (McGue and Gottesman, 1989). When following these subjects for a period of time it is possible to map their development and compare individuals who remain well with those who become ill. Differences in imaging data between people at high risk who are healthy at the time of study and healthy controls are indicative of the genetic component for schizophrenia. Understanding the developmental course of schizophrenia is of importance to improve existing treatments, but also to establish intervention programs. With this objective, the Edinburgh High Risk study of Schizophrenia was initiated (Hodges et al., 1999). For this study, people were recruited who had two or more first degree relatives with schizophrenia (Hodges et al., 1999). They were at an age typical for onset of the disease (16 - 25 years, Häfner et al., 1993), and at the start of the study none of the high risk subjects was diagnosed with either psychotic symptoms or schizophrenia. In total 146 subjects and 36 healthy control subjects (without a family history of psychiatric disease) were followed for a period of 10 years, during which 17 individuals who had a baseline structural scan developed schizophrenia (Johnstone et al., 2005; Lawrie et al., 2007). During these 10 years, 5 structural MRI scans were taken at 2 year intervals. At baseline (i.e., the first round of scans) various differences between the high risk group and the healthy control group have been reported using region of interest analysis. People at high risk had smaller thalami and amygdala-hippocampal complex than healthy controls (Lawrie et al., 1999; 2001), an increased prefrontal gyrification index (i.e., an increase of folding complexity; Harris, et al., 2004) and less prefrontal grey matter volume (McIntosh et al., 2011). However, using voxel-based morphometry (VBM) differences between the healthy control group and the high risk group in the baseline scans have only been found after a small volume correction (Job et al., 2005) or after using additional information (McIntosh et al., 2006; 2007). Within individuals, VBM showed changes of grey matter volume between two time points (Lawrie et al., 2001; Lawrie et al., 2002; Job et al., 2006; McIntosh et al., 2011).

The differences that have been found in the EHRS between healthy controls and high risk subjects with region of interest approaches and with small volume corrections, suggest that structural differences at whole brain level are subtle. Additionally, in the EHRS, differences have been found at whole brain level when change of grey matter over two time points was studied. Possibly, these subtle structural disruptions might have been filtered out during warping procedures used by VBM. To further investigate structural differences associated with high genetic risk of schizophrenia, the next Section gives on overview of other such studies.

4.6 Other studies about genetic high risk of schizophrenia

Studies, other than the EHRS, that have investigated familial high risk of schizophrenia can be categorised into twin studies, including twins that are discordant for schizophrenia (Suddath et al., 1990; Baare et al., 2001; Cannon et al., 2002; van Haren et al., 2004; Hulshoff Pol, Schnack, Mandl et al., 2006; Borgwardt et al., 2010), studies that investigated offspring from patients with schizophrenia (Rajarethinam et al., 2004; Bhojraj et al., 2010), studies that investigated healthy parents from patients with schizophrenia (Lui et al., 2009) and finally people at high risk because they have first degree relatives (Vogeley et al., 2001; Keshavan et al., 2007; Cannon et al., 1998; Staal et al., 2000; Marcelis et al., 2003; Boos et al., 2007; Ho, 2007; Gogtay et al., 2003; Jou et al., 2005; DeLisi et al., 2006; Diwadkar et al., 2006; Goghari et al., 2006; McDonald et al., 2006; Falkai et al., 2007; Goghari et al., 2007; Honea et al., 2008; Chan et al., 2011). Here only the differences between unaffected relatives of schizophrenia patients and healthy controls are discussed because these are of most interest in high risk studies. None of these studies included longitudinal data and therefore no information exists about differences between people at high risk who later developed the illness. Although longitudinal studies do exist that focus on people at high *clinical* risk, these studies will not be discussed here because these people are considered to be in a 'prodromal' phase just before onset of the disease, and therefore they are not comparable to familial high risk studies where subjects at high risk are clinically healthy at baseline (clinical high risk refers to people who are experiencing symptoms of psychosis, not necessarily with a familial background of schizophrenia, see for example: Pantelis et al., 2003; Borgwardt et

al., 2008; Fusar-Poli, Broome et al., 2011; Fusar-Poli, Crossley et al., 2011. For reviews and meta-analyses see: Jung et al., 2009; Correll et al., 2010; Fusar-Poli, Borgwardt et al., 2010).

Using region of interest analysis, twin studies have reported that the twin discordant for schizophrenia has on average lower overall grey matter volume than the healthy co-twin (Baare et al., 2001; Haren et al., 2004), and also less grey matter volume in the frontal lobe (Baare et al., 2001). Voxel-Based morphometry twin studies have found that discordant twins have on average less grey matter volume than the unaffected twins in the left medial orbitofrontal gyrus (Hulshoff Pol et al., 2006), dorsolateral and polar prefrontal cortex, Broca's area, supplementary motor areas, inferior sensorimotor strip, Wernicke's area and temporal pole (surface based automated whole brain analyses: Cannon et al., 2002). Some studies have found that patients from dizygotic twins were more similar to discordant monozygotic twins while their unaffected sibling was more similar to healthy control twins (Hulshoff Pol et al., 2006). Borgwardt et al. (2010) found that both concordant and discordant twins had less grey matter volume than healthy control twins in medial and inferior frontal cortex, anterior cingulate, precentral gyrus, caudate, lingual gyrus and cerebellar regions. They also found in discordant twins that the patients had less grey matter volume in the insula, superior temporal gyrus, precentral gyrus, posterior cingulate and paracentral lobule than their healthy siblings. In addition, they did not find any differences in grey matter volume between unaffected co-twins and healthy control twins.

Two studies have performed region of interest analysis to investigate differences between the children of patients with schizophrenia and healthy controls (Rajarethinam et al., 2004; Bhojraj et al., 2010). Rajarethinam et al. (2004) found that the risk subjects had less grey matter in the superior temporal gyrus than healthy controls. Bhojraj et al. (2010) investigated regions that are involved in the default mode network (a functional network in which the regions involved show less activation during tasks and more activation during rest, see: Raichle et al., 2001) and found that offspring of parents with schizophrenia had less grey matter than healthy controls in the lateral temporal nuclei, right precuneus, right inferior parietal lobule and left posterior cingulate cortex.

81

Furthermore they found a correlation in grey matter volume within the offspring group between the right dorso-lateral prefrontal cortex and the right anterior cingulate cortex that was stronger than in the healthy control group.

One study that compared parents of schizophrenic patients with healthy controls found that the parents had less grey matter volume in the right insula extending to the right temporal lobe and the right parietal lobule (Lui et al., 2009). However, strictly speaking, these parents were unlikely to develop schizophrenia themselves, since they were past the onset age of the disease.

In studies that involved unaffected siblings of schizophrenic patients, some reported less overall grey matter volume in siblings when compared to controls (Cannon et al., 1998), but other studies failed to find such a difference (Staal et al., 2000; McDonald et al., 2006; Ho, 2007). Most studies have reported less grey matter volume in unaffected siblings when compared to healthy controls in the parietal (Gogtay et al., 2003; Ho, 2007), frontal and temporal lobes (Ho, 2007), right cingulate (Goghari et al. 2006), and the ventromedial and frontal pole (Rosso et al., 2010). However, a thicker cortex, increased grey matter volume and surface area in unaffected siblings has also been reported in the total left hemisphere, parahippocampal gyri and middle temporal gyri (Goghari et al., 2006). Furthermore, gyrification patterns have been found to be more complex in unaffected siblings in comparison with healthy controls in the first coronal slice anterior to the corpus callosum (Jou et al., 2005; Falkai et al., 2007). On the other hand, a decrease in gyrification complexity has been reported in a parietal-occipital slice in people who had more than one family member with schizophrenia when compared to subjects who had just one family member with the disease (Falkai et al., 2007). In addition, sulcal thickness of unaffected relatives was thinner than healthy controls in the inferior and superior temporal sulci, and a reversed asymmetry in the cingulate sulcus (Goghari et al., 2007).

Voxel-based morphometry studies have found differences at whole brain level in the dorsolateral prefrontal cortex, anterior cingulate, insula, superior and middle and inferior temporal gyri, the inferior frontal gyrus, precuneus (Diwadkar et al., 2006), the right fusiform gyrus (Marcelis et al., 2003) and cerebellum (Diwadkar et al., 2006; Marcelis et al., 2003). Furthermore, Marcelis et al. (2003) reported that unaffected relatives had more grey matter in the left superior frontal

gyrus than healthy controls. However, Honea et al. (2008) failed to find differences between unaffected siblings and healthy controls.

To conclude, differences in grey matter structure have been found in relatives of schizophrenia patients when compared to healthy controls, however, some studies did not find such differences. Furthermore, a variety of regions has been reported to be involved, and of all studies just three have compared groups using analysis that did not involve a priori defined region of interest. Two of these studies failed to find differences at whole brain level (Job et al., 2003; Honea et al., 2008). Therefore it can be concluded that grey matter disturbances in healthy people at high genetic risk for schizophrenia are subtle.

The work in the next Chapter investigated whether the method presented in Chapter 3 was more sensitive to such subtle disruptions than traditional voxel-based methods in the EHRS sample. Also, the next Chapter will be the first study to describe network properties in people at high genetic risk of schizophrenia.

5. Study II: Investigating network properties of networks based on intracortical similarities extracted from individuals at high genetic risk of schizophrenia

The work in this Chapter is the first study to investigate individual morphological networks in a sample of people at high genetic risk of schizophrenia before manifestation of the illness.

5.1 Introduction

The disconnectivity theory of schizophrenia (e.g., Friston and Frith, 1995) has recently been investigated in MRI data with tools from graph theory (Basset al., 2008; Liu et al., 2008; Alexander-Bloch et al., 2010; Lynall et al., 2010; van den Heuvel et al., 2010; Wang et al., 2010; Zalesky et al., 2010; Lord et al., 2011; Yu et al., 2011). These studies have found topological disturbances in networks of people with schizophrenia when compared to healthy subjects in grey matter (Basset al., 2008), white matter (van den Heuvel et al., 2010; Zalesky et al., 2010) and functional MRI (Liu et al., 2008; Alexander-Bloch et al., 2010; Wang et al., 2010; Lynall et al., 2010; Lord et al., 2011; Yu et al., 2011). None of these studies included people at high genetic risk of the disease, and therefore it remains unknown whether topological disturbances are present before illness onset.

In this Chapter the topology of individual morphological networks from the Edinburgh High Risk study of Schizophrenia (EHRS) was investigated for the first time. Previously, focal differences have been reported in the EHRS using region of interest approaches and small volume corrections (Lawrie et al., 2001; Lawrie et al., 2002; Harris, Whalley et al., 2004; Job et al., 2005; Job et al., 2006; McIntosh et al., 2011), however, differences at whole brain level in the first round of scans when all subjects were clinically healthy have not been found. Therefore it was investigated here whether the new method would be more sensitive to subtle disruptions in brain structure than traditional group based methods.

Before this important question was studied, the method was first further validated by comparing the graph property values from the current healthy control group

with those from the Calibrain study (Chapter 3). Furthermore, network property values were studied within the high risk sample in relation to disease outcome.

5.2 Methods

Individual grey matter networks were extracted from the first round of scans of the EHRS using the same cube-size as discussed in Chapter 3 (i.e., 3 x 3 x 3 voxels of 2 x 2 x 2 mm^3). For details concerning this method the reader is referred to Chapter 3 (Section 3.2). In the following Sections methodological details specific to the current sample will be explained.

5.2.1 Subjects

The data used here was previously collected for the Edinburgh High Risk study of Schizophrenia (Hodges et al., 1999; Johnstone et al., 2000; 2005), in which 181 participants had undergone a structural scan at baseline. This sample consisted of 36 healthy controls (19 female, mean age = 21.17, SD = 2.37), who had no family history of psychiatric illness and 146 participants who had an increased genetic risk to develop schizophrenia and without a personal history of psychiatric illness. The high risk participants were identified throughout Scotland on the basis that they had at least two first- or second-degree relatives affected with schizophrenia (Hodges et al., 1999). At the start of the study all participants were clinically healthy. Seventeen of the high risk subjects developed schizophrenia during the study (6 female, mean age = 20.22, SD = 2.66). Of the people who remained well 57 subjects experienced psychotic symptoms at some point during the study (32 female, mean age = 21.20, SD = 3.05), and 72 participants never experienced psychotic symptoms (34 female, mean age = 21.52, SD = 2.88). Three participants were excluded because their segmentations did not contain enough anatomical detail due to failure of segmentation (n = 1), overestimation (n = 2) or underestimation (n = 1) of grey matter, rendering them unsuitable for morphological network extraction (all males, three from the high risk with symptoms and one from the healthy controls). The groups did not differ in their gender distribution ($\chi^2(3) = 3.69$, $p = 0.16$).

5.2.2 Acquisition and preprocessing of the images

The current study used structural T1 weighted MRI scans that were previously described in Job et al. (2003). Briefly, scanning was performed in a 1 Tesla 42 SPE Siemens (Erlangen, Germany) Magneton scanner. T1 weighted scans were acquired using a 3D magnetisation prepared rapid acquisition gradient echo (MPRAGE) sequence consisting of a 180° inversion pulse followed by a fast low angle shot (FLASH) collection (flip angle 12°, TR = 10 ms, TE = 4 ms, TI = 200 ms and relaxation delay time 500 ms, field of view 250 mm x 250 mm) to give 128 contiguous 'slices' of 1.88 mm thickness. Next the scans were preprocessed with Statistical Parameter Mapping software version 99 (SPM99, http://www.fil.ion.ucl.ac.uk/spm/spm99.html) running in MATLAB version 5.3 (The Mathworks, Natick, MA, USA) and using a study specific template as described in Job et al. (2003). The resulting grey matter segmentations in native space were used in this study to extract individual networks.

5.2.3 Statistical analyses

Networks were extracted as described in detail in Chapter 3. The binarised networks contained on average 6901 nodes (SD = 667). For each network, 20 random networks were created, and the following metrics were computed in Matlab: the sparsity, the average degree, the clustering coefficient and its ratio with an average clustering coefficient from 20 random networks (γ), the average minimum path length and its ratio with an average minimum path length from 20 random networks (λ), and the small world coefficient. The betweenness coefficient was omitted from the current analysis, because it was strongly correlated with the average degree (r = 0.95) in Chapter 3. Nodes were identified as hubs when they had a degree value higher than one standard deviation above the networks mean degree.

In Table 6 it can be seen that the network property values were significantly different from a normal distribution and therefore for all subsequent comparisons, non-parametric tests were used. The network property values of the healthy control group were compared using two-sample Mann-Whitney U tests with those from the Calibrain study (Chapter 3) to further validate the new method. Next, it was investigated whether the high risk and healthy groups

differed in the distribution of the network property values using two sample t-tests, with a Welch modification to the degrees of freedom when the variance was not equal between the groups. These analyses were repeated to compare subgroups within the high risk group (people who remained well throughout the study, people who experienced symptoms at some point during the study and people who later became ill) with ANOVAs instead of t-tests. The intercorrelations between the network property values were compared between the groups with Z tests, after performing a Fisher transformation on the correlation coefficients ($Z = \frac{1}{2}ln\frac{1+r}{1-r}$, Z is the transformed variable and r the correlation coefficient to be compared, see: Fisher, 1921). Because at multiple statistical tests were performed for all group comparisons, the p-value was corrected for multiple comparisons with the false discovery rate (Benjamini and Hochberg, 1995). All statistical analyses were implemented and performed in R version 2.12.1.

Table 6

Anderson-Darling test for normality of the distribution of graph property values

Property	Group			
	HC	HR well	HR symp	HR ill
size	0.86*	1.10**	0.52	0.66
degree	0.86*	0.62	0.67	0.26
L	0.97*	1.25**	0.30	1.02**
C	0.59	1.15**	0.71	0.32
σ	0.27	0.87*	0.995*	0.60
BC	-	-	-	-
S	0.53	1.46***	0.83*	0.60

Significance levels Anderson-Darling test: *** = $p < 0.001$,** = $p < 0.01$, * = $p < 0.05$
HC is the healthy control group, *HR well* is subgroup from the EHRS that remained well, *HR symp* is subgroup from the EHRS that acquired symptoms, HR ill is subgroup of EHRS that became ill, *L* is average path length, *C* is the average clustering coefficient, σ is the small world coefficient, *BC* is the betweenness coefficient, *S* is sparsity level.

5.3 Results

In this Section the results from the planned comparisons are discussed first, followed by exploratory analyses that were performed to study the clinical value of the network properties. The exploratory analyses investigated whether differences in the spatial distribution of the network hubs (i.e, nodes with a degree value higher than one standard deviation above the networks mean) could be predictive of group membership.

5.3.1 Comparing graph properties of the current healthy sample and the Calibrain sample

Figure 8 displays the distributions of the graph property values that were compared between the Calibrain sample from the study of Chapter 3 and the current healthy control sample. The networks from the Calibrain sample were of similar size as the current sample (U = 217, Z = -0.62, p_{FDR} = 0.54; Figure 7a), and so any other differences between these groups cannot be explained in terms of network size.

Using the same approach to determine the threshold of the networks led to significantly sparser networks in the current healthy sample (15%) than in the Calibrain sample (23%, U = 0, Z = -5.42, p_{FDR} = 1.07 x 10^{-7}; Figure 7b). Possibly the decrease in intracortical similarities in the current sample might be caused by additional noise to the data caused by the lower scanner strength that was used to acquire the MRI scans (1T instead of the 1.5T in the Calibrain sample). Scanner noise was quantified by calculating the signal-to-noise ratio (SNR. Computed for each slice containing grey matter as: = 0.66 * mean(grey matter) / standard deviation (background); Kaufman et al., 1989; Dietrich et al., 1997). However, possibly due to the use of a phantom to increase segmentation accuracy in the EHRS sample, the SNR was *better* for the EHRS sample (U = 466, p_{FDR} = 1.15 x10^{-6}; Figure 8h). Alternatively, the addition of edges in the Calibrain sample might be explained by a difference in variability in the cubes: If cubes vary less in their grey matter structure, then they might show more similarities. This was confirmed with a Mann Witney U test (U = 490, Z = 5.42, p_{FDR}= 1.07 x 10^{-7}; see Figure 8g), and might explain other differences between the groups in graph property values.

89

The average degree and clustering coefficient were also significantly higher in the Calibrain sample than the current healthy sample (respectively: U = 8, Z = -5.25, p_{FDR} = 2.08 x 10^{-7}; U = 1, Z = -5.40, p_{FDR} = 1.07 x 10^{-7}; Figure 7c and 7d), this might be explained by the high positive correlation between these properties and sparsity (see: Table 2 and Table 6). The average minimum path length was significantly lower in the Calibrain sample than in the current healthy control sample (U = 490, Z = 5.42, p_{FDR} = 1.07 x 10^{-7}; Figure 7e). Finally the Calibrain sample showed a significantly lower small world coefficient than the current healthy control sample (U = 490, Z = 5.42, p_{FDR} = 1.07 x 10^{-7}; Figure 7f).

Figure 9 shows the distribution of the degrees from 14 randomly sampled individual subjects of the EHRS healthy controls, and the group average. The spatial degree distribution shows a higher contrast than can be seen in Figure 6 of Chapter 3, because the EHRS networks were sparser than the Calibrain networks. Interestingly, the spatial distributions of nodes that show a relatively high degree, the hubs, are qualitatively similar to in those in Figure 6. This was confirmed by a strong correlation of the number of hubs in anatomical areas between the two studies (left hemisphere: ϱ = 0.97, p = 4.39 x 10^{-7}; right hemisphere: ϱ = 0.97, p = 3.42 x 10^{-7}). In addition, the interrelationships between the network property values were similar between the groups (see Table 7 and Table 2. Range of absolute Z values: 0.06 - 2.02; range of p_{FDR}-values: 0.53 - 0.95), suggesting that these interrelationships are a stable property of morphological networks based on intracortical similarities.
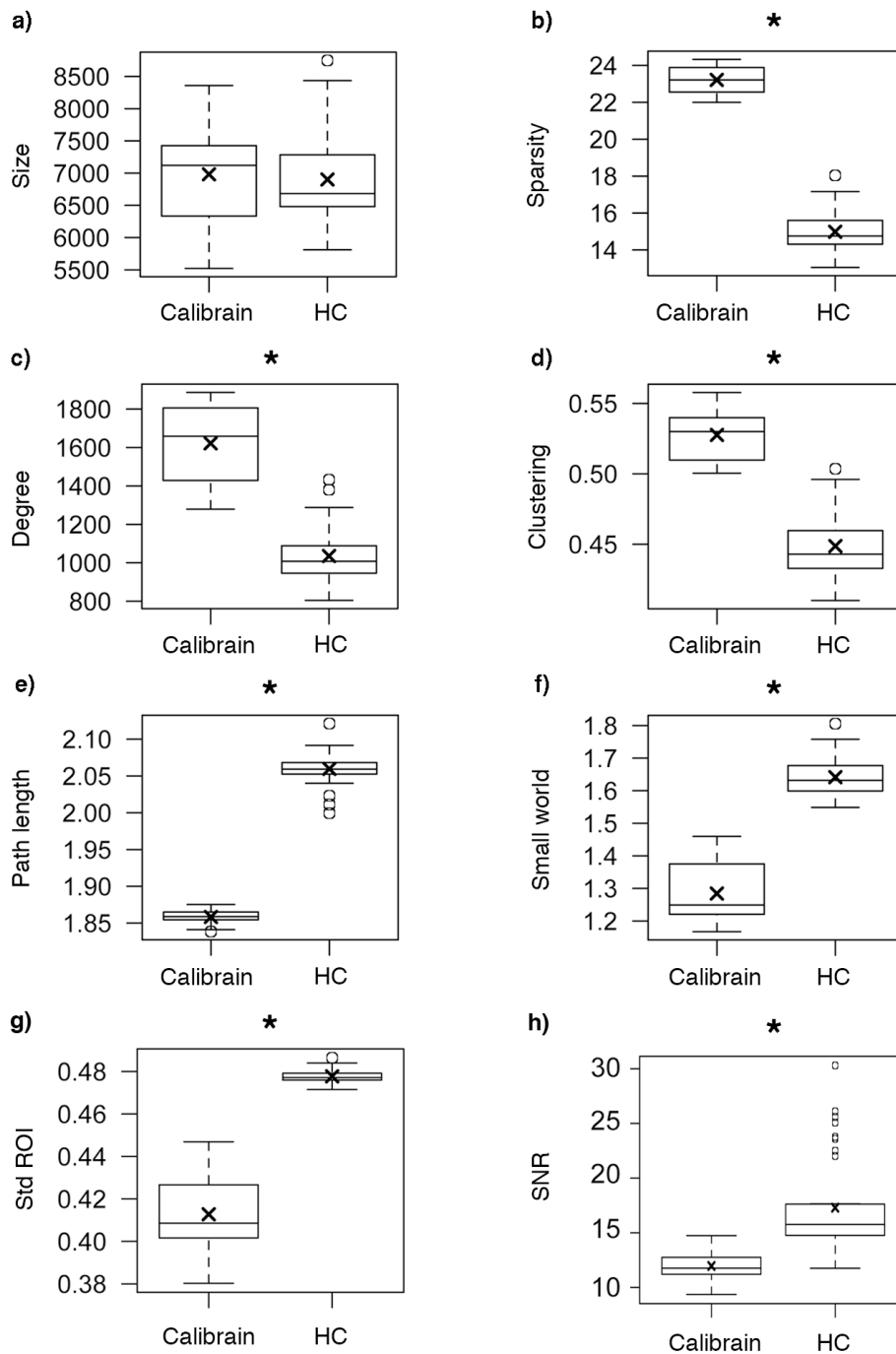
Figure 8. Comparison between the Calibrain sample of Chapter 3 and the current healthy control sample (HC) of a) size, b) sparsity, c) degree, d) average clustering coefficient, e) average minimum path length, f) small world coefficient, g) variability in the ROIs and h) the SNR of the scans. The middle horizontal line in the boxes indicates the median value, the cross the mean value, the bottom and top of the boxes indicate the 25th and 75th percentiles, the circles outside the whiskers indicate outliers and the asterisk indicates a significant difference between the means of these distributions ($p_{FDR} < 0.01$).

Table 7

Pairwise Spearman's rank correlations between the values of the graph properties computed across the healthy subjects (HC) at baseline compared to correlations in the high risk sample (HR)

	V		L		C		σ		S	
	HC	HR	HC	HR	HC	HR	HC	HR	HC	HR
d	0.86***	0.84***	-0.32	-0.1	0.68***	0.50***	0.70***	0.57***	0.63***	0.43***
V	1	1	-0.27	-0.1	0.28	0.04	0.44**	0.37***	0.19	-0.05
L			1	1	-0.21	0.14	-0.11 †	0.45*** †	-0.28	-0.03
C					1	1	0.79***	0.61***	0.98***	0.96***
σ							1	1	0.75***	0.44***
S									1	1

Significance levels Spearman's ρ: *** $= p < 0.001$, ** $= p < 0.01$, * $= p < 0.05$. Significance level of the Z test: † $= p_{FDR} < 0.05$ (two-tailed).

d is the degree, V the number of nodes (network size), L is the minimum path length, C the clustering coefficient, σ the small world coefficient, S is the sparsity, HC is healthy control subgroup, HR is high risk sample.
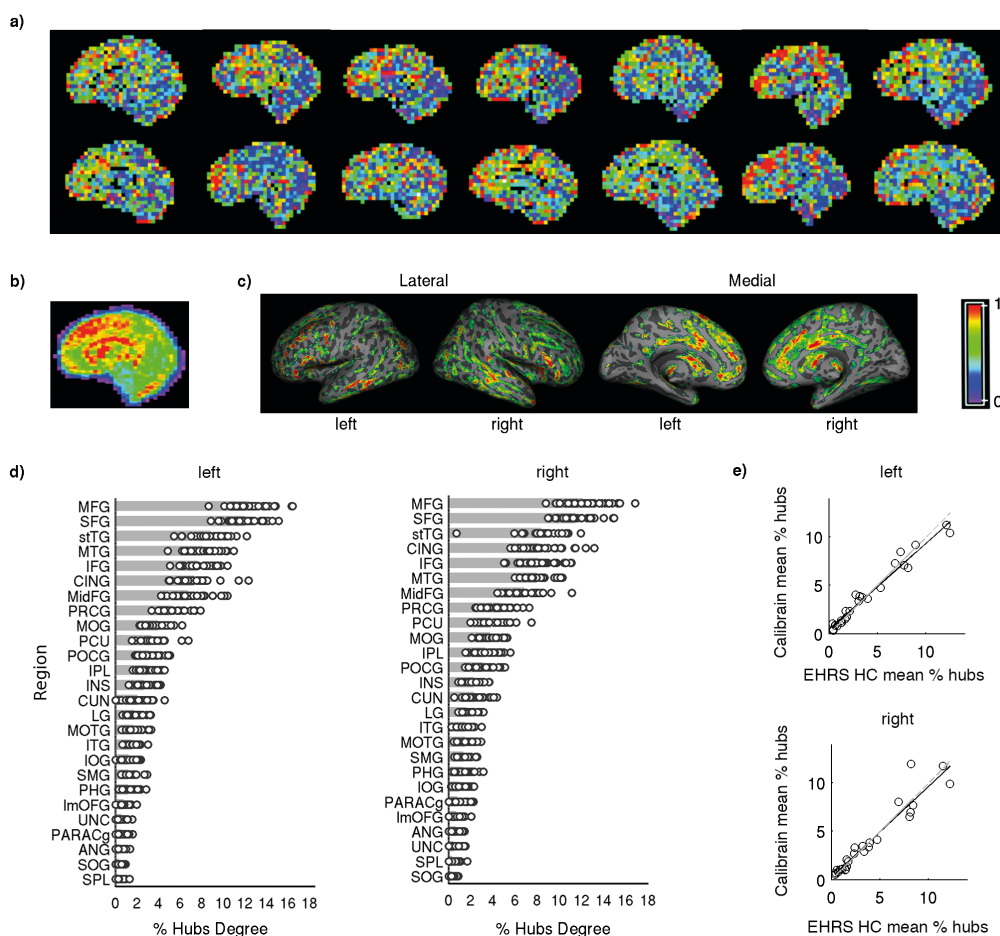
Figure 9. a) A plot of the degree of all cubes for one slice (right medial hemisphere) from 14 randomly chosen individual subjects of the healthy EHRS sample. The degrees were standardised by their maximal value. Warmer colours indicate that a cube has more structural similarities with other cubes in the brain than cubes with cooler colours. b) Shows the group average across 35 subjects of the degree patterns after warping to standard MNI space, which supports that most subjects have hubs along the right medial surface of the brain. c) Shows the spatial distribution of hubs (nodes with a degree higher than one standard deviation above the mean) averaged over all 35 subjects and plotted on a surface. To quantify the spatial degree distribution, the average percentage of hubs was plotted for both hemispheres based on the degree (d). (e) shows the high correspondence of the % of hubs for all anatomical areas in the left and right hemisphere between the EHRS and the Calibrain sample from Chapter 3.

5.3.2 Comparing graph properties between people with and without increased risk of schizophrenia

No differences were found between the healthy and high risk group in any of the network properties, suggesting that the overall organisation of the intracortical similarities is not disrupted in people at high generic risk of schizophrenia (Figure 10).
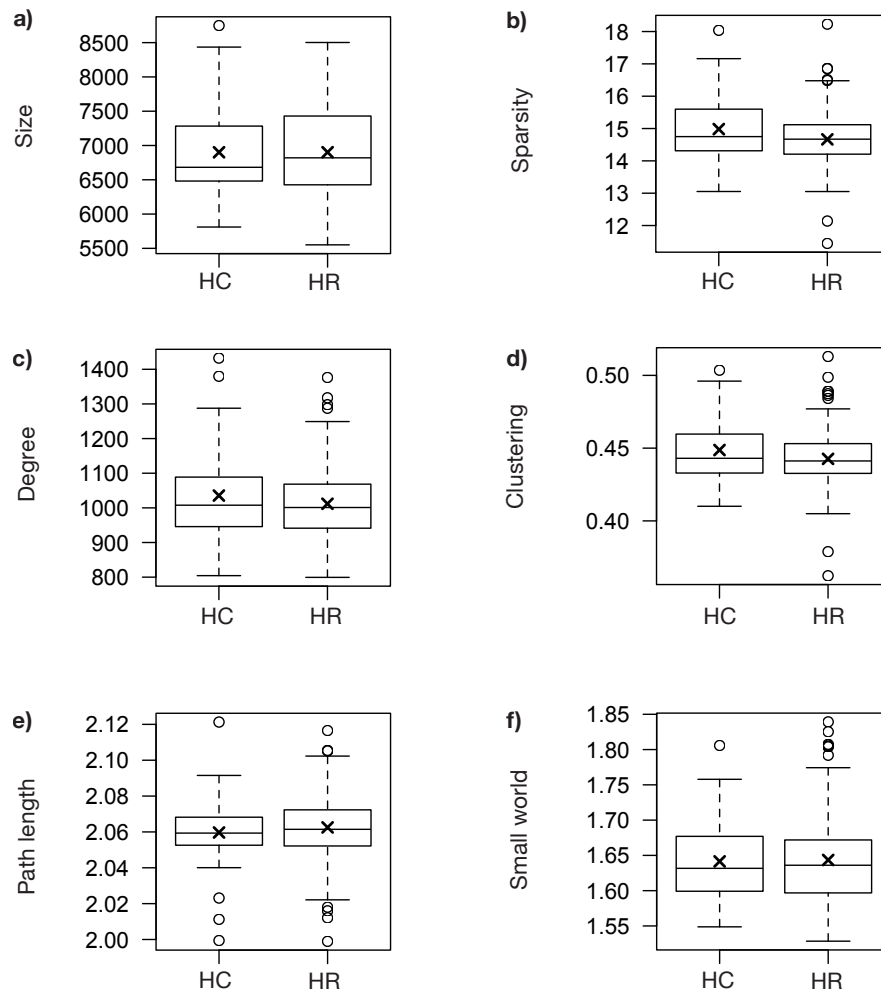
Figure 10. The distributions of a) size, b) sparsity, c) degree,d) clustering coefficient, e) minimum path length and f) the small world coefficient in the healthy control (HC) and high risk (HR) samples. The middle horizontal line in the boxes indicates the median value, the cross the mean value, the bottom and top of the boxes indicate the 25th and 75th percentiles, and the circles outside the whiskers are outliers. None of the distributions showed significant differences between the two groups.

5.3.3 Comparing correlation patterns of graph theoretical properties between people with and without increased risk of schizophrenia

Network properties have been reported to be interrelated (e.g., He, Chen, et al. 2007; Bassett et al. 2008, 2010; He et al. 2008; Fornito et al. 2010; van Wijk et al. 2010; Zalesky et al. 2010; Tijms et al., 2011). Here it was studied with separate Z tests whether the correlations summarised in Table 7 would differ between the high risk and healthy control groups (after a Fisher transformation of the correlation values). As can be seen in Figure 11, the high risk group showed a significant positive relationship between the average minimum path length and the small world property ($\varrho = 0.45$, $p = 2.19 \times 10^{-8}$) that was significantly different from the healthy control group ($\varrho = -0.11$, $p = 0.54$); $Z = 3..03$, $p_{FDR} = 0.04$). This correlation was unexpected, because the small world coefficient requires the division of the average minimum path length by the random path length to be around one and therefore should not be related to the small world coefficient. On the other hand, the small world property by itself does not give detailed information about the connectivity topology, and therefore it is possible that in the high risk group a larger path length is needed to achieve a similar small world property as the healthy control group. However, the difference in correlation might also be explained by the difference in sample size.

Table 8

Pairwise Spearman's rank correlation values between graph properties over subjects in three subgroups of the high risk group: no-symptoms (NS), symptoms (S) and ill (I).

	V			L			C			σ			S		
	NS	S	I	NS	S	I	NS	S	I	NS	S	I	NS	S	I
d	0.85***	0.84***	0.83***	-0.04	-0.10	-0.37	0.51***	0.44***	-0.08	0.62***	0.57***	-0.10	0.41***	0.40**	-0.18
V	1	1	1	0.03	-0.10	-0.59*	0.08	-0.01	-0.52*	0.52*** †	0.34*	-0.41 †	-0.05	-0.08	-0.63**
L				1	1	1	-0.05 †	0.25	0.74** †	0.40***	0.42***	0.83***	-0.22 †	0.10	0.59* †
C							1	1	1	0.50***	0.66***	0.87***	0.95***	0.96***	0.91***
σ										1	1	1	0.30*	0.51***	0.79***
S													1	1	1

Significance levels Spearman's ρ: *** = $p < 0.001$, ** = $p < 0.01$, ** = $p < 0.05$*.

Significance levels Z test: pairs that show differences at $p_{FDR} < 0.05$ (two-tailed) are indicated with †.

d is the degree, V the number of nodes (network size), L is the minimum path length, C the clustering coefficient, σ the small world coefficient and s the sparsity.

Correlation of degree - degree is omitted for space reasons.
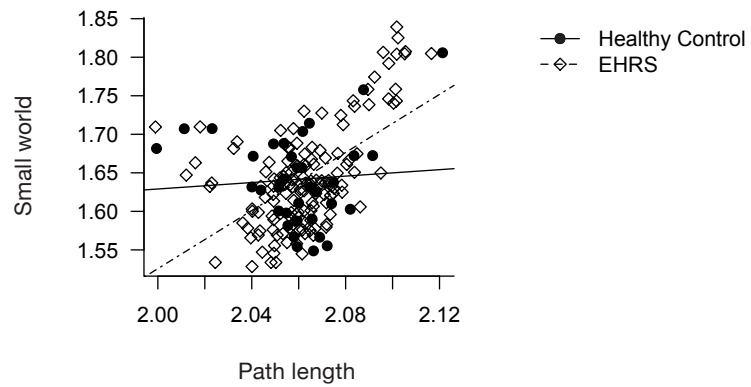
Figure 11. Scatterplot of the small world coefficient values and the average minimum path length. The high risk group (EHRS) showed a positive relationship between these two variables (diamonds, dashed regression line) but the healthy control group did not (circle, solid regression line).

5.3.4 Comparing graph properties within the high risk sample

Here, it was investigated whether there were any differences in network properties within the high risk sample that were related to disease outcome: people who never experienced symptoms (n = 72), people who at some point during the study experienced symptoms (n = 54) and people who were later diagnosed with schizophrenia (n =17). The groups were compared using non-parametric Kruskal Wallis tests, which do not require normality of the data and are robust to outliers.

Figure 12 contains box plots of the network property distributions in the three subgroups. The groups showed significant differences in the median network sparsity (Kruskal-Wallis $\chi^2(2)$ = 8.95, p_{FDR} = 0.03; Figure 12b), median degree (Kruskal-Wallis $\chi^2(2)$ = 10.94, p_{FDR} = 0.03; Figure 12c) and median clustering coefficient (Kruskal-Wallis $\chi^2(2)$ = 7.43, p_{FDR} = 0.048; Figure 12d).

Post-hoc tests indicated that only the no-symptom and ill subgroups differed significantly: (median sparsity of the ill group: 15.15%; 95% confidence interval: 14.77% - 15.32%; median sparsity of the no symptom group:14.51%; 95% confidence interval: 14.06% - 14.89%; difference in degree means = 78.92, 95% family-wise confidence interval = 9.50 - 148.34, p_{FDR} = 0.02; difference in clustering coefficient means = 0.01, 95% family-wise confidence interval = 0.0012 - 0.03, p_{FDR} = 0.03). Even though each individual network in each group had the same chance to include 5% spurious connections in their networks, the high risk group who later became ill showed more intracortical similarities, a higher degree and more clustering than the high risk without symptoms group.

To explore the origin of the increase of similarities, it was tested whether the groups differed in the variability of the grey matter values in the cubes (computed as the standard deviation in the cubes, Figure 12g) and the signal-to-noise ratio (SNR) of the scans (SNR was computed for each slice containing grey matter as: = 0.66 * mean(grey matter) / standard deviation (background)), and then averaged over slices). The groups did not differ in either variability of grey matter in the cubes, nor in the SNR of the scans.
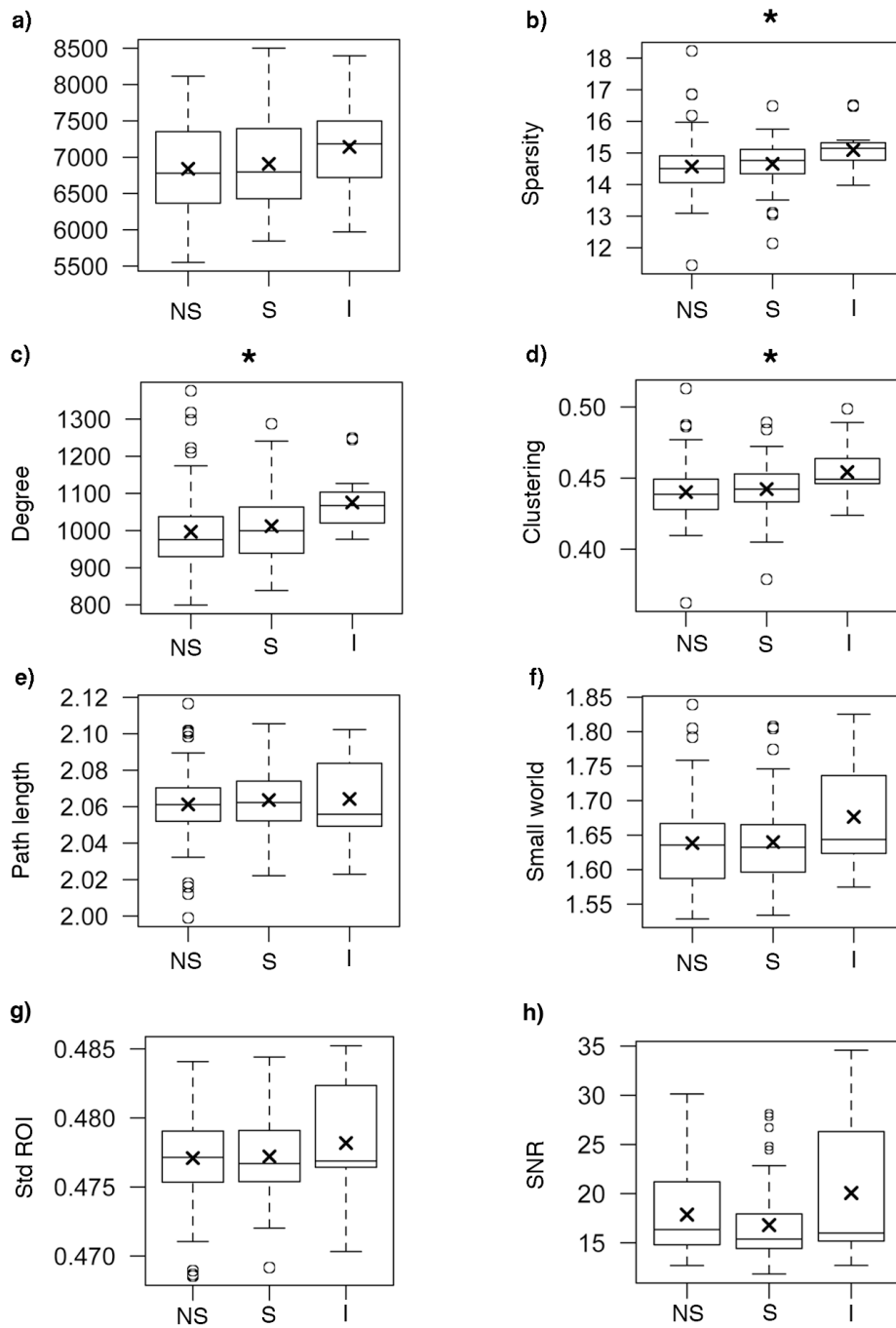
Figure 12. The distributions of a) size, b) sparsity, c) degree,d) clustering coefficient, e) minimum path length, f) the small world coefficient, g) variability in the ROIs and h) the SNR in the no-symptom (NS), symptom (S) and ill (I) high risk subgroups. The middle horizontal line in the boxes indicates the median value, the cross the mean value, the bottom and top of the boxes indicates the 25th and 75th percentiles, and the circles outside the whiskers indicate outliers. The asterisk indicates significant differences between the ill and no-symptom groups with $p_{FDR} < 0.05$.

5.3.5 Differences in graph theoretical property interrelationships between the high risk subgroups

Here it was investigated whether the high risk subgroups differed in their network property correlation patterns (see Table 8). No differences were found in correlation values between the symptom group and the other two groups. Possibly this might reflect that the symptom group represents a transient group between being well and becoming ill.

The well and ill subgroups showed differences in three correlation values: between the average path length and sparsity ($Z = -3.06$, $p_{FDR} = 0.01$), average path length and clustering ($Z = -3.39$, $p_{FDR} = 0.005$), and between the network size and the small world value ($Z = 3.45$, $p_{FDR} = 0.005$).

The ill subgroup showed a positive correlation between sparsity and the average minimum path length ($\varrho = 0.59$, $p = 0.01$), that was absent in the well group ($\varrho = -0.22$, $p = 0.07$). Such a relationship might occur when networks contain smaller clusters, that are densely interconnected but show less dense connectivity between the clusters. When clusters are less efficiently connected, this would lead to an increase in average minimum path length. This explanation was supported by the positive relationship between average path length and clustering coefficient that was only found in the ill group (Figure 13b; $\varrho = 0.74$, $p = 0.001$). Furthermore, only the well group showed a positive relationship between the small world coefficient and network size ($\varrho = 0.52$, $p = 2.5 \times 10^{-6}$).

Finally, the positive relationship between the average minimum path length and the small world coefficient was found in all high risk subgroups.
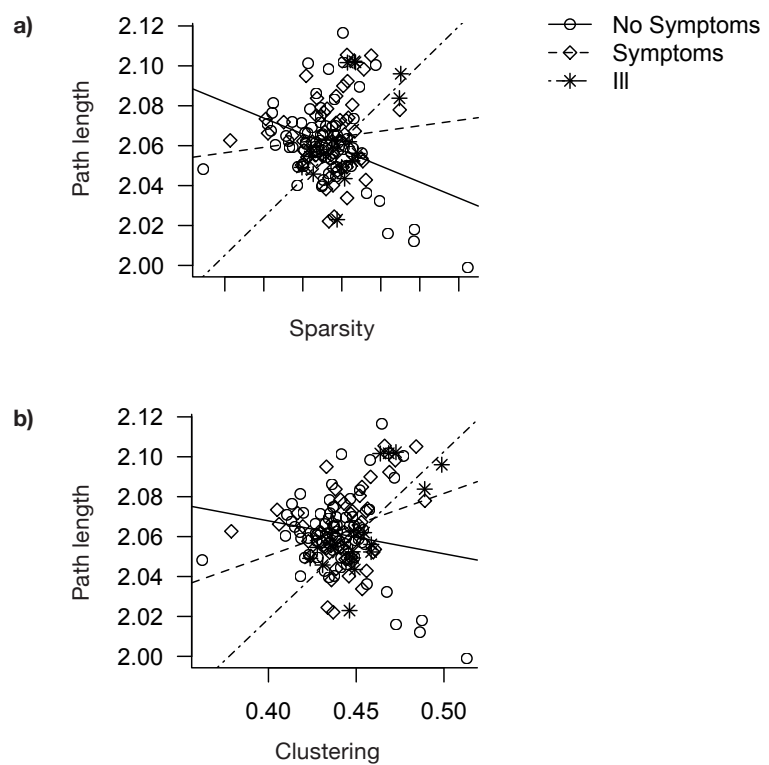
Figure 13. Scatterplots of a) average minimum path length and sparsity, b) average minimum path length and the clustering coefficient for the no-symptom (open circles and a solid line), symptom (open diamonds and a dashed line) and ill subgroups (asterisks with a dot-dashed line).

5.3.6 Exploratory analyses: classification of group membership

The diagnostic value of the method was explored by testing whether group membership could be predicted from differences in the spatial distribution of degree hubs. The exploratory analyses will be explained first, followed by the results.

Because each node of the individual networks can be characterised with a degree value, it was necessary to reduce the dimensionality of the data set (i.e., 'large p, small n'-problem; see: Green, 1991; Peduzzi et al., 1995; 1996; Babyak, 2004). This was done by computing the number of degree hubs for specific anatomical areas, reducing an average of 6901 variables to 52. The anatomical areas were extracted from the networks with an anatomical mask, that was constructed using the WFU Pickatlas tool within SPM5 as described in Chapter 3 (see: Table 4). The number of hubs from every anatomical area was used as a predictor variable in a logistic regression model to predict group membership for each hemisphere separately (26 variables per hemisphere). Three global network properties (sparsity, average degree and average clustering coefficient) were included as covariates. Because the smallest group contained 17 subjects, it was necessary to further reduce the dimensionality of the dataset to avoid overfitting. This was achieved with automatic variable selection with random forests for logistic regression (Prinzie and van den Poel, 2008). A random forest is a classifier model that is built from randomly constructed prediction models (in this case logistic regression models). A random forest is robust to overfitting because it estimates models from different bootstrap samples of the data, using randomly sampled predictor variables (Breiman, 2001). A random forest can be used as a classifier for new observations by aggregating information from all the models combined by using e.g., majority voting (Breiman, 2001; Liaw and Wiener, 2002). It also gives a generalisation error, that is computed from the observations that were not used to estimate the regression models (i.e. the out-of-bag (OOB) data, see: Efron and Tibshirani, 1997). Furthermore, a random forest can also be used for automated variable selection, by randomly permuting the corresponding column in the OOB data for each variable and comparing the correctly classified percentage with that from the intact OOB data, resulting in an importance score. An importance score > 0 means that the variable is important, because the

percentage of correctly classified instances decreases in the randomised situation. An importance score of equal or lower than zero means that randomising the observations of this variable does not alter the classification accuracy and therefore is not important. Random forests have been widely and successfully used in classification research were there are many more predictor variables than observations (the so-called 'small n, large p problem'. See, e.g., in gene association studies: Braga-Neto et al., 2004; Huang et al., 2005; Diaz-Uriarte and Alvarez de Andres, 2006). Classification accuracy was further improved by sampling the same number of observations from every group (i.e., undersampling: see e.g., Burez and van den Poel, 2009). In a random forest two parameters need to be set: 1. the number of trees (i.e., logistic regression models, here set to 1000) and 2. the number of predictor variables to be sampled for each regression model. Here the rule of thumb was used of 10 ~ 15 observations per predictor variable in the regression model (Green, 1991; Peduzzi et al., 1995; 1996; Babyak, 2004), resulting in 3 variables per model when comparing the high risk group to the healthy controls, and in 1 variable per model for the high risk subgroup comparisons. All statistical analyses were implemented and performed in R version 2.12.1 using the mlogitBMA package.

5.3.6.1 Healthy control versus high risk: left hemisphere

When all the predictor variables and degree, clustering and sparsity were used to construct a random forest, the average generalisation error of the resulting classifier was 51% (95% confidence interval = 46% - 55%), which was at chance level. The top three variables from Table 9, which lists the variables with an importance score higher than 0, were: the angular gyrus, sparsity and the superior parietal lobule. These variables were selected to construct a logistic regression model and the generalisation error was estimated using bootstrap validation (using a thousand random bootstrap samples). The average generalisation error improved to 41% (95% confidence interval: 37% - 45%), suggesting that sparsity in combination with a higher number of hubs in the left angular gyrus and superior parietal lobule is related to an increased genetic risk of schizophrenia.

5.3.6.2 Healthy control versus high risk: right hemisphere

The random forest classifier using all predictor variables from the right hemisphere performed around chance level (average generalisation error = 0.52%; 95% confidence interval = 47% - 57%). Including only the top three variables from Table 8 (middle temporal gyrus, precuneus and the postcentral gyrus) improved the performance of the classifier slightly to 46%, but the 95% confidence interval still included chance level (41% - 50%), indicating that there were no reliable differences between the groups in the spatial distribution of the hubs in the right hemisphere.

Table 9

The standardised importance score of the predictor variables for the left and right hemisphere, when comparing people with and without an increased risk for schizophrenia.

Left	Z score	Right	Z score
Angular gyrus	7.35	Middle temporal gyrus	2.75
sparsity	3.82	Precuneus	1.84
Superior Parietal Lobule	3.44	Postcentral gyrus	0.63
Uncus	3.19	Medial occipitotemporal gyrus	0.61
Cingulate areas	2.13	sparsity	0.44
Inferior occipital gyrus	1.88	Cingulate areas	0.30
Precentral gyrus	1.30	Cuneus	0.17
Medial occipito-temporal gyrus	0.93	Superior/transverse temp gyrus	0.14
Cuneus	0.73	Middle occipital gyrus	0.07

5.3.6.3 Comparisons between the high risk subgroups

Here the results of three comparisons within the high risk group are presented.

5.3.6.3.1.1 Global network properties of the non-ill and ill high risk subgroups

Because within the subgroups significant differences were found in the average degree, clustering coefficient and sparsity, it was first explored whether these variables could reliably distinguish people who later became ill from those who did not. Bootstrap validation showed that models including only sparsity, degree or the average clustering coefficient had an average generalisation error above chance level. However, none of these models could reliably classify the ill sub group from the non-ill subgroup, because the generalisation error of these models included chance level. Models with a combination of these three variables also did not improve classification of the ill subgroup. In the next Section it was explored whether adding information about the number of hubs from anatomical areas improved classification.

5.3.6.3.1.2 Differences in the hub distribution over the left hemisphere of the non-ill and ill high risk subgroups

The average generalisation error of a random forest classifier that included all the available predictor variables, sparsity, degree and clustering coefficient as covariates, was worse than chance level (53%). As can be seen in Table 10, none of the anatomical areas had an importance score higher than sparsity, degree or clustering, suggesting the increase of average degree in the ill subgroup was not specific to any anatomical area in the left hemisphere.

5.3.6.3.1.3 Differences in the hub distribution over the right hemisphere of the non-ill and ill high risk subgroups

The average generalisation error of a random forest classifier that included all the available predictor variables, sparsity, degree and clustering coefficient as covariates, was 44%, but the 95% confidence interval included chance level (36% - 51%). Table 10 shows that the degree and the angular gyrus had the highest importance score and therefore bootstrap validation with a thousand random

samples was performed for a logistic regression model using just these two variables. This model had an average generalisation error of 30% (95% confidence interval: 23% - 35%) which was better than chance. People who remained well were classified with an accuracy of 70% (95% confidence interval: 64% - 75%) and people who later became ill were classified with an accuracy of 71% correct (95% confidence interval 60% - 83%). These exploratory results suggest that the number of hubs in the right angular gyrus in combination with the degree could reliably predict whether people at high risk of schizophrenia become ill or not.

Table 10
The standardised importance score of the predictor variables for the left and right hemisphere when comparing non-ill (i.e., no-symptom and symptom combined) and ill subgroups.

Left	Z score	Right	Z score
Degree	6.68	Degree	5.57
Clustering	5.82	Angular gyrus	5.46
Sparsity	4.71	Postcentral gyrus	5.33
Insula	2.57	Precuneus	3.88
Medial occipito-temporal gyrus	2.51	Clustering	3.81
Inferior parietal gyrus	2.18	Sparsity	3.61
Superior occipital gyrus	1.88	Paracentral lobule	2.46
Superior/transverse temporal gyrus	1.85	Parahippocampal gyrus	2.38
Middle frontal gyrus	1.79	Inferior parietal gyrus	2.28
Uncus	1.68	Superior/transverse temporal gyrus	1.97
Precuneus	0.97	Middle temporal gyrus	1.92
Precentral gyrus	0.71	Medial frontal gyrus	1.84
Postcentral gyrus	0.67	Uncus	1.58
Angular gyrus	0.60	Precentral gyrus	1.32
Superior frontal gyrus	0.23	Superior occipital gyrus	0.87
		Cingulate areas	0.81
		Middle frontal gyrus	0.73
		Superior parietal lobule	0.55

5.3.6.3.2.1 Global network properties of the no-symptom and ill high risk subgroups

Because the no-symptom and ill subgroups had significantly different average and/or median values for the sparsity, degree and clustering coefficient, it was first explored whether these properties could predict group membership. Bootstrap validation with a thousand random samples suggested that the average degree was sufficient to distinguish the no-symptom from the ill group with an average generalisation error better than chance 31% (95% confidence interval: 25% - 36%). Both groups were classified higher than chance (well: mean = 71% (64% - 78%); ill: mean = 67%, 57% - 80%). A model including just sparsity also performed better than chance with an average generalisation error of 32% (26% - 37%). Using only the clustering coefficient was insufficient to reliably classify group membership, because the confidence interval of the ill group included chance level. Including both sparsity and the degree did not improve the performance of the degree-only model, (average mean = 31%, 95% confidence interval: 23%-37%).

The next Section explores whether adding information of the hub areas improves classification of the degree-only or sparsity-only models.

5.3.6.3.2.2 Differences in the hub distribution over the left hemisphere between the no-symptom and ill high risk subgroups

The average generalisation error of a random forest classifier that included all the available predictor variables, sparsity and degree as covariates, was 48%, which was worse than using just the degree. None of the anatomical areas had an importance score higher than sparsity or degree (Table 11), suggesting the increase in average degree was not specific to any anatomical area in the left hemisphere in the ill subgroup.

5.3.6.3.2.3 Differences in the hub distribution over the right hemisphere between the no-symptom and ill high risk subgroups

The random forest classifier that randomly sampled one variable from all the right hemispheric anatomical areas, sparsity and degree had generalisation error of 44%, but the 95% confidence interval included chance level (35% - 52%). Table

11 lists the predictor variables with the highest importance scores of which the top two were the angular gyrus and the average degree. The angular gyrus contained on average more hubs in the ill group (3.23) than the no-symptom group (2.28). Bootstrap validation of a logistic model including just the angular gyrus and the degree performed better than the full random forest, and also better than the degree only model with an average error rate of 27% (95% confidence interval = 26% - 33%). Also the classification of the groups improved (well mean = 72%, 95% confidence interval =65%-79%; ill mean = 74%, 95% confidence interval = 60% - 79%). These results suggest that people at high genetic risk of schizophrenia who later become ill have a higher average degree than people who remain well, and that this increase is specific to the angular gyrus. Furthermore this results suggests that this method could potentially be used as a diagnostic tool.

Table 11
The standardised importance score of the predictor variables for the left and right hemisphere when comparing high risk no-symptom and ill subgroups.

Left	Z score	Right	Z score
Degree	8.34	Angular gyrus	6.20
Sparsity	7.85	Degree	5.89
Insula	5.54	Postcentral gyrus	5.48
Precentral gyrus	5.15	Sparsity	5.30
Middle temporal gyrus	3.26	Paracentral gyrus	5.09
Superior occipital gyrus	2.62	Precuneus	5.06
Middle frontal gyrus	1.18	Inferior frontal gyrus	3.26
Cuneus	1.12	Medial frontal gyrus	3.21
Medial occipitotemporal gyrus	1.12	Cingulate areas	2.83
Lingual gyrus	0.72	Superior temporal gyrus	2.29
Supramarginal gyrus	0.64	Paracentral gyrus	2.07
Angular gyrus	0.31	Inferior parietal gyrus	2.01
		Middle occipital gyrus	1.79
		Superior frontal gyrus	1.69
		Precentral gyrus	1.55
		Uncus	0.79

5.3.6.3.3.1 Differences in the global network properties between the symptom and ill high risk subgroups

First it was explored whether sparsity, degree and the clustering coefficient could predict group membership. Bootstrap validation with a thousand random bootstrap samples suggested that although the average generalisation error of the degree (35%, 95% confidence interval = 28% - 35%), clustering coefficient (39%, 95% confidence interval = 31% - 45) and the sparsity (37%, 95% confidence interval: 31% - 42%) was better than chance level (50%), the 95% confidence interval of the classification of the ill group included for all models chance level, suggesting that the groups cannot be reliably classified using just one of these variables. Combining these variables did not improve classification.

5.3.6.3.3.2 Differences in the hub distribution over the left hemisphere between the symptom and ill high risk subgroups

The random forest classifier that randomly sampled one variable from all the right hemispheric anatomical areas and sparsity, clustering and degree had generalisation error of 45%, its 95% confidence interval included chance level (38% - 54%) indicating that it did not perform better than chance level. Sparsity had the highest importance score in Table 12, indicating that information from the left anatomical areas could not be used to improve the classification of the groups.

5.3.6.3.3.3 Differences in the hub distribution over the right hemisphere between the symptom and ill high risk subgroups

The generalisation error of the random forest classifier that randomly sampled one variable from all the right anatomical areas, sparsity and degree had generalisation error of 45% and its 95% confidence interval included chance level (38% - 54%). The most important variable in Table 12 was the paracentral lobule that contained more hubs in the ill group than the symptom group. A logistic regression model that included just the paracentral lobule, performed better than chance with a generalisation error of just 35% (95% confidence interval: 27% - 41%). However, the confidence interval of the generalisation error specific for the ill group still included chance level (mean 34%, 95% confidence interval: 29% - 50%). Adding the second highest predictor variable (i.e., the degree) to the logistic regression

model improved the generalisation error to 34%, and also both classes were correctly classified (symptom class: mean = 64%, 95% confidence interval: 59% - 71%; ill class: mean = 67%, 95% confidence interval: 57% - 83%).

Table 12
The standardised importance score of the predictor variables for the left and right hemisphere within the high risk group: symptoms versus ill.

Left	Z score	Right	Z score
Sparsity	4.41	Paracentral lobule	5.60
Middle temporal gyrus	4.25	Degree	5.34
Degree	3.04	Precuneus	4.80
Inferior parietal lobule	2.34	Postcentral gyrus	3.78
Insula	1.80	Sparsity	3.37
Superior occipital gyrus	1.78	Cuneus	3.27
Supramarginal gyrus	1.30	Superior occipital gyrus	2.53
Lat and med orbitofrontal gyrus	0.68	Angular gyrus	2.20
Angular gyrus	0.46	Medial frontal gyrus	2.04
Inferior frontal gyrus	0.24	Cingulate areas	1.59
Precentral gyrus	0.19	Superior frontal gyrus	1.32
Cuneus	0.10	Superior parietal lobule	0.65
		Inferior parietal lobule	0.46
		Uncus	0.44

5.4 Relationship of hubs and symptoms within the high risk group

Here it was further explored whether the differences found between the groups were correlated to symptom severity at the start of the study and genetic liability.

Earlier symptom severity of schizotypal cognitions as measured with the RISC (Rust Inventory of Schizotypal Cognitions; Rust, 1988) has been reported to be significantly different between all three subgroups of the EHRS (Johnstone, 2005). However, at whole brain level, no significant correlations have been found with grey matter density at baseline within the EHRS subgroups (Lymer et al., 2006). Only after applying a small volume correction, Lymer et al. (2006) found a strong positive relationship between symptom severity and grey matter density of the left superior temporal gyrus was found in the ill subgroup.

Table 13 lists the anatomical areas that showed a significant rank correlation with the RISC across all subjects in the EHRS and for each subgroup separately. All these correlations were of moderate strength, and none survived correction for multiple hypothesis testing with false discovery rate. No significant correlations were found for the left superior frontal gyrus, however, correlations were found for the left inferior and middle frontal gyri.

Table 13

Significant rank correlations rho (*p*-value) of the Rust Inventory of Schizotypal Cognitions (RISC) with number of hubs in the EHRS groups

Anatomical area	Group			
	All	well	symptom	ill
left inferior frontal gyrus	-0.16 (0.05)	-0.32 (0.006)	ns	ns
left middle frontal gyrus	ns	ns	ns	0.56 (0.02)
left insula	ns	ns	-0.33 (0.02)	ns
left middle occipital gyrus	-0.18 (0.03)	ns	ns	ns
left inferior occipital gyrus	ns	ns	0.32 (0.02)	ns
right cingulate gyrus	0.19 (0.02)	ns	ns	ns
right middle temporal gyrus	ns	-0.36 (0.002)	ns	ns
right middle occipital gyrus	ns	ns	ns	0.50 (0.04)

5.5 Discussion

In the present study, the properties of grey matter networks were studied for the first time in a sample of people at high genetic risk for schizophrenia (from the Edinburgh High Risk study of Schizophrenia). In addition, the new method was further validated by comparing the healthy control sample with the study of Chapter 3. It was found that only the size of the networks was similar for both groups, but all other network properties were different. Possibly these differences were related noise arising from scanners of different strength, because the groups showed differences in the variability of grey matter intensity values in the cubes. Interestingly, the spatial distribution of the degree over anatomical areas was highly stable and also the interrelationships between the network property values were similar in both groups.

In the EHRS study, global network properties were similar between the high risk and healthy control groups, but the only the high risk group showed a positive correlation between the average minimum path length and the small world coefficient. Within the high risk group, networks from people who later became ill contained more intracortical similarities, an increased average degree and average clustering coefficient in comparison to networks from people who did not had any symptoms. Network property values of people who experienced symptoms during the study were intermediate between the two other high risk groups. Furthermore, the diagnostic potential of the new method was supported by exploratory results, where people who later became ill could be classified up to an accuracy of 74%. The number of hubs in the left angular gyrus and superior parietal lobule could predict whether someone had an increased risk of schizophrenia or not (an average prediction accuracy of 59%). The number of hubs in the right angular lobe differentiated people at risk who later became ill from those who did not (an average prediction accuracy of 73%). People at high risk who experienced symptoms had less hubs in the right paracentral lobule than people who later became ill (an average prediction accuracy of 65.5%).

These results suggest that the new method offers a more sensitive approach than traditional methods to analyse grey matter data. The remainder of this Section will discuss the issues specific to the current study. For a discussion of general issues regarding the new method the reader is referred to Chapter 6.

5.5.1 Validation of the method

The networks from the EHRS healthy sample showed less intracortical similarities than those from the Calibrain study. This discrepancy might be explained by the difference in scanner strength, because scans from a 1T scanner (in the EHRS study) contained more noise in their cubes than the scans from a 1.5T scanner (in the Calibrain study). Because the groups did not differ in network size, it is likely that the differences in all other network property values are related to the difference in network sparsity. However, these differences did not affect the spatial distribution of local degree values across the anatomical areas, because this was highly stable between studies. The interrelationships between the network property values were also stable. These findings suggest that comparisons between scans acquired with different scanner strengths should be limited to stable network properties.

5.5.2 Differences in network properties: healthy versus high risk groups

The high risk group showed a positive relationship between average minimum path length and the small world property, which is suggestive of a disrupted network topology because such a correlation did not exist in the healthy control group. Alternatively, this difference in correlation is caused by the difference in group size. Furthermore, the groups did not show differences in their global network properties, suggesting that the global level of organisation was not affected in people with a genetic risk of schizophrenia. This result is in line with previous anatomical network studies in established schizophrenia that also found global network property values were comparable with those from healthy controls (Bassett et al., 2008; van den Heuvel et al., 2010; Lord et al., 2011; but also see Zalesky et al., 2010).

5.5.3 Differences in network properties related to disease outcome

Within the high risk group it was found that people who later became ill had more intracortical similarities (i.e., the networks more densely connected), resulting in a higher average degree and clustering coefficient. The difference in sparsity could not be related to differences in noise in the scans, suggesting that this findings is

specific to disease outcome. At this point it is unclear what underlies the increase in intracortical similarities. An important next step is to investigate how these differences are related to other anatomical measures that have been reported to be involved in schizophrenia such as, for example, cortical thickness (e.g., White et al. 2003; Kuperberg et al., 2003; Narr et al., 2004; Jung et al., 2009) or change of grey matter volume over time (e.g., Pantelis et al., 2003; Job et al., 2005; Borgwardt et al., 2008; Sun et al., 2009).

Furthermore, only the ill subgroup showed two positive correlations of the average minimum path length with network sparsity and the clustering coefficient. These correlations could be caused by the increase in intracortical similarities. These finding suggests that an imbalance in clustering and minimum path length exists in people at high risk who later become ill, and this explanation should be further tested in future research.

5.5.4 Increase of hubs in the parietal regions of the high risk group

In exploratory analysis it was found with automated variable selection that the left angular gyrus and superior parietal lobule in combination with sparsity could predict whether an individual was at increased risk for schizophrenia or not. More specifically, these regions contained more hubs in people with an increased risk for schizophrenia than in people without such risk. Furthermore, within the high risk group, the right angular gyrus contained more hubs in people who later became ill than in people who remained well. Lastly, the right paracentral lobule contained more hubs in people who became ill than people who later experienced symptoms.

Surprisingly, while previous studies mostly have reported differences in temporal and frontal lobes in people at high genetic risk for schizophrenia (at either whole brain level or with region of interest analysis), none of these regions were found to be significantly different between group. However, the number of hubs in temporal, frontal, cingulate and occipital regions did show weak to moderately strong correlations with symptom severity as measured with the RISC (Rust, 1988). The number of hubs in the parietal regions, that predicted group membership, however did not not correlate with symptom severity. The rest of this Section will further speculate about the role of parietal regions in a network.

The number of hubs in the parietal regions, that predicted group membership, however did not not correlate with symptom severity. The rest of this Section will further speculate about the role of parietal regions in a network

The angular gyrus is part of the inferior parietal lobule, which is implicated in language and thought processing and has been hypothesised to be disrupted in schizophrenia (Pearlson, 1997; Shenton, 2001; for a review of the involvement of the parietal cortex in schizophrenia see: Torrey, 2007). It receives reciprocal connections from the prefrontal cortex, hippocampus, amygdala, septum and temporal lobe regions (Cavada and Goldman-Rakic 1989; Seltzer and Pandya, 1984). In functional, white and grey matter MRI studies disruptions involving the parietal regions in schizophrenia have been reported (e.g., Schlaepfer et al., 1994; Wright et al., 1995; Frederikse et al., 2000; Wilke et al., 2001; Hulshoff Poll et al., 2001; Buchanan et al., 2004; Whalley et al., 2004; Nierenberg et al., 2005; Whalley et al., 2005; Whalley et al., 2006; Zhou et al., 2007; Liu et al., 2008; Whitfield et al., 2009; Alexander-Bloch et al., 2010; Lynall et al., 2010; Nenadic et al., 2010; van den Heuvel et al., 2010; Wang et al. 2010).

Reductions of grey matter in the left angular gyrus and inferior parietal regions have been reported in established schizophrenia (Schlaepfer et al., 1994; Frederikse et al., 2000; Wilke et al., 2001; Hulshoff Poll et al., 2001; Nierenberg et al., 2005; Zhou et al., 2007). Studies have found negative correlations between inferior parietal grey matter volume and symptom severity (Wright et al., 1995; Wilke et al., 2001; Nenadic et al., 2010) and with deficits in sustained attention (Salgado-Pineda et al., 2003). Furthermore, Buchanan et al., (2004) found a grey matter volume correlation between the left angular gyrus and left inferior gyrus in people with schizophrenia, but not in healthy controls (however, also see: Zhou et al., 2007), providing more evidence that the morphological properties of these areas play a role in schizophrenia.

Further evidence for a hub role of the left inferior parietal cortex in schizophrenia has been provided by a DTI network study (van den Heuvel et al., 2010). This study also found a decrease of clustering and the average minimum path length in the right paracentral lobule in patients with schizophrenia when compared to healthy controls.

Functional MRI studies involving the EHRS have also found disruptions of the parietal cortex during a sentence completion task (Whalley et al., 2004). Furthermore, people at high risk for schizophrenia showed increased fronto-parietal functional connectivity when seeded from the inferior parietal cortex (Whalley et al., 2005), which was predictive of illness (Whalley et al., 2006).

Other functional MRI studies also reported differences in parietal activation in people at high clinical risk of schizophrenia (Gogtay et al. 2003; Borgwardt et al., 2007; Jung et al., 2009; Lui et al., 2009; Jacobson et al., 2010; Dazzan et al., 2011; Lord et al., 2011; and for established schizophrenia see e.g., Thompson et al., 2001; Voets et al., 2008). Only one graph theoretical study exists that studied fMRI networks in people at clinical high risk of the disease, and they reported that people at high clinical risk had an increased betweenness centrality in the superior parietal regions (among other regions) in comparison with healthy controls (Lord et al., 2011), again indicating a hub role of this region in schizophrenia.

In established schizophrenia the inferior parietal lobe has also been identified as a hub region (Wang et al., 2010), based on increased of functional connectivity (also see Yu et al., 2011b). Another study found that left inferior parietal regions showed less clustering and a larger average path length (in resting state data: Liu et al., 2008; note however, other studies only found differences in the right parietal regions: Alexander-Bloch et al., 2010; Lynall et al., 2010). Additionally, the default mode network of patients with schizophrenia showed stronger fMRI correlations between prefrontal and parietal regions than healthy first degree relatives of patients with schizophrenia, who in turn showed moderately stronger correlations than healthy controls (Whitfield et al., 2009).

All these studies in different modalities have found that parietal regions are involved in schizophrenia. This leads to the question as to why these regions have not been indicated in previous group based analyses in the grey matter data. Parietal regions show high variability between individuals (e.g., Kennedy et al., 1998), which might be the reason why traditional VBM did not find differences at whole brain level in the EHRS. The new method did find differences, possibly because patterns of intracortical similarities were examined within an individual cortex without the need of warping scans into a standard space. These results

support the hypothesis that networks based on intracortical similarity provide a concise, statistical description that is more sensitive to subtle structural disturbances than traditional group based methods. However, it remains to be established, why these regions show an increase in intracortical similarities. Possibly, the increased risk of schizophrenia is related to differences in cortical development. During healthy development, grey matter volume in the parietal and prefrontal regions peaks at around 11-12 years of age, after which it decreases during adolescence (Jernigan et al., 1991; Giedd et al., 1999; Sowell et al., 2003; Paus et al., 2005). Because onset of schizophrenia usually occurs during adolescence, it has been hypothesised that these regions lag behind in development in people at high genetic risk of disease (e.g., Douaud et al., 2009). This question needs to be further investigated, for example, by mapping changes over time in the individual morphological networks and possibly in combination with functional networks.

5.5.5 Methodological limitations

Exploratory analyses were performed to investigate whether the spatial distribution of the hubs could be used to classify the subjects in different groups. An automated procedure, random forest, was used to select anatomical regions that were predictive of group membership. Although the classification rates were higher than chance level, it should be investigated whether they can be improved. Recently two other studies using information from morphological networks, have shown high classification accuracy (> 80%) when distinguishing healthy elderly people from people with minor cognitive impairment (Zhou et al., 2011) and Alzheimer's disease (Dai et al., 2011) using support vector machines (SVM). SVM were tried in the present study as well, but they did not work as well as the logistic regression models. Logistic regression has been reported to perform comparable to support vector machines, therefore future research should investigate whether variable selection could be improved (Bray et al., 2009). Possibly other network properties could be added to achieve a lower generalisation error (e.g., the clustering coefficient, see Bassett et al., 2008). However it must be noted that although the smallest group contained just 17 individuals, group membership could be predicted with a generalisation error as

low as 26%. It might also be possible, that the higher classification accuracy in ageing studies can be explained by the fact that structural differences between healthy and demented elderly are more pronounced than in the present high risk study, where all people were healthy.

This is the first study that provides evidence of differences the structure of grey matter using graph theory in a sample of healthy people at high genetic risk for schizophrenia. The findings were in line with previously reported findings in genetic and clinical high risk studies. This implies that patterns of intracortical similarity within individual cortices contain important information relevant to function. Future research should focus on studying the mechanisms that underly intracortical similarities.

6. Overview, conclusions and future research

In this thesis it was examined whether it was possible to extract morphological networks from individual grey matter segmentations from magnetic resonance imaging scans (MRI).

In Chapter 2 it was discussed that the morphology of the human cortex is complex and not well understood. Graph theory has been used to study human cortical morphology, but a limitation of existing methods is that they extract a single morphological network from group averaged data. Averaging cortical morphology across subjects can be problematic and subtle structural differences that are of most interest for clinical studies can be filtered out. Moreover, inter-individual cortical variation has been suggested to determine individual differences in cognitive function (e.g., Schwarzkopf et al., 2010) and therefore it is important to have a concise description of individual cortices.

The major contribution of this thesis was the development of a new method to extract individual grey matter from MRI scans in Chapter 3. This method divided the cortex into small three-dimensional regions of interest, which served as the nodes of the network that were connected based on their structural similarity. The method was tested on data from a sample of healthy people who were scanned at two different time points. The most important finding was that the topological organisation of the resulting networks was significantly different from random networks. The network property values that were found were comparable with those reported in group derived morphological networks of similar sparsity and two fMRI networks, and they were consistent over two time points. The main conclusion in this Chapter was that patterns of intracortical similarities give a concise statistical description of individual cortical morphology.

Chapter 4 presented an overview of schizophrenia and mainly discussed studies that investigated grey matter MRI in people at high genetic risk of schizophrenia. Findings reported in healthy subjects who were at increased risk to develop schizophrenia show inconsistencies: while some studies found structural differences at whole brain level using traditional voxel-based morphometry methods, most studies did not. In spite of the inconsistent findings at whole brain level analyses, many region of interest analysis studies have reported differences

in grey matter at baseline that might be predictive of the disease. The main conclusion of Chapter 4 was that differences in cortical structure related to high genetic risk of schizophrenia must be subtle and for that reason might remain undetected by traditional automated whole brain analyses.

In Chapter 5 it was investigated whether the new method presented in this thesis would more sensitive than traditional methods when studying cortical morphological differences between people with and without an increased genetic risk for schizophrenia from the EHRS (i.e., the Edinburgh High Risk study of Schizophrenia). Several subtle differences were found between the high risk and healthy control sample. For example, a correlation between minimum path length and the small world coefficient, which was suggestive of a disturbed network topology, only occurred in the high risk group. Also, differences in network topology within the high risk sample could be related to disease outcome. The results from Chapter 5 supported that the new method is more sensitive than traditional VBM methods to subtle cortical disruptions and is therefore of importance for the study of cortical structure in clinical populations.

The remainder of the current Chapter will discuss potential explanations for the results found in this thesis, followed by a discussion of how the method could be improved and other suggestions for future research, followed by the final conclusions.

6.1 Intracortical similarities

At this point it is only possible to speculate about the mechanisms that underlie intracortical similarities and their relationship to connectivity. One possible explanation comes from the axon tension theory that was proposed by van Essen (1997). He posited that axons between connected cortical areas cause a mechanical force, resulting in a tension that pulls connected areas together whereas unconnected areas simply drift apart. Furthermore this hypothesis also explains how differences in cortical areas arise, when, for example, more tension applied to a cortical region results in thinner cortex. This prediction was later verified by Hilgetag and Barbas (2005; 2006), who showed with a series of tracer studies in monkey that tension from axons shifts cortical layers resulting in either thinner (heavily pulled on) or thicker cortex. Removing parts of cortex during

embryonic development can result in a disturbed cortical morphology, which also supports the axonal tension hypothesis (Goldman et al., 1978; Kolb et al., 1994; but for an alternative explanation also see Toro and Burnod, 2005). In the human brain using structural MRI, Im et al. (2006) found that about fifty percent of the variance in the fractal dimension of the cerebral cortex could be explained by cortical thickness and folding area. They suggested that a high fractal dimension, is related to a thinner and more convoluted cortex, and that this relationship is in keeping with the axon tension theory. Finally, Casanova et al. (2009) reported that in comparison to healthy controls, people with autism had a reduced gyral window, which is measured by the depth of gyral white matter and gives an indication of the space available for connections to and from the cortex. This measure was correlated with abnormalities in micro-columnar arrangement of neurons. These findings suggest that similarity in cortical structure might arise as a consequence of axonal tension between two connected areas.

Alternatively, intracortical similarities might be related to functional connectivity. In Chapter 3 it was found that the anatomical areas that contained the highest percentage of hubs (i.e., regions that show more similarities with all other nodes in the network than average) showed a striking correspondence with the functional default mode network (i.e., regions that show increased activation during rest and decreased activation during tasks see e.g., Raichle et al., 2001). In addition, experience driven activity and/or plasticity could cause regions to be more morphologically similar. For example, Andrews et al. (1997) demonstrated that experience driven plasticity can lead to coordinated morphological changes within an individual brain. Also, parietal regions, which are part of the default mode network, were shown to be different in people at increased genetic risk of schizophrenia in Chapter 5 and in other MRI studies, further suggesting an overlap between functional connectivity and patterns of intracortical similarities.

The above research indicates that anatomical and/or functional connectivity of the brain can have an effect on its morphology and this should be further investigated. The new method contributes to this issues by providing a way to study these important questions within individual cortices.

6.1.2 Disruptions of intracortical similarity patterns in high risk of schizophrenia

The new method provides the opportunity to describe the morphology of grey matter for an individual cortex. So instead of warping individual scans to a standard space to compare groups, cortices can be compared by averaging the descriptive statistics from the scans' native space without the need to use a prior model to define anatomical areas. Because the scans can be described in their native space, the sensitivity to detect subtle differences between clinical groups is increased and this was demonstrated in Chapter 5: people at high risk of schizophrenia showed a different correlation between the average minimum path length and the small world coefficient than people without such risk. Also, it was found that the angular gyrus showed the most differences between groups, where it contained the least hubs in healthy people, and the most hubs in people at high risk who later became ill. The results of Chapter 5 support the neurodevelopmental hypothesis discussed in Chapter 4, because they indicate that subtle morphological differences exist that are related to an increased risk of schizophrenia and subsequent disease outcome.

The differences found in the exploratory analyses were subtle and could predict group membership up to an accuracy of 74%. However it must be noted, that the smallest group contained just 17 people and therefore need to be validated with a different (larger) sample. It must be mentioned that the EHRS is an unique dataset and it would be difficult to create a similar or larger dataset. Possibly the areas found to be predictive of schizophrenia could also be predictive in other high risk groups, for example, in people who are at high risk of schizophrenia for cognitive reasons (e.g., the Edinburgh Study of Comorbidity could be used, see: Johnstone et al., 2007). In addition, it could be further investigated whether adding topological information can increase the classification accuracy.

Because this study found subtle topological disruptions that could be related to the genetic risk of schizophrenia and the consequent development of the disease, more research should aim to understand the underlying causes of these disruptions. A next step should be to study changes of network topologies during the development of schizophrenia. Specifically, it would be interesting to investigate whether dysfunctional connectivity arises at a specific point. The new

method could contribute to further understanding of cortical structure and function interactions by combining individual anatomical networks with individual functional imaging data at different time points during the development of the illness in the Edinburgh High Risk study of Schizophrenia.

6.2 Unresolved issues and future research

6.2.1 Methodological issues

The nodes of the networks had a fixed resolution that was based on the lowest possible scale that can measure both folding and thickness (Kiselev et al., 2003), combined with a voxel size that is generally used in functional MRI studies. For future research it needs to be tested how different spatial resolutions will influence the results. For example, a single node could be used to slide over all dimensions of the grey matter volume to better match the convolution of the brain. However, this would introduce more (redundant) correlations due to overlap of the cubes and would also produce networks with a very large size. An alternative for the use of a rigid template to define ROIs, could be the use of 'scale-space'. Scale-space is a theoretical framework to represent signals (including images) across multiple spatial scales. With this framework features of an image can be detected that are invariant for the change of scale in an image, without a priori information about what type of object is being studied (Witkin, 1983; Florack et al, 1992; Koenderink, 1994; Lindeberg, 1994). In other words, such a framework would be able to extract interesting features from an image that are independent of scale, in contrast to the use of a rigid template. Briefly, a multi-scale representation of a feature in an image can extracted by convoluting the image with Gaussians of varying widths, and the feature is then constructed as the ordered set of signals that represent structures at coarser spatial scales. Lowe (2004) described a method that uses scale space to extract features from 3D structures in multiple images that are scale and rotation invariant. The present method could use such features as nodes in individual grey matter networks, which can be connected when the feature vectors are similar.

The present method is not rotation invariant. Addition of noise due to maximisation of the similarity coefficient for rotation was limited by only using angles that did not require interpolation to correct for rotation when computing the

correlation coefficient. A simulation study (with the use of a simplified model to represent structural MRI) demonstrated that approximately 1% of the similarities could have been missed using just these angles. The distribution of the degree and clustering coefficient over the nodes of a network was highly stable for networks extracted with angle multiples of 90° and 45°. These results in combination with those from the simulation study strongly suggest that using angle multiples of 45° to maximise the correlation coefficient is sufficient to describe morphological network topology. However future research could study whether network property values would change if the spheres were to be used as nodes, since spheres can be rotated for arbitrary degrees more easily than cubes. Alternatively, as mentioned above, the use of scale space could make similarity measurements between grey matter structures independent of scaling and rotation (e.g., Lowe, 1994; Toews et al., 2010). Related to scale-space, specific methods to quantify shape exist that use operators that are invariant for rotation, among which a techniques that uses spherical harmonics (SPHARM: Uthama et al., 2007;McKeown et al., 2007) or wavelet-based attribute vectors (Xue et al., 2004). SPHARM has been used to characterise the shape of predefined regions of interest, resulting in feature vectors. For the present work, the cubes could be represented with such feature vectors. Alternatively, wavelet attribute vectors can be defined for individual voxels (Xue et al., 2004), eliminating the need for rigidly extracted ROIs. Future research should aim to investigate how these types of operators can improve the current method.

Addition of noise to the data was limited by keeping the MRI scans in their native space, but voxels might still have been assigned to the incorrect tissue class during segmentation (e.g., due to partial volume effects). However, as the method mostly concerns the spatial relationship between voxels within small cortical areas, these errors should not have a prominent effect on the results. This issue was explored by comparing network properties of networks using different grey matter intensity levels to classify voxels as being grey matter, and no differences in the network properties were found, suggesting that the method is robust to such misclassification. Nevertheless, in Chapter 4 it was found that different scanners were related to differences network property values. The Calibrain study that used a 1.5T scanner resulted in more densely connected

networks than the EHRS study (1T), even though both studies had the same 5% chance of including spurious connections. The scans from both studies differed in how they were corrected for bias field signal (i.e., intensity inhomogeneities resulting from a low-frequency, smooth signal produced by the scanner). The EHRS scans were bias corrected with help of a phantom, which provides a physical estimate of the bias field. The Calibrain scans were corrected in SPM5, which estimates the bias field retrospectively with a mathematical model that is based on surface fitting. The main difference is that the retrospective method does not use a priori information about the bias field, which has been used in the EHRS scans by means of a phantom. Both methods have limitations. While the use of a phantom could still leave as much as 30% of the inhomogeneity in the scans (Vovk et al., 2007), the mathematical model could be unstable, introducing a spurious solution (Hou et al., 2006). The differences methods used for bias field correction could therefore have caused a the difference in the number of similarities found between the two studies. In addition, the lower scanner strength was related to more noise in the EHRS data (measured as an increase in standard deviation in the distribution of grey matter intensity values), which might have caused the decrease of similarities found in this sample. However, the spatial distribution of the degree over the nodes in the networks was not affected, suggesting that this network characteristic is robust to different scanners. Related to this issue, the method was also applied to a cohort of elderly individuals (healthy, with mild cognitive impairment and Alzheimer's disease). Structural templates needed to be constructed for this elderly population, because standard segmentation with SPM5 led to grey matter segmentations of poor quality. This preliminary study showed that the network properties were dramatically lower than those from the young and healthy Calibrain cohort, and that this effect could also be related to more noise in the data.

The spatial distributions in a network of hubs based on the degree or betweenness centrality showed a strong positive correlation with the size of an anatomical region. This relationship might explain why those regions have been indicated as hubs in other studies as well, illustrating how a priori anatomical templates can influence results and that it is important to develop alternative anatomical parcellation schemes that lead to similarly sized anatomical regions

(for examples see: Hagman et al., 2007; Meunier et al., 2009; Zalesky et al., 2010). The current method does not require a priori parcellation schemes and therefore the results can be easily projected on any other alternative.

6.2.2 Network comparison

It is important to note the comparison of individual networks is an important problem, because the number of nodes and the average degree influence the network property values, as shown here and in recent studies (He, Chen et al., 2007; Bassett et al., 2008; He et al., 2008; Bassett et al., 2010; Fornito et al., 2010; Zalesky et al., 2010; van Wijk et al., 2010). As a consequence, the highly stable number of nodes in the networks from Chapter 3 might have caused the stability of the degree, average minimum path length and the betweenness coefficient.

Such intricate relationships between different topological properties greatly complicate the comparison of networks, when everything but the property of interest should be held constant. Unfortunately, this is not always possible. With the current approach the number of nodes could not be kept constant because the subjects were analysed in native space to keep their individual variability intact. But, when individual brains are warped into a standard space where the same number of nodes are defined for all individual subjects, some nodes might not be present in their native space (or might consist of a slightly different combination of gyri: e.g., Paus et al. (1996) showed in a sample of 247 subjects that small percentage of them did not have a paracingulate sulcus in either the left (8%) or right (15%) hemisphere). In addition to the number of nodes, the number of edges in a network could be kept constant. However, such a procedure will introduce spurious connections, because edges might not exist in some individuals. In this thesis all individual networks had the same 5% chance of spurious connections. A disadvantage of this approach is that it can result in different spatial degree distributions for all individuals. As discussed in the previous Section, the non-uniform distribution of the degree and clustering coefficient values of the nodes seems to be stable for different sparsity levels of the networks, implying that this might not be a problem when comparing the spatial distribution of local network property values. The work in this thesis also

suggests that sparsity might have a more important influence on other network properties than network size. For example, network from the Calibrain study and the EHRS healthy sample were comparable in size, but differed significantly in all other network properties. In addition, a preliminary correlation analysis across the studies summarised in Table 1, demonstrates that the small world property was unrelated to the size of the networks ($r = 0.12$), and (weakly) negatively correlated to sparsity ($r = -0.30$, $p = 4.63 \times 10^{-5}$). Also, two other fMRI studies qualitatively showed more variability between sparsity levels than between different network sizes in network property values (Fornito et al., 2010; Hayasaka et al., 2010). However, the size of white matter networks directly determines the sparsity: anatomical regions that have a smaller size will have a lower probability to contain a white matter tract (Zalesky et al., 2010).

How to compare different networks raises important methodological issues that deserve more attention (Sporns et al. 2005; Rubinov and Sporns, 2010; van Wijk et al., 2010), but lie outside the scope of this thesis. The present method contributes to these issues, by offering an approach that can be applied to different modalities to extract networks in a similar manner per individual or group.

6.2.3 Networks and structural MRI

One interesting finding in this thesis was that most hubs were located along the medial surface of the cortex. This means that cubes covering this area show more similarities with other cubes in the brain than average. At this point it is not clear why this region has more intracortical similarities than other regions and this should be further investigated in future research.

Only the basic network properties of individual morphological networks were studied in the current work to facilitate the interpretation of the results. In the future more complex issues should be studied, such as, for example, whether hubs show similarities with nodes in a specific area (suggesting increased local connectivity, nodes closer together are more similar) or whether these patterns are more widespread (then the cubes would represent a feature that characterises some general aspect of cortical morphology).

In Chapter 3 it was found that the property values of morphological networks tend to remain in a small range (assessed for similar network sparsity),

for example, the small world coefficient varied between 1.15 and 1.47. Also, the distribution of hubs was highly similar over individuals, suggesting that intracortical similarities might underly the covariance of cortical volume and thickness between regions over subjects. It would be interesting to extract both types of networks from the same sample to further investigate how these networks overlap.

The new method shows some resemblance to methods that compute the fractal dimension. Those methods result in one value, the fractal dimension, which indicates whether structures are repeated at different spatial resolutions. By assessing morphological similarities within a fixed spatial resolution that keep intact the spatial information present in the cortex, the new method demonstrated that it is possible to represent the morphology of the cortex as a network. It would be interesting to study how intracortical similarities contribute to the fractal dimension, by using different spatial resolutions for the cubes. Preliminary studies have been performed during the development of the new method, to investigate this relationship. The fractal dimension could easily be computed with the use of the 'box-counting' method, that overlays a grid of cubes over the grey matter segmentation and then the number of non-empty cubes is counted separately for different resolutions of the cubes (first implementation for 3D MRI scans: Chuang et al., 1991). The log of the resulting counts can then be plotted against the log of the resolution of the cubes (i.e., the number of voxels in one dimension) and the slope of the line that fits through the points is an indication of the fractal dimension. Next, it was explored whether graph theoretical properties of the network would change for different resolutions of the cubes, to understand how patterns of intracortical similarities would contribute to the fractal dimension. However, it was not straightforward how to further investigate the relationship of the networks with the fractal dimension, because the method to binarise the networks identified all correlations higher than what would be expected at random. A solution for this thresholding problem at coarser spatial scales could be to correlate every cube in the scan with their spatial information intact, with all other cubes of the scan of which their spatial information is removed. Preliminary attempts have been made to implement this alternative way of generating an empirical null-distribution to correct for multiple testing, but these attempts failed

because it is not straightforward as to how to combine this information into a single model to derive a threshold. These preliminary findings might indicate that the topology of individual morphological networks is specific to the spatial scale used to extract the network, but this needs to be further explored.

Around the same time when the present method was published, Zhou et al. (2011) proposed a method to extract hierarchical anatomical networks at an individual basis by combining all structural information at different spatial resolutions in a single network, which potentially could also be used in combination with the present method to further examine the relationship of anatomical networks and the fractal dimension. It must be noted that they did not report the resulting graph properties.

The network properties of the individually extracted morphological networks were different from DTI networks of similar size. Not a single study could be found that investigated DTI networks of similar size and sparsity to the present networks, leaving the question whether the network properties would become more similar if investigated at similar sparsity level. However, some white matter studies reported in Table 1 (Chapter 2) of smaller size but similar sparsity as the networks from this thesis, demonstrated similar small world values, again supporting the important role of sparsity for determining network property values.

Recently, Gong et al. (2011) systematically studied the properties of group derived cortical thickness networks and DTI and found evidence for a similar organisation in network topology in both modalities. However, 60% of the cortical thickness correlations did not converge with DTI connectivity suggesting that these correlations are caused by other factors (e.g., functional connectivity). With the new method, the direct relationship between morphological and white matter networks can be further investigated by, for example, combining the current method with that of Hagmann et al. (2007) that extracts large scale white matter networks from individual cortices. Such work would also provide more insight into the axonal tension hypothesis (van Essen, 1997).

Other studies have shown that functional signals can also arise in the absence of DTI traced tracts (e.g., Honey et al., 2009). The robustness of the current network analysis should be further investigated within a multimodal

approach combing structural MRI, DTI and functional MRI. The present method allows for the direct comparison within an individual of connectivity matrices derived from different imaging modalities, such as functional MRI and DTI. Such a general multimodal approach should be used in future research to further test the biological validity of intra-cortical similarities. Because matrices across different imaging modalities can be derived within the same subject, converging and diverging patterns of connectivity across modalities can be determined at the single subject level. For example, it can be directly tested whether in the absence of a DTI traced tract structural similarities overlap with temporal correlations. Furthermore, inter-individual variability in the connectivity matrices across modalities can then be established. By combing sMRI and fMRI it would also be possible to test the hypothesis that similarities in cortical structure might be caused by experience driven plasticity.

6.3 The structure-function relationship

So what do intracortical similarities actually mean in relation to brain function? Recently a few studies have began to explore the structure function relationship of the brain using tools from graph theory in cat (Zemanova et al., 2006; Binzegger et al., 2009), macaque (Honey et al., 2007; 2008) and human brain (Alstott et al., 2009; Honey et al., 2009; Rubinov et al., 2009). In these studies fMRI signals in nodes were simulated using computational neuronal population models, that were connected according to a connectivity matrix (usually derived from axon tracing in animals or DTI data in the human case). Interestingly, Honey et al. (2007; 2009) found that functional correlations can arise from these networks in the absence of a direct anatomical connection. However, these studies did not validate their functional models with real (resting-state) fMRI data. It is important to investigate this further because actual fMRI signals might only weakly correspond to simulated hemodynamic signals (Horwitz et al., 2005).

This framework is excellent to further investigate whether regions that have a cortically similar structure have a correlated fMRI signal and whether the functional patterns would follow those from the default mode network as well.

6.4 Final conclusion

The major contribution of this work was a new method to investigate morphological network properties in individual cortices. Every study including the current work has its limitations. For now the new method offers a concise, statistical description of the morphology of individual cortices to contribute to study subtle morphological differences between groups. Finally, the new method has been demonstrated to be of importance for studies involving clinical populations.

Bibliography

Achard, S., & Bullmore, E. (2007). Efficiency and cost of economical brain functional networks. *PLoS Computational Biology*, *3*(2), e17:0174-0183. doi:10.1371/journal.pcbi.0030017

Achard, S., Salvador, R., Whitcher, B., Suckling, J., & Bullmore, E. (2006). A resilient, low-frequency, small-world human brain functional network with highly connected association cortical hubs. *The Journal of Neuroscience*, *26*(1), 63-72. doi:10.1523/JNEUROSCI.3874-05.2006

Albert, R., & Barabási, A.L. (2002). Statistical mechanics of complex networks. *Reviews of Modern Physics*, *74*, 47-97.

Alexander-Bloch, A., Gogtay, N., Meunier, D., Birn, R., Clasen, L., Lalonde, F., Lenroot, R., et al. (2010). Disrupted modularity and local connectivity of brain functional networks in childhood-onset schizophrenia. *Frontiers in Systems Neuroscience*, *4*, 147:1-16. doi:10.3389/fnsys.2010.00147

Alstott, J., Breakspear, M., Hagmann, P., Cammoun, L., & Sporns, O. (2009). Modeling the impact of lesions in the human brain. *PLoS Computational Biology*, *5*(6), e1000408:1-12. doi:10.1371/journal.pcbi.1000408

Andrews, T. J., Halpern, S.D., & Purves, D. (1997). Correlated size variations in human visual cortex, lateral geniculate nucleus, and optic tract. *The Journal of Neuroscience*, *17*(8), 2859-2868.

Armstrong, E., Schleicher, A., Omran, H., Curtis, M., & Zilles, K. (1995). The ontogeny of human gyrification. *Cerebral Cortex*, *5*(1), 56-63.

Ashburner, J., & Friston, K.J. (2000). Voxel-based morphometry - The methods. *NeuroImage*, *11*, 805-821.

Ashburner, J., & Friston, K.J. (2005). Unified segmentation. *NeuroImage*, *26*(3), 839-851. doi:10.1016/j.neuroimage.2005.02.018

Astolfi, L., Fallani, F.D.V., Cincotti, F., Mattia, D., Marciani, M. G., Bufalari, S., Salinari, S., et al. (2007). Imaging functional brain connectivity patterns from high-resolution EEG and fMRI via graph theory. *Psychophysiology*, *44*, 880-893.

Baare, W.F.C., van Oel, C.J., Hulshoff Pol, H.E., Schnack, H.G., Durston, S., Sitskoorn, M.M., & Kahn, R.S. (2001). Volumes of brain structures in twins discordant for schizophrenia. *Archives of General Psychiatry*, *58*(1), 33-40.

Babyak, M.A. (2004). What you see may not be what you get: A brief, nontechnical introduction to overfitting in regression-type models. *Psychosomatic Medicine*, *66*(3), 411-421.

Barbas, H. (1986). Pattern in the laminar origin of corticocortical connections. *The Journal of Comparative Neurology*, *252*, 415-422.

Barbas, H, & Rempel-Clower, N. (1997). Cortical structure predicts the pattern of corticocortical connections. *Cerebral Cortex*, *7*(7), 635-646.

Barrat, A., Barthélemy, M., Pastor-Satorras, R., & Vespignani, A. (2004). The architecture of complex weighted networks. *Proceedings of the National Academy of Sciences of the United States of America*, *101*(11), 3747-3752.

Bartley, A.J., Jones, D.W., & Weinberger, D.R. (1997). Genetic variability of human brain size and cortical gyral patterns. *Brain*, *120*, 257-269.

Bassett, D.S., & Bullmore, E.T. (2006). Small-world brain networks. *The Neuroscientist*, *12*(6), 512-523. doi:10.1177/1073858406293182

Bassett, D.S., & Bullmore, E.T. (2009). Human brain networks in health and disease. *Current Opinion in Neurology*, *22*(4), 340-347.

Bassett, D.S., Bullmore, E., Verchinski, B.A., Mattay, V.S., Weinberger, D.R., & Meyer-Lindenberg, A. (2008). Hierarchical organization of human cortical networks in health and schizophrenia. *The Journal of Neuroscience*, *28*(37), 9239-9248. Society for Neuroscience.

Bassett, D.S., & Gazzaniga, M.S. (2011). Understanding complexity in the human brain. *Trends in Cognitive Sciences*, *15*(5), 200-209. doi:10.1016/j.tics.2011.03.006

Bassett, D.S., Brown, J.A, Deshpande, V., Carlson, J.M., & Grafton, S.T. (2011). Conserved and variable architecture of human white matter connectivity. *NeuroImage*, *54*(2), 1262-1279. doi:10.1016/j.neuroimage.2010.09.006

Belleville, S., Mellah, S., Gilbert, B., Fontaine, F., & Gauthier, S. (2011). Training-related brain plasticity in subjects at risk of developing Alzheimer's disease. *Brain*, *134*(6), 1623-1634. doi:10.1093/brain/awr037

Benjamini, Y., & Hochberg, Y. (1995). Controlling the false discovery rate: a practical and powerful approach to multiple testing. *Journal of the Royal Statistical Society. Series B.*, *57*(1), 289-300.

Benjamini, Y., & Yekutieli, D. (2001). The control of the false discovery rate in multiple testing under dependency. *The Annals of Statistics*, *29*(4), 1165-1188.

Bernhardt, B.C., Chen, Z., He, Y., Evans, A.C, & Bernasconi, N. (2011). Graph-theoretical analysis reveals disrupted small-world organization of cortical thickness correlation networks in temporal lobe epilepsy. *Cerebral Cortex*. doi:10.1093/cercor/bhq291

Bernhardt, B.C., Rozen, D.A, Worsley, K.J., Evans, A.C., Bernasconi, N., & Bernasconi, A. (2009). Thalamo–cortical network pathology in idiopathic

generalized epilepsy: Insights from MRI-based morphometric correlation analysis. *NeuroImage*, *46*(2), 373-381. doi:10.1016/j.neuroimage. 2009.01.055

Bhojraj, T.S., Prasad, K.M., Eack, S.M., Francis, A.N., Montrose, D.M, & Keshavan, M.S. (2010). Do inter-regional gray-matter volumetric correlations reflect altered functional connectivity in high-risk offspring of schizophrenia patients? *Schizophrenia Research*, *118*(1-3), 62-68. doi: 10.1016/j.schres.2010.01.019

Binzegger, T., Douglas, R.J., & Martin, K.A.C. (2009). Topology and dynamics of the canonical circuit of cat V1. *Neural Networks*, *22*(8), 1071-1078. doi: 10.1016/j.neunet.2009.07.011

Bohbot, V.D., Lerch, J., Thorndycraft, B., Iaria, G., & Zijdenbos, A.P. (2007). Gray matter differences correlate with spontaneous strategies in a human virtual navigation task. *The Journal of Neuroscience*, *27*(38), 10078-10083. doi:10.1523/JNEUROSCI.1763-07.2007

Bonnici, H.M., Moorhead, T.W.J., Stanfield, A.C., Harris, J.M, Owens, D.G., Johnstone, E.C., & Lawrie, S.M. (2007). Pre-frontal lobe gyrification index in schizophrenia, mental retardation and comorbid groups: An automated study. *October*, *35*(NeuroImage), 648 - 654. doi:10.1016/j.neuroimage. 2006.11.031

Boos, H., Aleman, A, Cahn, W., Hulshoff Pol, H., & Kahn, R.S. (2007). Brain volumes in relatives of patients with schizophrenia: a meta-analysis. *Archives of General Psychiatry*, *64*(3), 297-304.

Borgefors, G., Nyström, I., & di Baja, G.S. (1997). Connected components in 3D neighbourhoods. *10th Scandinavian conference on image analysis* (pp. 567-572). Lappeeranta: Pattern Recognition Society, Finland.

Borgwardt, S.J., McGuire, P.K, Aston, J., Gschwandtner, U., Pflüger, M.O., Stieglitz, R.-D., Radue, E.-W., et al. (2008). Reductions in frontal, temporal and parietal volume associated with the onset of psychosis. *Schizophrenia Research*, *106*(2-3), 108-114. doi:10.1016/j.schres.2008.08.007

Borgwardt, S.J., Picchioni, M.M., Ettinger, U., Toulopoulou, T., Murray, R., & McGuire, P.K. (2010). Regional gray matter volume in monozygotic twins concordant and discordant for schizophrenia. *Biological Psychiatry*, *67*(10), 956-964. doi:10.1016/j.biopsych.2009.10.026

Borgwardt, S.J., Riecher-Rössler, A., Dazzan, P., Chitnis, X., Aston, J., Drewe, M., Gschwandtner, U., et al. (2007). Regional gray matter volume abnormalities in the at risk mental state. *Biological Psychiatry*, *61*, 1148 -1156. doi:10.1016/j.biopsych.2006.08.009

Braga-Neto, U., Hashimoto, R., Dougherty, E.R., Nguyen, D.V., & Carroll, R.J. (2004). Is cross-validation better than resubstitution for ranking genes? *Bioinformatics*, *20*(2), 253-258. doi:10.1093/bioinformatics/btg399

Bray, S., Chang, C., & Hoeft, F. (2009). Applications of multivariate pattern classification analyses in developmental neuroimaging of healthy and clinical populations. *Frontiers in Human Neuroscience*.

Breiman, L. (2001). Random forests. *Machine Learning*, *45*, 5-32.

Buchanan, R.W., Francis, A., Arango, C., Miller, K., Lefkowitz, D.M., McMahon, R. P., Barta, P.E., et al. (2004). Morphometric assessment of the heteromodal association cortex in schizophrenia. *American Journal of Psychiatry*, *161*, 322-331.

Buckner, R.L., Sepulcre, J., Talukdar, T., Krienen, F.M., Liu, H., Hedden, T., Andrews-Hanna, J.R., et al. (2009). Cortical hubs revealed by intrinsic functional connectivity: Mapping, assessment of stability, and relation to Alzheimer's disease. *The Journal of Neuroscience*, *29*(6), 1860-1873. doi: 10.1523/JNEUROSCI.5062-08.2009

Bullmore, E.T., & Bassett, D.S. (2011). Construction and interpretation of complex networks derived from human neuroimaging data. *Annual Review of Clinical Psychology*, *7*, 113-140.

Bullmore, E., Brammer, M., Harvey, I., Persaud, R., Murray, R., & Ron, M. (1994). Fractal analysis of the boundary between white matter and cerebral cortex in magnetic resonance images: a controlled study of schizophrenic and manic-depressive patients. *Psychological Medicine*, *24*(3), 771-781.

Bullmore, E., & Sporns, O. (2009). Complex brain networks: graph theoretical analysis of structural and functional systems. *Nature Reviews Neuroscience*, *10*, 186-198. doi:10.1038/nrn2575

Bullmore, E., Barnes, A., Bassett, D.S., Fornito, A., Kitzbichler, M., Meunier, D., & Suckling, J. (2009). NeuroImage generic aspects of complexity in brain imaging data and other biological systems. *NeuroImage*, *47*(3), 1125-1134. doi:10.1016/j.neuroimage.2009.05.032

Burdette, J.H., Laurienti, P.J., Espeland, M.A., Morgan, A., Telesford, Q., Vechlekar, C.D., Hayasaka, S., et al. (2010). Using network science to evaluate exercise-associated brain changes in older adults. *Frontiers in Aging Neuroscience*, *2*, 23:1-10. doi:10.3389/fnagi.2010.00023

Burez, J., & van den Poel, D. (2009). Handling class imbalance in customer churn prediction. *Expert Systems with Applications*, *36*(3), 4626-4636. doi: 10.1016/j.eswa.2008.05.027

Cannon, T.D., van Erp, T.G.M., Huttunen, M., Lönnqvist, J., Salonen, O., Valanne, L., Poutanen, V.P., et al. (1998). Regional gray matter, white matter, and cerebrospinal fluid distributions in schizophrenic patients, their siblings, and controls. *Archives of General Psychiatry*, *55*(12), 1084-1091.

Cannon, T.D., Thompson, P.M., Erp, T.G.M.V., Toga, A.W, Poutanen, V.-P., Huttunen, M., Lonnqvist, J., et al. (2002). Cortex mapping reveals

regionally specific patterns of genetic and disease-specific gray-matter deficits in twins discordant for schizophrenia. *Proceedings of the National Academy of Sciences of the United States of America*, *99*(5), 3228-3233.

Casanova, Manuel F., El-Baz, A., Mott, M., Mannheim, G., Hassan, H., Fahmi, R., Giedd, J., et al. (2009). Reduced gyral window and corpus callosum size in autism: possible macroscopic correlates of a minicolumnopathy. *Journal of Autism and Developmental Disorders*, *39*, 751-764. doi:10.1007/s10803-008-0681-4

Cavada, C., & Goldman-Rakic, P.S. (1989). Posterior parietal cortex in rhesus monkey: II. Evidence for segregated corticocortical networks linking sensory and limbic areas with the frontal lobe. *The Journal of Comparative Neurology*, *287*(4), 422-445. doi:10.1002/cne.902870403

Cecchi, G.A., Rao, A.R., Centeno, M.V., Baliki, M., Apkarian, A.V., & Chialvo, Dante R. (2007). Identifying directed links in large scale functional networks: Application to brain fMRI. *BMC Cell Biology*, *8*, S5:1-10. doi:10.1186/1471-2121-8-S1-S5

Chan, R.C.K., Di, X., McAlonan, G.M., & Gong, Q.-Y. (2011). Brain anatomical abnormalities in high-risk individuals, first-episode, and chronic schizophrenia: An activation likelihood estimation meta-analysis of illness progression. *Schizophrenia Bulletin*, *37*(1), 177-188. doi:10.1093/schbul/sbp073

Chanraud, S., Pitel, A.-L., Pfefferbaum, A., & Sullivan, E.V. (2011). Disruption of functional connectivity of the default-mode network in alcoholism. *Cerebral Cortex*, *21*(10), 2272-2281. doi:10.1093/cercor/bhq297

Chen, Z.J., He, Y., Rosa-Neto, P., Germann, J., & Evans, A.C. (2008). Revealing modular architecture of human brain structural networks by using cortical thickness from MRI. *Cerebral Cortex*, *18*(10), 2374-2381. doi:10.1093/cercor/bhn003

Chialvo, D.R. (2004). Critical brain networks. *Physica A*, *340*, 756 - 765. doi:10.1016/j.physa.2004.05.064

Chklovskii, D.B. (2004). Synaptic connectivity and neuronal morphology: Viewpoint two sides of the same coin. *Neuron*, *43*, 609-617.

Chklovskii, D.B., Mel, B.W., & Svoboda, K. (2004). Cortical rewiring and information storage. *Nature*, *431*, 782-788.

Cho, M.W., & Choi, M.Y. (2010). Brain networks: Graph theoretical analysis and development models. *International Journal of Imaging Systems and Technology*, *20*(2), 108-116. doi:10.1002/ima.20229

Chuang, K.S., Valentino, D.J., & Huang, H.K. (1991). Measurement of fractal dimension using 3-D technique. *Proceedings of SPIE* (Vol. 1445, pp. 341-347).

Cohen, R., Erez, K., Ben-Avraham, D., & Havlin, S. (2000). Resilience of the internet to random breakdowns. *Physical Review Letters*, *85*(21), 4626-4628.

Colibazzi, T., Zhu, H., Bansal, R., Schultz, R.T., Wang, Z., & Peterson, B.S. (2008). Latent volumetric structure of the human brain: exploratory factor analysis and structural equation modeling of gray matter volumes in healthy children and adults. *Human Brain Mapping*, *29*(11), 1302-1312. doi:10.1002/hbm.20466

Cook, M.J., Free, S.L., Manford, M.R.A., Fish, D.R., Shorvon, S.D., & Stevens, J.M. (1995). Fractal description of cerebral cortical patterns in frontal lobe epilepsy. *European Neurology*, *35*(6), 327-335.

Correll, C.U., Hauser, M., Auther, A.M., & Cornblatt, B.A. (2010). Research in people with psychosis risk syndrome: a review of the current evidence and future directions. *Journal of Child Psychology and Psychiatry*, *51*(4), 390-431. doi:10.1111/j.1469-7610.2010.02235.x

Dai, D., He, H., Vogelstein, J., & Hou, Z. (2011). Network-based classification using cortical thickness of AD patients. In K. Suzuki, F. Wang, S. Dinggang, & Y. Pingkun (Eds.), *Machine Learning in Medical Imaging* (pp. 193-200). Springer Berlin / Heidelberg.

Dazzan, P., Soulsby, B., Mechelli, A., Wood, S.J., Velakoulis, D., Phillips, L.J., Yung, A.R., et al. (2011). Volumetric abnormalities predating the onset of schizophrenia and affective psychoses: An MRI study in subjects at ultrahigh risk of psychosis. *Schizophrenia Bulletin*, 1-9. doi:10.1093/ schbul/sbr035

DeLisi, L.E. (2008). The concept of progressive brain change in schizophrenia: implications for understanding schizophrenia. *Schizophrenia Bulletin*, *34* (2), 312-321. doi:10.1093/schbul/sbm164

Delisi, L.E., Szulc, K.U., Bertisch, H., Majcher, M., Brown, K., Bappal, A., Branch, C.A., et al. (2006). Early detection of schizophrenia by diffusion weighted imaging. *Psychiatry Research: Neuroimaging*, *148*, 61 - 66. doi: 10.1016/j.pscychresns.2006.04.010

Deshpande, G., LaConte, S., James, G.A., Peltier, S., & Hu, X. (2009). Multivariate granger causality analysis of fMRI data. *Human Brain Mapping*, *30*, 1361-1373. doi:10.1002/hbm.20606

Dice, L.R. (1945). Measures of the amount of ecologic association between species. *Ecology*, *23*(3), 297-302.

Dijkstra, E.W. (1959). A note on two problems in connexion with graphs. *Numerische Mathematik*, *1*, 269-271.

Diwadkar, V.A., Montrose, D.M, Dworakowski, D., Sweeney, J. A., & Keshavan, M.S. (2006). Genetically predisposed offspring with schizotypal features:

An ultra high-risk group for schizophrenia? *Progress in Neuro-Psychopharmacology & Biology*, *30*, 230 - 238. doi:10.1016/j.pnpbp. 2005.10.019

Dombrowski, S.M., Hilgetag, C.C., & Barbas, H. (2001). Quantitative architecture distinguishes prefrontal cortical systems in the rhesus monkey. *Cerebral Cortex*, *11*(10), 975-988.

Dosenbach, N.U.F., Fair, D.A., Miezin, F.M., Cohen, A.L., Wenger, K.K., Dosenbach, R.A.T., Fox, M.D., et al. (2007). Distinct brain networks for adaptive and stable task control in humans. *Proceedings of the National Academy of Sciences of the United States of America*, *104*(26), 11073-11078.

Douaud, G., Mackay, C., Andersson, J., James, S., Quested, D., Ray, M.K., Connell, J., et al. (2009). Schizophrenia delays and alters maturation of the brain in adolescence. *Brain*, *132*, 2437-2448. doi:10.1093/brain/awp126

Draganski, B., Gaser, C, Busch, V., Schuierer, G., Bogdahn, U., & May, A. (2004). Neuroplasticity: Changes in grey matter induced by training. *Nature*, *427*, 311-312. doi:10.1038/427311a

Díaz-Uriarte, R., & Alvarez de Andrés, S. (2006). Gene selection and classification of microarray data using random forest. *BMC Bioinformatics*, *7*. doi:10.1186/1471-2105-7-3

Efron, B., & Tibshirani, R. (1997). Improvements on cross-validation: The . 632+ bootstrap method. *Journal of the American Statistical Association*, *92*(438), 548- 560.

Eguiluz, V.M., Chialvo, D.R., Cecchi, G.A., Baliki, M, & Apkarian, A.V. (2005). Scale-free brain functional networks. *Physical Review Letters*, *94*(1), 018102:1--4. doi:10.1103/PhysRevLett.94.018102

Erdős, P., & Rényi, A. (1960). On the evolution of random graphs. *Publications of the Mathematical Institute of the Hungarian Academy of Sciences*, *5*, 17-61. Retrieved from http://citeseerx.ist.psu.edu/viewdoc/download? doi=10.1.1.153.5943&rep=rep1&type=pdf

van Essen, D.C. (1997). A tension-based theory of morphogenesis and compact wiring in the central nervous system. *Nature*, *385*, 313-318.

Esteban, F.J., Sepulcre, J., de Miras, J.R., Navas, J., Vélez de Mendizábal, N., Goñi, J., Quesada, J.M., et al. (2009). Fractal dimension analysis of grey matter in multiple sclerosis. *Journal of the Neurological Sciences*, *282* (1-2), 67-71. doi:10.1016/j.jns.2008.12.023

Evans, A.C., Lee, J.M., Kim, S.I., Fukuda, H., Kawashima, R., He, Y., Jiang, T., et al. (2008). Human cortical anatomical networks assessed by structural MRI. *Brain Imaging and Behavior*, *2*(4), 289-299. doi:10.1007/ s11682-008-9034-3

Fair, D.A., Cohen, A.L., Power, J.D., Dosenbach, N.U.F., Church, J.A., Miezin, F.M., Schlaggar, B.L., et al. (2009). Functional brain networks develop from a "local to distributed" organization. *PLoS Computational Biology*, *5* (5), e1000381:1-14. doi:10.1371/journal.pcbi.1000381

Falkai, P., Honer, W.G., Kamer, T., Dustert, S., Vogeley, K., Schneider-Axmann, T., Dani, I., et al. (2007). Disturbed frontal gyrification within families affected with schizophrenia. *Journal of Psychiatric Research*, *41*, 805-813. doi:10.1016/j.jpsychires.2006.07.018

Fan, Y., Shi, F., Keith, J., Lin, W., Gilmore, J.H., & Shen, D. (2011). Brain anatomical networks in early human brain development. *NeuroImage*, *54* (3), 1862-1871. doi:10.1016/j.neuroimage.2010.07.025

Feinberg, I. (1983). Schizophrenia: Caused by a fault in programmed synaptic elimination during adolescence? *Journal of Psychiatric Research*, *17*(4), 319-334.

Ferrarini, L, Veer, I., Baerends, E., van Tol, M.-J., Renken, R.J., van der Wee, N.J.A., Veltman, D.J., et al. (2009). Hierarchical functional modularity in the resting-state human brain. *Human Brain Mapping*, *30*, 2220-2231.

Ferrarini, L., Veer, I.M., van Lew, B., Oei, N.Y.L., van Buchem, M.A., Reiber, J.H.C., Rombouts, S.A.R.B., et al. (2011). Non-parametric model selection for subject-specific topological organization of resting-state functional connectivity. *NeuroImage*, *56*(3), 1453-1462. doi:10.1016/j.neuroimage.2011.02.028

Fischl, B., & Dale, A.M. (2000). Measuring the thickness of the human cerebral cortex from magnetic resonance images. *Proceedings of the National Academy of Sciences of the United States of America*, *97*(20), 11050-11055. doi:10.1073/pnas.200033797

Fisher, R. A. (1921). On the "probable error" of a coefficient of correlation deduced from a small sample. *Metron*, *1*, 1-32.

Florack, L. M. J., Haar Romeny, ter, B. M., Koenderink, J. J., & Viergever, M. A. (1992). Scale and the differential structure of images. *Image and Vision Computing, 10*, 376–388.

da Fontoura Costa, L. (2005). Sznajd complex networks. *International Journal of Modern Physics C*, *16*(7), 1001-1016.

da Fontoura Costa, L., & Manoel, E.T.M. (2003). A percolation approach to neural morphometry and connectivity. *Neuroinformatics*, *1*, 65-80.

da Fontoura Costa, L., Barbosa, M.S., Coupez, V., & Stauffer, D. (2003). Morphological Hopfield networks. *Brain and Mind*, *4*, 91-105.

Fornito, A., Zalesky, A., & Bullmore, E.T. (2010). Network scaling effects in graph analytic studies of human resting-state fMRI data. *Frontiers in Systems Neuroscience*, *4*, 22:1-16. doi:10.3389/fnsys.2010.00022

Franco, A. R., Pritchard, A., Calhoun, V. D., & Mayer, A. R. (2009). Interrater and intermethod reliability of default mode network selection. *Human Brain Mapping, 30*, 2293–2303. doi:10.1002/hbm.20668

Fransson, P., Aden, U., Blennow, M., & Lagercrantz, H. (2011). The functional architecture of the Infant brain as revealed by resting-state fMRI. *Cerebral Cortex*, *21*(1), 145-154. doi:10.1093/cercor/bhq071

Frederikse, M., Lu, A., Aylward, E., Barta, P., Sharma, Tonmoy, & Pearlson, G. (2000). Sex differences in inferior parietal lobule volume in schizophrenia. *American Journal of Psychiatry*, *157*, 422-427.

Free, S.L., Sisodiya, S.M., Cook, M.J., Fish, D.R., & Shorvon, S.D. (1996). Three-dimensional fractal analysis of the white matter surface from magnetic resonance images of the human brain. *Cerebral Cortex*, *6*(6), 830-836.

Freeman, L.C. (1977). A set of measures of centrality based on betweenness. *Sociometry*, *40*(1), 35-41.

Friston, K.J., & Frith, C.D. (1995). Schizophrenia: A disconnection syndrome? *Clinical Neuroscience*, *3*(2), 89-97.

Friston, K.J. (1998). The disconnection hypothesis. *Schizophrenia Research*, *30*, 115-125.

Fusar-Poli, P., Borgwardt, S., Crescini, A., Deste, G., Kempton, M.J., Lawrie, S., McGuire, P, et al. (2010). Neuroanatomy of vulnerability to psychosis: A voxel-based meta-analysis. *Neuroscience and Biobehavioral Reviews*, *35*(5), 1175-1185. doi:10.1016/j.neubiorev.2010.12.005

Fusar-Poli, P, Broome, M.R., Woolley, J.B., Johns, L.C., Tabraham, P, Bramon, E, Valmaggia, L., et al. (2011). Altered brain function directly related to structural abnormalities in people at ultra high risk of psychosis: Longitudinal VBM-fMRI study. *Journal of Psychiatric Research*, *45*(2), 190-198. doi:10.1016/j.jpsychires.2010.05.012

Fusar-Poli, P., Crossley, N., Woolley, J., Carletti, F., Perez-iglesias, R., Broome, M., Johns, L., et al. (2011). Gray matter alterations related to P300 abnormalities in subjects at high risk for psychosis: Longitudinal MRI-EEG study. *NeuroImage*, *55*(1), 320-328. doi:10.1016/j.neuroimage.2010.11.075

Gerloff, C., & Hallett, M. (2010). Big news from small world networks after stroke. *Brain*, *133*(4), 952-956.

Geyer, S., Schleicher, A, & Zilles, K. (1999). Areas 3a, 3b, and 1 of human primary somatosensory cortex. *NeuroImage*, *10*(1), 63-83. doi:10.1006/nimg.1999.0440

Giedd, J.N., Blumenthal, J., Jeffries, N.O., Castellanos, F.X., Liu, H, Zijdenbos, A, Paus, T., et al. (1999). Brain development during childhood and adolescence: A longitudinal MRI study. *Nature Neuroscience*, *2*, 861-863.

Ginestet, C.E., & Simmons, A. (2011). Statistical parametric network analysis of functional connectivity dynamics during a working memory task. *NeuroImage*, *55*(2), 688-704. doi:10.1016/j.neuroimage.2010.11.030

Goghari, V.M., Rehm, K., Carter, C.S., & MacDonald, A.W. (2007). Sulcal thickness as a vulnerability indicator for schizophrenia. *The British Journal of Psychiatry*, *191*(3), 229-233. doi:10.1192/bjp.bp.106.034595

Goghari, V.M., Rehm, K., Carter, C.S., & MacDonald, A.W. (2007). Regionally specific cortical thinning and gray matter abnormalities in the healthy relatives of schizophrenia patients. *Cerebral Cortex*, *17*(2), 415-424. doi:10.1093/cercor/bhj158

Gogtay, N., Sporn, A., Clasen, L.S., Greenstein, D., Giedd, J.N., Lenane, M., Gochman, P.A., et al. (2003). Structural brain MRI abnormalities in healthy siblings of patients with childhood-onset schizophrenia. *American Journal of Psychiatry*, *160*(3), 549-571.

Goldman, P.S., & Galkin, T.W. (1978). Prenatal removal of frontal association cortex in the fetal rhesus monkey: anatomical and functional consequences in postnatal life. *Brain Research*, *152*(3), 451-485.

Gong, G., He, Y., Concha, L., Lebel, C., Gross, D. W., Evans, A. C., & Beaulieu, C. (2009). Mapping anatomical connectivity patterns of human cerebral cortex using in vivo diffusion tensor imaging tractography. *Cerebral cortex (New York, N.Y.: 1991)*, *19*(3), 524-36. doi:10.1093/cercor/bhn102

Gong, G., Rosa-Neto, P., Carbonell, F., Chen, Z.J., He, Y., & Evans, A.C. (2009). Age- and gender-related differences in the cortical anatomical network. *The Journal of Neuroscience*, *29*(50), 15684 -15693. doi:10.1523/JNEUROSCI.2308-09.2009

Gong, G., He, Y., & Evans, A.C. (2011). Brain connectivity: Gender makes a difference. *The Neuroscientist*, 1-17. doi:10.1177/1073858410386492

Gong, G., He, Y., Chen, Z.J., & Evans, A.C. (2011). Convergence and divergence of thickness correlations with diffusion connections across the human cerebral cortex. *NeuroImage*. doi:10.1016/j.neuroimage.2011.08.017

Gountouna, V.-E., Job, D.E., McIntosh, A.M, Moorhead, T.W.J., Lymer, G.K.L., Whalley, H.C., Hall, J., et al. (2010). Functional Magnetic Resonance Imaging (fMRI) reproducibility and variance components across visits and

scanning sites with a finger tapping task. *NeuroImage*, *49*(1), 552-560. doi: 10.1016/j.neuroimage.2009.07.026

Green, S.B. (1991). How many subjects does it take to do a regression analysis. *Multivariate Behavioral Research*, *26*(3), 499-510. doi:10.1207/ s15327906mbr2603_7

Greicius, M.D, Krasnow, B., Reiss, A.L., & Menon, V. (2003). Functional connectivity in the resting brain: A network analysis of the default mode hypothesis. *Proceedings of the National Academy of Sciences of the United States of America*, *100*(1), 253-258. doi:10.1073/pnas.0135058100

Greicius, M.D., Supekar, K., Menon, V., & Dougherty, R.F. (2009). Resting-state functional connectivity reflects structural connectivity in the default mode network. *Cerebral Cortex*, *19*(1), 72-78. doi:10.1093/cercor/bhn059

Ha, T.H., Yoon, U., Lee, K.J., Shin, Y.W., Lee, J.-M., Kim, I.Y., Ha, K.S., et al. (2005). Fractal dimension of cerebral cortical surface in schizophrenia and obsessive-compulsive disorder. *Neuroscience Letters*, *384*, 172-176. doi: 10.1016/j.neulet.2005.04.078

Hafner, H., Maurer, K., Löffler, W., & Riecher-Rössler, A. (1993). The influence of age and sex on the onset and early course of schizophrenia. *The British Journal of Psychiatry*, *162*(1), 80-86. doi:10.1192/bjp.162.1.80

Hagmann, P., Kurant, M., Gigandet, X., Thiran, P., Wedeen, V.J., Meuli, R., & Thiran, J.-P. (2007). Mapping human whole-brain structural networks with diffusion MRI. *PloS One*, *2*(7), e597:1-9. doi:10.1371/journal.pone. 0000597

Hagmann, P., Cammoun, L., Gigandet, X., Meuli, R., Honey, C. J., Wedeen, V. J., & Sporns, O. (2008). Mapping the structural core of human cerebral cortex. *PLoS Biology*, *6*(7), e159. doi:10.1371/journal.pbio.0060159

Harris, J.M, Yates, S., Miller, P., Best, J.J.K, Johnstone, E.C., & Lawrie, S.M. (2004). Gyrification in first-episode schizophrenia: A morphometric study. *Biological Psychiatry*, *55*(2), 141-147.

Harris, J.M., Whalley, H., Yates, S., Miller, P., Johnstone, E.C., & Lawrie, S.M. (2004). Abnormal cortical folding in high-risk individuals: A predictor of the development of schizophrenia? *Biological Psychiatry*, *56*, 182-189. doi: 10.1016/j.biopsych.2004.04.007

Harrison, P.J. (1999). The neuropathology of schizophrenia: A critical review of the data and their interpretation. *Brain*, *122*(4), 593-624. doi:10.1093/brain/ 122.4.593

Hayasaka, S., & Laurienti, P.J. (2010). Comparison of characteristics between region-and voxel-based network analyses in resting-state fMRI data. *NeuroImage*, *50*(2), 499-508. doi:10.1016/j.neuroimage.2009.12.051

He, Y., & Evans, A. (2010). Graph theoretical modeling of brain connectivity. *Current Opinion in Neurology*, *23*(4), 341-350. doi:10.1097/WCO. 0b013e32833aa567

He, Y., Chen, Z.J., & Evans, A.C. (2007). Small-world anatomical networks in the human brain revealed by cortical thickness from MRI. *Cerebral Cortex*, *17* (10), 2407-2419. doi:10.1093/cercor/bhl149

He, Y., Chen, Z., & Evans, A. (2008). Structural insights into aberrant topological patterns of large-scale cortical networks in Alzheimer's disease. *The Journal of Neuroscience*, *28*(18), 4756-4766. doi:10.1523/JNEUROSCI. 0141-08.2008

He, Y., Chen, Z., Gong, G., & Evans, A. (2009). Neuronal networks in Alzheimer's disease. *The Neuroscientist*, *15*(4), 333-350. doi: 10.1177/1073858409334423

He, Y., Dagher, A., Chen, Z., Charil, A., Zijdenbos, A., Worsley, K., & Evans, A. (2009). Impaired small-world efficiency in structural cortical networks in multiple sclerosis associated with white matter lesion load. *Brain*, *132*, 3366-3379. doi:10.1093/brain/awp089

He, Y., Wang, J., Wang, L., Chen, Z.J., Yan, C., Yang, H., Tang, H., et al. (2009). Uncovering Intrinsic Modular Organization of Spontaneous Brain Activity in Humans. *PLoS One*, *4*(4), e5226:1-18. doi:10.1371/journal.pone. 0005226

Hilgetag, C.C, & Barbas, H. (2005). Developmental mechanics of the primate cerebral cortex. *Anatomy and Embryology*, *210*, 411-417. doi:10.1007/ s00429-005-0041-5

Hilgetag, C.C, & Barbas, H. (2006). Role of mechanical factors in the morphology of the primate cerebral cortex. *PLoS computational biology*, *2* (3), e22: 0146-0159. doi:10.1371/journal.pcbi.0020022

Ho, B.-C. (2007). MRI brain volume abnormalities in young, nonpsychotic relatives of schizophrenia probands are associated with subsequent prodromal symptoms. *Schizophrenia Research*, *96*, 1 - 13. doi:10.1016/ j.schres.2007.08.001

Hodges, A., Byrne, M., Grant, E., & Johnstone, E. (1999). People at risk of schizophrenia. Sample characteristics of the first 100 cases in the Edinburgh High-Risk Study. *The British journal of Psychiatry*, *174*, 547-553.

Honea, R.A., Meyer-Lindenberg, A., Hobbs, K.B., Pezawas, L., Mattay, V.S., Egan, M.F., Verchinski, B., et al. (2008). Is gray matter volume an intermediate phenotype for schizophrenia? A voxel-based morphometry study of patients with schizophrenia and their healthy siblings. *Biological Psychiatry*, *63*, 465-474. doi:10.1016/j.biopsych.2007.05.027

Honey, C.J., Sporns, O., Cammoun, L., Gigandet, X., Thiran, J.P., Meuli, R., & Hagmann, P. (2009). Predicting human resting-state functional connectivity from structural connectivity. *Proceedings of the National Academy of Sciences of the United States of America*, *106*(6), 2035-2040. doi:10.1073/pnas.0811168106

Honey, C.J., & Sporns, O. (2008). Dynamical consequences of lesions in cortical networks. *Human Brain Mapping*, *29*(7), 802-809. doi:10.1002/hbm.20579

Honey, C.J., Kötter, R., Breakspear, M., & Sporns, O. (2007). Network structure of cerebral cortex shapes functional connectivity on multiple time scales. *Proceedings of the National Academy of Sciences of the United States of America*, *104*(24), 10240-10245. doi:10.1073/pnas.0701519104

Honey, C.J., Thivierge, J.-P., & Sporns, O. (2010). Can structure predict function in the human brain? *NeuroImage*, *52*(3), 766-776. doi:10.1016/j.neuroimage.2010.01.071

Horwitz, B., Warner, B., Fitzer, J., Tagamets, M.-A, Husain, F.T., & Long, T.W. (2005). Investigating the neural basis for functional and effective connectivity. Application to fMRI. *Philosophical Transactions of the Royal Society of London. Series B, Biological Sciences*, *360*, 1093-1108. doi:10.1098/rstb.2005.1647

Hou, Z. (2006). A review on MR Image intensity inhomogeneity correction. *Int J Biomed Imag*, 2006. doi:10.1155/IJBI/2006/49515

Huang, X., Pan, W., Grindle, S., Han, X., Chen, Y., Park, S.J., Miller, L.W., et al. (2005). A comparative study of discriminating human heart failure etiology using gene expression profiles. *BMC Bioinformatics*, *6*(1), 205:1--15. doi:10.1186/1471-2105-6-205

Hulshoff Pol, H.E., Schnack, H.G., Mandl, R.C.W., van Haren, N.E.M., Koning, H., Collins, D.L., Evans, A.C., et al. (2001). Focal gray matter density changes in schizophrenia. *Archives of General Psychiatry*, *58*(12), 1118-1125. doi:10.1001/archpsyc.58.12.1118

Hulshoff Pol, H.E., Schnack, H.G., Mandl, C.W., Brans, R.G.H., van Haren, N.E.M, Baaré, W.F.C., van Oel, C.J., et al. (2006). Gray and white matter density changes in monozygotic and same-sex dizygotic twins discordant for schizophrenia using voxel-based morphometry. *Human Brain Mapping*, *31*, 482 - 488.

Humphries, M.D., Gurney, K., & Prescott, T.J. (2006). The brainstem reticular formation is a small-world, not scale-free, network. *Proceedings of the Royal Society. Series B: Biological Sciences*, *273*, 503-511. doi:10.1098/rspb.2005.3354

Hyde, K.L., Lerch, J., Norton, A., Forgeard, M., Winner, E., Evans, A.C., & Schlaug, G. (2009). Musical training shapes structural brain development.

The Journal of Neuroscience, *29*(10), 3019 -3025. doi:10.1523/ JNEUROSCI.5118-08.2009

Hänggi, J., Wotruba, D., & Jäncke, L. (2011). Globally altered structural brain network topology in grapheme-color synesthesia. *The Journal of Neuroscience*, *31*(15), 5816-5828.

Im, K., Lee, J.-M., Lyttelton, O., Kim, S.H., Evans, A.C., & Kim, S.I. (2008). Brain size and cortical structure in the adult human brain. *Cerebral Cortex*, *18*(9), 2181-2191. doi:10.1093/cercor/bhm244

Im, K., Lee, J.-M., Yoon, U., Shin, Y.-W., Hong, S.B., Kim, I.Y., Kwon, J.S., et al. (2006). Fractal dimension in human cortical surface: multiple regression analysis with cortical thickness, sulcal depth, and folding area. *Human Brain Mapping*, *27*(12), 994-1003. doi:10.1002/hbm.20238

Iturria-Medina, Y., Pérez Fernández, A., Morris, D.M., Canales-Rodríguez, E.J., Haroon, H.A., García Pentón, L., Augath, M., et al. (2011). Brain hemispheric structural efficiency and interconnectivity rightward asymmetry in human and nonhuman primates. *Cerebral Cortex*, *21*(1), 56-67. doi:10.1093/cercor/bhq058

Iturria-Medina, Y., Sotero, R.C., Canales-Rodríguez, E.J., Alemán-Gómez, Y., & Melie-García, L. (2008). Studying the human brain anatomical network via diffusion-weighted MRI and Graph Theory. *NeuroImage*, *40*(3), 1064-1076. doi:10.1016/j.neuroimage.2007.10.060

Jablensky, A. (1995). Schizophrenia: Recent epidemiologic issues. *Epidemiologic Reviews*, *17*(1), 10-20.

Jacobson, S., Kelleher, I., Harley, M., Murtagh, A., Clarke, M., Blanchard, M., Connolly, C., et al. (2010). Structural and functional brain correlates of subclinical psychotic symptoms in 11 – 13 year old schoolchildren. *NeuroImage*, *49*(2), 1875-1885. doi:10.1016/j.neuroimage.2009.09.015

Jehee, J.F.M., & Murre, J.M.J. (2008). The scalable mammalian brain: emergent distributions of glia and neurons. *Biological Cybernetics*, *98*, 439-445. doi: 10.1007/s00422-008-0228-y

Jelinek, H.F., & Fernandez, E. (1998). Neurons and fractals: How reliable and useful are calculations of fractal dimensions? *Journal of Neuroscience Methods*, *81*, 9-18.

Jernigan, T.L., Trauner, D.A., Hesselink, J.R., & Tallal, P.A. (1991). Maturation of human cerebrum observed in vivo during adolescence. *Brain*, *114*, 2037-2049.

Jiang, J., Zhu, W., Shi, F., Zhang, Y., Lin, L., & Jiang, T. (2008). A robust and accurate algorithm for estimating the complexity of the cortical surface. *Journal of Neuroscience Methods*, *172*(1), 122-130. doi:10.1016/ j.jneumeth.2008.04.018

Job, D.E., Whalley, H.C, McIntosh, A.M, Owens, D.G.C., Johnstone, E.C., & Lawrie, S.M. (2006). Grey matter changes can improve the prediction of schizophrenia in subjects at high risk. *BMC Medicine*, *4*, e29:1-4. doi: 10.1186/1741-7015-4-29

Job, D.E., Whalley, T.H.C., Johnstone, E.C, & Lawrie, S.M. (2005). Grey matter changes over time in high risk subjects developing schizophrenia. *NeuroImage*, *25*, 1023 - 1030. doi:10.1016/j.neuroimage.2005.01.006

Johnstone, E C. (2005). Predicting schizophrenia: Findings from the Edinburgh High-Risk Study. *The British Journal of Psychiatry*, *186*(1), 18-25. doi: 10.1192/bjp.186.1.18

Johnstone, E.C, Frith, C.D, Crow, T.J, Husband, J., & Kreel, L. (1976). Cerebral ventricular size and cognitive impairment in chronic schizophrenia. *The Lancet*, *308*(7992), 924-926.

Johnstone, E.C, Owens, D.G.C, Hoare, P., Gaur, S., Spencer, M. D., Harris, J., Stanfield, A.W., et al. (2007). Schizotypal cognitions as a predictor of psychopathology in adolescents with mild intellectual impairment. *The British Journal of Psychiatry*, *191*(6), 484-492. doi:10.1192/bjp.bp. 106.033514

Johnstone, E.C., Abukmeil, S.S., Byrne, M., Clafferty, R., Grant, E., Hodges, A., Lawrie, S.M., et al. (2000). Edinburgh high risk study — findings after four years: Demographic , attainment and psychopathological issues. *Schizophrenia Research*, *46*, 1-15.

Jou, R.J., Hardan, A.Y., & Keshavan, M.S. (2005). Reduced cortical folding in individuals at high risk for schizophrenia: A pilot study. *Schizophrenia Research*, *75*, 309 - 313. doi:10.1016/j.schres.2004.11.008

Jung, W.H., Jang, J.H., Byun, M.S., An, S.K., & Kwan, J.S. (2010). Structural brain alterations in individuals at ultra-high risk for psychosis: A review of magnetic resonance imaging studies and future directions. *Journal of Korean Medical Science*, *25*, 1700-1709. doi:10.3346/jkms. 2010.25.12.1700

Jung, W.H., Kim, J.S., Jang, J.H., Choi, J.-S., Jung, M.H., Park, J.-Y., Han, J.Y., et al. (2010). Cortical thickness reduction in individuals at ultra-high-risk for psychosis. *Schizophrenia Bulletin*, *37*(4), 839-849. doi:10.1093/schbul/ sbp151

Kaiser, M. (2011). A tutorial in connectome analysis: Topological and spatial features of brain networks. *NeuroImage*, *57*(3), 892-907. doi:10.1016/ j.neuroimage.2011.05.025

Kaufman, L., Kramer, D. M., Crooks, L. E., & Ortendahl, D. A. (1989). Measuring signal-to-noise ratios in MR imaging. Radiology, 173, 265–267.

Kennedy, D.N., Lange, N., Makris, N., Bates, J., Meyer, J., & Caviness, V.S. (1998). Gyri of the human neocortex: An MRI-based analysis of volume and variance. *Cerebral Cortex*, *8*(4), 372-384.

Keshavan, M.S., Montrose, D.M., Pierri, J.N., Dick, E.L., Rosenberg, D.R., Talagala, L., & Sweeney, J.A. (1997). Magnetic resonance imaging and spectroscopy in offspring at risk for schizophrenia: Preliminary studies. *Progress in Neuro-Psychopharmacology & Biological Psychiatry*, *21*, 1285-1295.

King, R.D., George, A.T., Jeon, T., Hynan, L.S., Youn, T.S., Kennedy, D.N., Dickerson, B., et al. (2009). Characterization of atrophic changes in the cerebral cortex using fractal dimensional analysis. *Brain Imaging and Behavior*, *3*(2), 154-166. doi:10.1007/s11682-008-9057-9

Kiselev, V.G., Hahn, K.R., & Auer, D.P. (2003). Is the brain cortex a fractal? *NeuroImage*, *20*(3), 1765-1774. doi:10.1016/S1053-8119(03)00380-X

Klyachko, V.A., & Stevens, C.F. (2003). Connectivity optimization and the positioning of cortical areas. *Proceedings of the National Academy of Sciences of the United States of America*, *100*(13), 7937-7941. doi:10.1073/pnas.0932745100

Koenderink, J. J. (1984). The structure of images. *Biological Cybernetics, 50*, 363–370.

Kolb, B., Gibb, R., & van der Kooy, D. (1994). Neonatal frontal cortical lesions in rats alter cortical structure and connectivity. *Brain Research*, *645*(1-2), 85-97.

Kulynych, J.J., Luevano, L.F., Jones, Douglas W., & Weinberger, D.R. (1997). Cortical abnormality in schizophrenia: An in vivo application of the gyrification index. *Biological Psychiatry*, *41*, 995-999.

Kuperberg, G.R., Broome, M.R., McGuire, P.K., David, A.S., Eddy, M., Ozawa, F., Goff, D., et al. (2003). Regionally localized thinning of the cerebral cortex in schizophrenia. *Archives of General Psychiatry*, *60*(9), 878-888.

Latora, V., & Marchiori, M. (2001). Efficient behavior of small-world networks. *Physical Review Letters*, *87*(19), 198701(1-4). doi:10.1103/PhysRevLett.87.198701

Lawrie, S.M., McIntosh, A.M., Hall, J., Owens, D.G.C., & Johnstone, E.C. (2008). Brain structure and function changes during the development of schizophrenia: The evidence from studies of subjects at increased genetic risk. *Schizophrenia Bulletin*, *34*(2), 330-340. doi:10.1093/schbul/sbm158

Lawrie, S.M., Whalley, H., Kestelman, J.N., Abukmeil, S.S., Byrne, M., Hodges, A., Rimmington, J.E., et al. (1999). Magnetic resonance imaging of brain in people at high risk of developing schizophrenia. *Lancet*, *353*(9146), 30-33. doi:10.1016/S0140-6736(98)06244-8

Lawrie, S.M., Whalley, H.C., Abukmeil, S.S., Kestelman, J.N., Donnelly, L., Miller, P., Best, J.J.K., et al. (2001). Brain structure, genetic liability, and psychotic symptoms in subjects at high risk of developing schizophrenia. *Biological Psychiatry*, *49*, 811-823.

Lerch, J.P, Worsley, K., Shaw, W.P., Greenstein, D.K., Lenroot, R.K., Giedd, J., & Evans, A.C. (2006). Mapping anatomical correlations across cerebral cortex (MACACC) using cortical thickness from MRI. *NeuroImage*, *31*(3), 993-1003. doi:10.1016/j.neuroimage.2006.01.042

Lewis, J. (1995). Fast normalized cross-correlation. *Vision Interface*. Retrieved from http://citeseerx.ist.psu.edu/viewdoc/download?doi=10.1.1.21.6062&rep=rep1&type=pdf

Li, H., Xue, Z., Cui, K., & Wong, S.T.C. (2011). Diffusion tensor-based fast marching for modeling human brain connectivity network. *Computerized Medical Imaging and Grapics*, *35*(3), 167-178. doi:10.1016/j.compmedimag.2010.07.008

Li, Y., Liu, Y., Li, J., Qin, W., Li, K., Yu, C., & Jiang, T. (2009). Brain anatomical network and intelligence. *PLoS Computational Biology*, *5*(5), e1000395:1-17. doi:10.1371/journal.pcbi.1000395

Liao, W., Ding, J., Marinazzo, D., Xu, Q., Wang, Z, Yuan, C., Zhang, Z., et al. (2011). Small-world directed networks in the human brain: Multivariate Granger causality analysis of resting-state fMRI. *NeuroImage*, *54*, 2683-2694.

Liaw, A., & Wiener, M. (2002). Classification and regression by randomForest. *RNews*, *2*, 18-22.

Lindeberg, T. (1993). Discrete derivative approximations with scale-space properties: A basis for low-level feature extraction. *Journal of Mathematical Imaging and Vision, 3*, 349–376.

Liu, Y., Liang, M., Zhou, Y., He, Y., Hao, Y., Song, M., Yu, C., et al. (2008). Disrupted small-world networks in schizophrenia. *Brain*, *131*, 945-961. doi:10.1093/brain/awn018

Lo, C.-Yi, Wang, P.-N., Chou, K.-H., Wang, J., He, Y., & Lin, C.-P. (2010). Diffusion tensor tractography reveals abnormal topological organization in structural cortical networks in Alzheimer's disease. *The Journal of Neuroscience*, *30*(50), 16876 -16885. doi:10.1523/JNEUROSCI.4136-10.2010

Lord, L.-D., Allen, P., Expert, P., Howes, O., Lambiotte, R., McGuire, P., Bose, S. K., et al. (2011). Characterization of the anterior cingulate's role in the at-risk mental state using graph theory. *NeuroImage*, *56*(3), 1531-1539. doi: 10.1016/j.neuroimage.2011.02.012

Lowe, D. G. (2004). Distinctive image features from scale-invariant keypoints. *International Journal of Computer Vision*, *60*, 91–110.

Luce, R.D., & Perry, A.D. (1949). A method of matrix analysis of group structure. *Psychometrika*, *14*(1), 95-116.

Lui, S., Deng, W., Huang, X., Jiang, L., Ouyang, L., Borgwardt, S.J., Ma, X., et al. (2009). Neuroanatomical differences between familial and sporadic schizophrenia and their parents: An optimized voxel-based morphometry study. *Psychiatry Research: Neuroimaging*, *171*(2), 71-81. doi:10.1016/j.pscychresns.2008.02.004

Lv, B., Li, J., He, H., Li, M., Zhao, M., Ai, L., Yan, F., et al. (2010). Gender consistency and difference in healthy adults revealed by cortical thickness. *NeuroImage*, *53*(2), 373-382. doi:10.1016/j.neuroimage.2010.05.020

Lv, Y.-T., Yang, H., Wang, D.-Y., Li, S.-Y., Han, Y., Zhu, C.-Z., He, Y., et al. (2008). Correlations in spontaneous activity and gray matter density between left and right sensorimotor areas of pianists. *Neuroreport*, *19*(6), 631-634. doi:10.1097/WNR.0b013e3282fa6da0

Lymer, G., Job, D., William, T., Moorhead, J., McIntosh, A., Owens, D., Johnstone, E., et al. (2006). Brain-behaviour relationships in people at high genetic risk of schizophrenia. NeuroImage, 33(1), 275–285.

Lynall, M.-E., Bassett, D.S., Kerwin, R., McKenna, P.J., Kitzbichler, M., Muller, U., & Bullmore, E. (2010). Functional connectivity and brain networks in schizophrenia. *The Journal of Neuroscience*, *30*(28), 9477-9487. doi: 10.1523/JNEUROSCI.0333-10.2010

Maguire, E.A., Gadian, D.G., Johnsrude, I.S., Good, C.D., Ashburner, J., Frackowiak, R.S.J., & Frith, C.D. (2000). Navigation-related structural change in the hippocampi of taxi drivers. *Proceedings of the National Academy of Sciences of the United States of America*, *97*(8), 4398-4403.

Mainen, Z.F., & Sejnowski, T.J. (1996). Influence of dendritic structure on firing pattern in model neocortical neurons. *Nature*, *382*(6589), 363-366. doi: 10.1038/382363a0

Mandelbrot, B.B. (1967). How long is the coast of Britain? Statistical self-similarity and fractional dimension. *Science*, *156*, 636-638.

Mandelbrot, B.B. (1985). Self-affine fractals and fractal dimension. *Physica Scripta*, *32*(4), 257-260. doi:10.1088/0031-8949/32/4/001

Marcelis, M., Suckling, J., Woodruff, P., Hofman, P., Bullmore, E., & van Os, J. (2003). Searching for a structural endophenotype in psychosis using computational morphometry. *Psychiatry Research: Neuroimaging*, *122*, 153-167. doi:10.1016/S0925-4927(02)00125-7

Marín, O., & Rubenstein, J.L.R. (2003). Cell migration in the forebrain. *Annual Review of Neuroscience*, *26*, 441-483. doi:10.1146/annurev.neuro. 26.041002.131058

Maslov, S., & Sneppen, K. (2002). Specificity and stability in topology of protein networks. *Science*, *296*, 910-913. doi:10.1126/science.1065103

McAlonan, G.M., Cheung, V., Cheung, C., Suckling, J., Lam, G.Y., Tai, K.S., Yip, L., et al. (2005). Mapping the brain in autism. A voxel-based MRI study of volumetric differences and intercorrelations in autism. *Brain*, *128*, 268-276. doi:10.1093/brain/awh332

McDonald, C., Marshall, N., Sham, P.C., Bullmore, E.T., Schulze, K., Chapple, B., Bramon, E., et al. (2006). Regional brain morphometry in patients with schizophrenia or bipolar disorder and their unaffected relatives. *American Journal of Psychiatry*, *163*(3), 478-487.

McGraw, K.O., & Wong, S.P. (1996). Forming inferences about some intraclass correlation coefficients. *Psychological Methods*, *1*(1), 30-46. doi: 10.1037/1082-989X.1.1.30

McGue, M., & Gottesman, I.I. (1989). Genetic linkage in schizophrenia: Perspectives from genetic epidemiology. *Schizophrenia Bulletin*, *15*(3), 453-464.

McKeown, M. J., Uthama, A., Abugharbieh, R., Palmer, S., Lewis, M., & Huang, X. (2008). Shape (but not volume) changes in the thalami in Parkinson disease. *BMC Neurology, 8*, 8. doi:10.1186/1471-2377-8-8

McIntosh, A.M., Baig, B.J., Hall, J., Job, D., Whalley, H.C., Lymer, G.K.S., Moorhead, T.W.J., et al. (2007). Relationship of catechol-O-methyltransferase variants to brain structure and function in a population at high risk of psychosis. *Biological Psychiatry*, *61*(10), 1127-1134.

McIntosh, A.R., & Korostil, M. (2008). Interpretation of neuroimaging data based on network concepts. *Brain Imaging and Behavior*, *2*, 264-269. doi: 10.1007/s11682-008-9031-6

McIntosh, A.M., Job, D.E., Moorhead, W.J., Harrison, L.K., Whalley, H.C., Johnstone, E.C., & Lawrie, S.M. (2006). Genetic liability to schizophrenia or bipolar disorder and its relationship to brain structure. *American Journal of Medical Genetics Part B (Neuropsychiatric Genetics)*, *141B*, 76 - 83. doi:10.1002/ajmg.b.30254

McIntosh, A.M., Owens, D.C., Moorhead, W.J., Whalley, H.C, Stanfield, A.C., Hall, J., Johnstone, E.C., et al. (2011). Longitudinal volume reductions in people at high genetic risk of schizophrenia as they develop psychosis. *Biological Psychiatry*, *69*(10), 953-958. doi:10.1016/j.biopsych. 2010.11.003

Mechelli, A., Crinion, J.T., Noppeney, U., O'Doherty, J., Ashburner, J, Frackowiak, R.S., & Price, C.J. (2004). Structural plasticity in the bilingual brain. *Nature*, *431*, 757. doi:10.1038/431757a

Mechelli, A., Friston, K.J., Frackowiak, R.S., & Price, C.J. (2005). Structural covariance in the human cortex. *The Journal of neuroscience*, *25*(36), 8303-8010. doi:10.1523/JNEUROSCI.0357-05.2005

Meunier, D., Lambiotte, R., Fornito, A., Ersche, K.D., & Bullmore, E.T. (2009). Hierarchical modularity in human brain functional networks. *Frontiers in Neuroinformatics*,*3*, 37:1-12. doi:10.3389/neuro.11.037

Milgram, S. (1967). The small world problem. *Psychology Today*, *2*(1), 60-67.

Mitelman, S.A., Buchsbaum, M.S., Brickman, A.M., & Shihabuddin, L. (2005). Cortical intercorrelations of frontal area volumes in schizophrenia. *NeuroImage*, *27*(4), 753-770. doi:10.1016/j.neuroimage.2005.05.024

Modinos, G., Vercammen, A., Mechelli, A., Knegtering, H., McGuire, P.K., & Aleman, A. (2009). Structural covariance in the hallucinating brain: a voxel-based morphometry study. *Journal of Psychiatry and Neuroscience*, *34*(6), 465-469.

Moorhead, T.W.J., Gountouna, V.-E., Job, D.E., McIntosh, A.M., Romaniuk, L., Lymer, G.K.S., Whalley, H.C., et al. (2009). Prospective multi-centre voxel based morphometry study employing scanner specific segmentations: procedure development using CaliBrain structural MRI data. *BMC Medical Imaging*, *9*, 8:1-12. doi:10.1186/1471-2342-9-8

Moorhead, T.W.J., Harris, J.M., Stanfield, A.C., Job, D.E., Best, J.J.K., Johnstone, E.C., & Lawrie, S.M. (2006). Automated computation of the gyrification index in prefrontal lobes: Methods and comparison with manual implementation. *NeuroImage*, *31*, 1560 - 1566. doi:10.1016/j.neuroimage.2006.02.025

Moskowitz, A., & Heim, G. (2011). Eugen Bleuler's Dementia Praecox or the group of schizophrenias (1911): A centenary appreciation and reconsideration. *Schizophrenia Bulletin*, *37*(3), 471-479. doi:10.1093/schbul/sbr016

Muir, D.R., & Douglas, R.J. (2011). From neural arbors to daisies. *Cerebral Cortex*, *21*(5), 1118-1133. doi:10.1093/cercor/bhq184

Murray, R.M., & Lewis, S.W. (1987). Is schizophrenia a neurodevelopmental disorder? *British Medical Journal*, *295*(6600), 681-682.

Murre, J.M.J., & Sturdy, D.P.F. (1995). The connectivity of the brain: Multi-level quantitative analysis. *Biological Cybernetics*, *73*(6), 529–545.

Nakamura, T., Hillary, F.G., & Biswal, B.B. (2009). Resting network plasticity following brain injury. *PLoS One*, *4*(12), e8220:1-9. doi:10.1371/journal.pone.0008220

Narr, K.L., Bilder, R.M., Toga, A.W., Woods, R.P., Rex, D.E., Szesko, P.R., Robinson, D, et al. (2004). Mapping cortical thickness and gray matter concentration in first episode schizophrenia. *Cerebral Cortex*, *15*(6), 708-719. doi:10.1093/cercor/bhh172

Narr, K., Thompson, P., Sharma, T., Moussai, J., Zoumalan, C., Rayman, J., & Toga, A. (2001). Three-dimensional mapping of gyral shape and cortical surface asymmetries in schizophrenia: Gender effects. *The American Journal of Psychiatry*, *158*(2), 244-255.

Narr, K.L., Toga, A.W., Szeszko, P., Thompson, P.M., Woods, R.P., Robinson, D., Sevy, S., et al. (2005). Cortical thinning in cingulate and occipital cortices in first episode schizophrenia. *Biological Psychiatry*, *58*, 32- 40. doi:10.1016/j.biopsych.2005.03.043

Nenadic, I., Smesny, S., Schlo, R.G.M., Sauer, H., & Gaser, C. (2010). Auditory hallucinations and brain structure in schizophrenia: Voxel-based morphometric study. *The British Journal of Psychiatry*, *196*, 412-413. doi:10.1192/bjp.bp.109.070441

Nesvag, R., Lawyer, G., Varnäs, K., Fjell, A., Walhovd, K., Frigessi, A., Jönsson, E., et al. (2008). Regional thinning of the cerebral cortex in schizophrenia: Effects of diagnosis, age and antipsychotic medication. *Schizophrenia Research*, *98*, 16-28. doi:10.1016/j.schres.2007.09.015

Newman, M.E.J. (2003). The structure and function of complex networks. *SIAM Review*, *45*(2), 167-256. doi:10.1137/S003614450342480

Nierenberg, J., Salisbury, D.F., Levitt, J.J., David, E.A., McCarley, R.W., & Shenton, M.E. (2005). Reduced left angular gyrus volume in first-episode schizophrenia. *American Journal of Psychiatry*, *162*(8), 1539-1541.

Nikou, C., Heitz, F., & Armspach, J. (1999). Robust voxel similarity metrics for the registration of dissimilar single and multimodal images. *Pattern Recognition*, *32*(8), 1351-1368. doi:10.1016/S0031-3203(98)00167-8

Noble, W.S. (2009). How does multiple testing correction work? *Nature Biotechnology*, *27*(12), 1135-1137. Nature Publishing Group. doi:10.1038/nbt1209-1135

Ourselin, S., Roche, A., Prima, S., & Ayache, N. (2000). Block matching: A general framework to improve robustness of rigid registration of medical images. In S. Delp, A. DiGoia, & B. Jaramaz (Eds.), *Medical Image Computing and Computer-Assisted Intervention – MICCAI 2000* (pp. 557-566). Springer Berlin / Heidelberg.

Pan, W.-J., Wu, G., Li, C.-X., Lin, F., Sun, J., & Lei, H. (2007). Progressive atrophy in the optic pathway and visual cortex of early blind Chinese adults: A voxel-based morphometry magnetic resonance imaging study. *NeuroImage*, *37*(1), 212-220. doi:10.1016/j.neuroimage.2007.05.014

Pantelis, C., Velakoulis, D., McGorry, P.D., Wood, S.J., Suckling, J., Phillips, L.J., Yung, A.R., et al. (2003). Neuroanatomical abnormalities before and after onset of psychosis: A cross-sectional and longitudinal MRI comparison. *The Lancet*, *361*, 281-288.

Paus, T. (2005). Mapping brain maturation and cognitive development during adolescence. *Trends in Cognitive Sciences*, *9*(2), 60-68.

Paus, T., Tomaiuolo, F., Otaky, N., MacDonald, D., Petrides, M., Atlas, J., Morris, R., et al. (1996). Human cingulate and paracingulate sulci: Pattern, variability, asymmetry, and probabilistic map. *Cerebral Cortex*, *6*(2), 207-214.

Pearlson, G.D. (1997). Superior temporal gyrus and planum temporale in schizophrenia: A selective review. *Progress in Neuro-Psychopharmacology and Biological Psychiatry*, *21*, 1203-1229.

Peduzzi, P., Concato, J., Feinstein, A.R., & Holford, T.R. (1995). Importance of events per independent variable in proportional hazards regression analysis. II. Accuracy and precision of regression estimates. *Journal of Clinical Epidemiology*, *48*(12), 1503-1510.

Peduzzi, P., Concato, J., Kemper, E., Holford, T.R., & Feinstein, A.R. (1996). Study of the number of events per variable in logistic regression analysis. *Journal of Clinical Epidemiology*, *49*(12), 1373-1379.

Penney, G.P., Griffin, L.D., King, A.P., & Hawkes, D.J. (2008). A novel framework for multi-modal intensity-based similarity measures based on internal similarity. In J. M. Reinhardt & J. P. Pluim (Eds.), *Medical Imaging 2008: Image Processing* (Vol. 6914, p. 69140X-69140X-10). San Diego,CA, USA: Proc. of SPIE. doi:10.1117/12.769402

Penttilä, J., Paillère-Martinot, M.-L., Martinot, J.-L., Mangin, J.-F., Burke, L., Corrigall, R., Frangou, S., et al. (2008). Global and temporal cortical folding in patients with early-onset schizophrenia. *Journal of the American Academy of Child and Adolescent Psychiatry*, *47*(10), 1125-1132.

Petrella, J. (2011). Use of graph theory to evaluate brain networks: A clinical tool for a small world? *Radiology*, *259*, 317-320.

Pezawas, L., Verchinski, B.A., Mattay, V.S., Callicott, J.H., Kolachana, B.S., Straub, R.E., Egan, M.F., et al. (2004). The brain-derived neurotrophic factor val66met polymorphism and variation in human cortical morphology. *The Journal of Neuroscience*, *24*(45), 10099-10102. doi: 10.1523/JNEUROSCI.2680-04.2004

Power, J.D., Fair, D.A., Schlaggar, B.L., & Petersen, S.E. (2010). The development of human functional brain networks. *Neuron*, *67*(5), 735-748. Elsevier Inc. doi:10.1016/j.neuron.2010.08.017

Prettejohn, B., Berryman, M., & McDonnell, M.D. (2011). Methods for generating complex networks with selected structural properties for simulations: A review and tutorial for neuroscientists. *Frontiers in Computational Neuroscience*, *5*, 11:1-18. doi:10.3389/fncom.2011.00011

Prinzie, A., & van den Poel, D. (2008). Random Forests for multiclass classification: Random MultiNomial Logit. *Expert Systems with Applications*, *34*, 1721-1732. doi:10.1016/j.eswa.2007.01.029

Raichle, M.E., MacLeod, A.M., Snyder, A.Z., Powers, W.J., Gusnard, D.A., & Shulman, G.L. (2001). A default mode of brain function. *Proceedings of the National Academy of Sciences of the United States of America*, *98*(2), 676-682. doi:10.1073/pnas.98.2.676

Raj, A., Mueller, S.G., Young, K., Laxer, K.D., & Weiner, M. (2010). Network-level analysis of cortical thickness of the epileptic brain. *NeuroImage*, *52* (4), 1302-1313. doi:10.1016/j.neuroimage.2010.05.045

Rajarethinam, R., Sahni, S., Rosenberg, D.R., & Keshavan, M.S. (2004). Reduced superior temporal gyrus volume in young offspring of patients with schizophrenia. *American Journal of Psychiatry*, *161*(6), 1121-1124.

Reijneveld, J.C., Ponten, S.C., Berendse, H.W., & Stam, C.J. (2007). The application of graph theoretical analysis to complex networks in the brain. *Clinical Neurophysiology*, *118*(11), 2317-2331. doi:10.1016/j.clinph.2007.08.010

Rosanoff, A.J., & Orr, F.I. (1911). A study of heredity in insanity in the light of the mendelian theory. *American Journal of Psychiatry*, *68*, 221-261.

Rubinov, M., & Sporns, O. (2010). Complex network measures of brain connectivity: Uses and interpretations. *NeuroImage*, *52*(3), 1059-1069. doi:10.1016/j.neuroimage.2009.10.003

Rubinov, M., McIntosh, A.R., Valenzuela, M.J., & Breakspear, M. (2009). Simulation of neuronal death and network recovery in a computational model of distributed cortical activity. *The American Journal of Geriatric Psychiatry*, *17*(3), 210-217. doi:10.1097/JGP.0b013e318187137a

Russakoff, D. B., Tomasi, C., Rohlfing, T., & Maurer, C.R. (2004). Image similarity using mutual information of regions. In T. Pajdla & J. Matas (Eds.), *Computer Vision - ECCV 2004* (pp. 596-607). Springer Berlin / Heidelberg.

Rust, J. (1988). The Rust Inventory of Schizotypal Cognitions (RISC). *Schizophrenia Bulletin*, *14*, 317. National Institute of Mental Health.

Rykhlevskaia, E., Gratton, G., & Fabiani, M. (2008). Combining structural and functional neuroimaging data for studying brain connectivity: A review. *Psychophysiology*, *45*(2), 173-187. doi:10.1111/j.1469-8986.2007.00621.x

Salgado-Pineda, P., Baeza, I., Pérez, M., Vendrell, P., Junqué, C., Bargallo, N., & Bernardo, M. (2003). Sustained attention impairment correlates to gray matter decreases in first episode neuroleptic-naive schizophrenic patients. *NeuroImage*, *19*, 365-375. doi:10.1016/S1053-8119(03)00094-6

Sallet, P.C., Elkis, H., Alves, T.M., Oliveira, J.R., Sassi, E., de Castro, C.C., Busatto, G.F., et al. (2003). Reduced cortical folding in schizophrenia: An MRI morphometric study. *American Journal of Psychiatry*, *160*(9), 1606-1613.

Salvador, R., Suckling, J., Coleman, M.R., Pickar, J.D., Menon, D., & Bullmore, E. (2005). Neurophysiological architecture of functional magnetic resonance images of human brain. *Cerebral Cortex*, *15*, 1332-1342.

Sanabria-Diaz, G., Melie-García, L., Iturria-Medina, Y., Alemán-Gómez, Y., Hernández-González, G., Valdés-Urrutia, L., Galán, L., et al. (2010). Surface area and cortical thickness descriptors reveal different attributes of the structural human brain networks. *NeuroImage*, *50*(4), 1497-1510. doi: 10.1016/j.neuroimage.2010.01.028

Sandu, A.-L., Rasmussen, I.-A., Lundervold, A., Kreuder, F., Neckelmann, G., Hugdahl, K., & Specht, K. (2008). Fractal dimension analysis of MR images reveals grey matter structure irregularities in schizophrenia. *Computerized Medical Imaging and Graphics*, *32*(2), 150-158.

Sanz-Arigita, E.J., Schoonheim, M.M., Damoiseaux, J.S., Rombouts, S.A.R.B., Maris, E., Barkhof, F., Scheltens, P., et al. (2010). Loss of "small-world" networks in Alzheimer's disease: Graph analysis of fMRI resting-state functional connectivity. *PLoS One*, *5*(11), e13788:1-14. doi:10.1371/journal.pone.0013788

Schaer, M., Cuadra, M.B., Tamarit, L., Lazeyras, F., Eliez, S., & Thiran, J.-P. (2008). A surface-based approach to quantify local cortical gyrification. *IEEE Transactions on Medical Imaging*, *27*(2), 161-170.

Schlaepfer, T.E., Harris, G.J., Tien, A.Y., Peng, L.W., Lee, S., Federman, E.B., Chase, G.A., et al. (1994). Decreased regional cortical gray matter volume in schizophrenia. *American Journal of Psychiatry*, *151*(6), 842-848.

Schmitt, J.E., Lenroot, R.K., Wallace, G.L., Ordaz, S., Taylor, K.N., Kabani, N., Greenstein, D., et al. (2008). Identification of genetically mediated cortical networks: A multivariate study of pediatric twins and siblings. *Cerebral Cortex*, *18*(8), 1737-1747.

Schwarz, A.J., & Mcgonigle, J. (2011). Negative edges and soft thresholding in complex network analysis of resting state functional connectivity data. *NeuroImage*, *55*(3), 1132-1146.

Schwarzkopf, D.S., Song, C., & Rees, G. (2010). The surface area of human V1 predicts the subjective experience of object size. *Nature Neuroscience*, *14* (1), 28-30.

Seltzer, B., & Pandya, D.N. (1984). Further observations on parieto-temporal connections in the rhesus monkey. *Experimental Brain Research.*, *55*(2), 301-312.

Sepulcre, J., Liu, H., Talukdar, T., Martincorena, I., Yeo, B.T.T., & Buckner, R.L. (2010). The organization of local and distant functional connectivity in the human brain. *PLoS Computational Biology*, *6*(6), e1000808:1-15. doi: 10.1371/journal.pcbi.1000808

Shattuck, D.W., Mirza, M., Adisetiyo, V., Hojatkashani, C., Salamon, G., Narr, K. L., Poldrack, R.A, et al. (2008). Construction of a 3D probabilistic atlas of human cortical structures. *NeuroImage*, *39*(3), 1064-80. doi:10.1016/ j.neuroimage.2007.09.031

Shenton, M.E., Dickey, C.C., Frumin, M., & McCarley, R.W. (2001). A review of MRI findings in schizophrenia. *Schizophrenia Research*, *49*, 1-52.

Sheppard, J.P., Wang, J.-P., & Wong, P.C.M. (2011). Large-scale cortical functional organization and speech perception across the lifespan. *PLoS One*, *6*(1), e16510:1-13. doi:10.1371/journal.pone.0016510

Shu, N., Liu, Y., Li, K., Duan, Y., Wang, J., Yu, C., Dong, H., et al. (2011). Diffusion tensor tractography reveals disrupted topological efficiency in white matter structural networks in multiple sclerosis. *Cerebral Cortex*. doi: 10.1093/cercor/bhr039

Shu, N., Liu, Y., Li, J., Li, Y., Yu, C., & Jiang, T. (2009). Altered anatomical network in early blindness revealed by diffusion tensor tractography. *PLoS One*, *4*(9), e7228:1-13. doi:10.1371/journal.pone.0007228

Sowell, E.R., Peterson, B.S., Thompson, P.M., Welcome, S.E., Henkenius, A.L., & Toga, A.W. (2003). Mapping cortical change across the human life span. *Nature Neuroscience*, *6*(3), 309-315.

Sowell, E.R., Thompson, P.M., Leonard, C.M., Welcome, S.E., Kan, E., & Toga, A.W. (2004). Longitudinal mapping of cortical thickness and brain growth in normal children. *The Journal of Neuroscience*, *24*(38), 8223-8231.

Spoormaker, V.I., Schro, M.S., Gleiser, P.M., Andrade, K.C., Dresler, M., Wehrle, R., Sämann, P.G., et al. (2010). Development of a large-scale functional brain network during human non-rapid eye movement sleep. *The Journal of Neuroscience*, *30*(34), 11379 -11387. doi:10.1523/JNEUROSCI. 2015-10.2010

Sporns, O. (2006). Small-world connectivity, motif composition, and complexity of fractal neuronal connections. *BioSystems*, *85*, 55-64. doi:10.1016/ j.biosystems.2006.02.008

162

Sporns, O. (2009). From complex networks to intelligent systems. In E. Sendhoff, O Sporns, H. Ritter, & K. Doya (Eds.), *Creating Brain-Like Intelligence* (pp. 15-30). Berlin, Heidelberg, Germany.: Springer Verlag.

Sporns, O. (2011). The non-random brain: Efficiency, economy, and complex dynamics. *Frontiers in Computational Neuroscience*, *5*, 5:1-13. doi: 10.3389/fncom.2011.00005

Sporns, O., & Zwi, J.D. (2004). The small world of the cerebral cortex. *Neuroinformatics*, *2*(2), 145-162.

Sporns, O., Chialvo, D.R., Kaiser, M., & Hilgetag, C.C. (2004). Organization, development and function of complex brain networks. *Trends in Cognitive Sciences*, *8*(9), 418-425.

Sporns, O., Tononi, G., & Kötter, R. (2005). The human connectome: A structural description of the human brain. *PLoS Computational Biology*, *1*(4), e42: 0245-0251. doi:10.1371/journal.pcbi.0010042

Staal, W.G., Hulshoff Pol, H.E., Schnack, H.G., Hoogendoorn, M.L.C., Jellema, K., & Kahn, R.S. (2000). Structural brain abnormalities in patients with schizophrenia and their healthy siblings. *American Journal of Psychiatry*, *157*(3), 416-421.

Stam, C.J. (2010). Characterization of anatomical and functional connectivity in the brain: A complex networks perspective. *International Journal of Psychophysiology*, *77*(3), 186-194.

Stepanyants, A., & Chklovskii, D.B. (2005). Neurogeometry and potential synaptic connectivity. *Trends in Neurosciences*, *28*(7), 387-394.

Stepanyants, A., Martinez, L.M., Ferecskó, A.S., & Kisvárday, Z.F. (2009). The fractions of short- and long-range connections in the visual cortex. *Proceedings of the National Academy of Sciences of the United States of America*, *106*(9), 3555-3560.

Suddath, R.L., Christison, G.W., Torrey, E.F., Casanova, M.F., & Weinberger, D.R. (1990). Anatomical abnormalities in the brains of monozygotic twins discordant for schizophrenia. *The New England Journal of Medicine*, *322* (12), 789-794.

Sun, L., Patel, R., Liu, J., Chen, K., Wu, T., Li, J., Reiman, E., et al. (2009). *Mining brain region connectivity for Alzheimer's disease study via sparse inverse covariance estimation. Proceedings of the 15th ACM SIGKDD international conference on nowledge discovery and data mining - KDD '09* (pp. 1335-1343). New York, NY, USA: ACM Press.

Supekar, K., Menon, V., Rubin, D., Musen, M., & Greicius, M.D. (2008). Network analysis of intrinsic functional brain connectivity in Alzheimer's disease. *PLoS Computational Biology*, *4*(6), e1000100:1-11. Retrieved from http://dx.plos.org/10.1371/journal.pcbi.1000100

Supekar, K., Musen, M., & Menon, V. (2009). Development of large-scale functional brain networks in children. *PLoS Biology*, *7*(7), e1000157:1-15. doi:10.1371/journal.pbio.1000157

Sur, M., & Rubenstein, J.L.R. (2005). Patterning and plasticity of the cerebral cortex. *Science*, *310*, 805-810.

Telesford, Q.K., Morgan, A.R., Hayasaka, S., Simpson, S.L., Barret, W., Kraft, R. A., Mozolic, J.L., et al. (2010). Reproducibility of graph metrics in fMRI networks. *Frontiers in Neuroinformatics*, *4*, 117:1-10. doi:10.3389/fninf. 2010.00117

Thomas, A.G., Marrett, S., Saad, Z.S., Ruff, D.A., Martin, A., & Bandettini, P.A. (2009). Functional but not structural changes associated with learning: An exploration of longitudinal Voxel-Based Morphometry (VBM). *NeuroImage*, *48*(1), 117-125.

Thompson, P.M., Schwartz, C., Lin, R.T., Khan, A.A., & Toga, A.W. (1996). Three-dimensional statistical analysis of sulcal variability in the human brain. *The Journal of Neuroscience*, *16*(13), 4261-4274.

Thompson, P.M., Lee, A.D., Dutton, R.A., Geaga, J.A., Hayashi, K.M., Eckert, M.A., Bellugi, U., et al. (2005). Abnormal cortical complexity and thickness profiles mapped in Williams syndrome. *The Journal of Neuroscience*, *25*(16), 4146-4158.

Thompson, P., Cannon, T.D, & Toga, A.W. (2002). Mapping genetic influences on human brain structure. *Annals of Medicine*, *34*, 523-536.

Tian, L., Wang, J., Yan, C., & He, Y. (2011). Hemisphere- and gender-related differences in small-world brain networks: A resting-state functional MRI study. *NeuroImage*, *54*(1), 191-202.

Tijms, B.M., Seriès, P., Willshaw, D.J., & Lawrie, S.M. (2011). Similarity-based extraction of individual networks from gray matter MRI scans. *Cerebral Cortex*, *in press*. doi:10.1093/cercor/bhr221

Toews, M., Wells, W., III, Collins, D. L., & Arbel, T. (2010). Feature-based morphometry: Discovering group-related anatomical patterns. *NeuroImage*, *49,* 2318-2327.

Torrey, E.F. (2007). Schizophrenia and the inferior parietal lobule. *Schizophrenia Research*, *97*(1-3), 215-225.

Toro, R., & Burnod, Y. (2005). A morphogenetic model for the development of cortical convolutions. *Cerebral Cortex*, *15*, 1900-1913. doi:10.1093/cercor/ bhi068

Tzourio-Mazoyer, N., Landeau, B., Papathanassiou, D., Crivello, F., Etard, O., Delcroix, N., & Joliot, M. (2002). Automated anatomical labeling of activations in SPM using a macroscopic anatomical parcellation of the MNI

MRI single-subject brain. *NeuroImage*, *15*, 273-289. doi:10.1006/nimg. 2001.0978

Uthama, A., Abugharbieh, R., Traboulsee, A., & McKeown, M. J. (2007). Invariant SPHARM shape descriptors for complex geometry in MR region of interest analysis. Conference proceedings: Annual International Conference of the IEEE Engineering in Medicine and Biology Society. IEEE Engineering in Medicine and Biology Society. Conference, 2007, 1322–1325. doi:10.1109/IEMBS.2007.4352541

Vaessen, M.J., Hofman, P.A.M., Tijssen, H.N., Aldenkamp, A.P., Jansen, J.F.A., & Backes, W.H. (2010). The effect and reproducibility of different clinical DTI gradient sets on small world brain connectivity measures. *NeuroImage*, *51*(3), 1106-1116.

Valencia, M., Pastor, M.A., Artieda, J., Martinerie, J., & Chavez, M. (2009). Complex modular structure of large-scale brain networks. *Chaos*, *19*, 023119:1-7.

Vancourt, T., Gu, Y., & Martin, C. (2005). Three-dimensional template correlation: Object recognition in 3D voxel data. *Proceedings of the Seventh International Workshop on Computer Architecture for Machine Perception*. (pp. 1-6). Washington D.C., USA: IEEE Computer Society.

van den Heuvel, M.P., Mandl, C.W., Stam, C.J, Kahn, S., & Hulshoff Pol, H.E. (2010). Aberrant frontal and temporal complex network structure in schizophrenia: A graph theoretical analysis. *The Journal of Neuroscience*, *30*(47), 15915-15926. doi:10.1523/JNEUROSCI.2874-10.2010

van den Heuvel, M.P., Stam, C.J., Boersma, M., & Hulshoff Pol, H.E. (2008). Small-world and scale-free organization of voxel-based resting-state functional connectivity in the human brain. *NeuroImage*, *43*(3), 528-39. doi:10.1016/j.neuroimage.2008.08.010

van den Heuvel, M.P., Stam, C.J, Kahn, S., & Hulshoff Pol, H.E. (2009). Efficiency of functional brain networks and intellectual performance. *The Journal of Neuroscience*, *29*(23), 7619 -7624. doi:10.1523/JNEUROSCI. 1443-09.2009

van Haren, N.E.M., Picchioni, M.M., McDonald, C., Marshall, N., Davis, N., Ribchester, T., Hulshoff Pol, H.E., et al. (2004). A controlled study of brain structure in monozygotic twins concordant and discordant for schizophrenia. *Biological Psychiatry*, *56*, 454 - 461. doi:10.1016/ j.biopsych.2004.06.033

van Ooyen, A., Duijnhouwer, J., Remme, M.W.H., & van Pelt, J. (2002). The effect of dendritic topology on firing patterns in model neurons. *Network: Computation in Neural Systems*, *13*(3), 311-325.

van Wijk, B.C.M., Stam, C.J., & Daffertshofer, A. (2010). Comparing brain networks of different size and connectivity density using graph theory. *PLoS One*, *5*(10), e13701:1-13. doi:10.1371/journal.pone.0013701

Venkatasubramanian, G., Jayakumar, P.N., Gangadhar, B.N., & Keshavan, M.S. (2008). Automated MRI parcellation study of regional volume and thickness of prefrontal cortex (PFC) in antipsychotic-naïve schizophrenia. *Acta Psychiatrica Scandinavica*, *117*(6), 420-431.

Voets, N.L., Hough, M.G., Douaud, G., Matthews, P.M., James, A., Winmill, L., Webster, P., et al. (2008). Evidence for abnormalities of cortical development in adolescent-onset schizophrenia. *NeuroImage*, *43*(4), 665-675.

Vogeley, K., Tepest, R., Pfeiffer, U., Schneider-Axmann, T., Maier, W., Honer, W.G., & Falkai, P. (2001). Right frontal hypergyria differentiation in affected and unaffected siblings from families multiply affected with schizophrenia: A morphometric MRI study. *The American journal of psychiatry*, *158*(3), 494-496.

Vovk, U., Pernus, F., & Likar, B. (n.d.). A review of methods for correction of intensity inhomogeneity in MRI. *IEEE Transactions on medical imaging*, *26*, 405–421. doi:10.1109/TMI.2006.891486

Wang, J., Wang, L., Zang, Y., Yang, H., Tang, H., Gong, Q., Chen, Z., et al. (2009). Parcellation-dependent small-world brain functional networks: A resting-state fMRI study. *Human Brain Mapping*, *30*, 1511-1523.

Wang, J., Zuo, X., & He, Y. (2010). Graph-based network analysis of resting-state functional MRI. *Frontiers in Systems Neuroscience*, *4*, 16:1-14. doi: 10.3389/fnsys.2010.00016

Wang, L., Zhu, C., He, Y., Zang, Y., Cao, Q., Zhang, H., Zhong, Q., et al. (2009). Altered small-world brain functional networks in children with attention-deficit/hyperactivity disorder. *Human Brain Mapping*, *30*, 638-649.

Wang, L., Li, Y., Metzak, P., He, Y., & Woodward, T.S. (2010). Age-related changes in topological patterns of large-scale brain functional networks during memory encoding and recognition. *NeuroImage*, *50*(3), 862-872.

Wang, L., Metzak, P.D., Honer, W.G, & Woodward, T.S. (2010). Impaired efficiency of functional networks underlying episodic memory-for-context in schizophrenia. *The Journal of Neuroscience*, *30*(39), 13171-13179.

Wang, L., Yu, C., Chen, H., Qin, W., He, Y., Fan, F., Zhang, Y., et al. (2010). Dynamic functional reorganization of the motor execution network after stroke. *Brain*, *133*, 1224-1238.

Watts, D.J., & Strogatz, S.H. (1998). Collective dynamics of "small-world" networks. *Nature*, *393*(6684), 440-442.

Weese, J., Rösch, P., Netsch, T., Blaffert, T., & Quist, M. (1999). Gray-value based registration of CT and MR images by maximization of local correlation. In C. Taylor & A. Colchester (Eds.), *Medical Image Computing and Computer-Assisted Intervention – MICCAI'99* (pp. 656-664). Springer Berlin/Heidelberg, Germany.

Weinberger, D.R. (1987). Implications of normal brain development for the pathogenesis of schizophrenia. *Archives of General Psychiatry*, *44*(7), 660-669.

Wen, W., He, Y., & Sachdev, P. (2011). Structural brain networks and neuropsychiatric disorders. *Current Opinion in Psychiatry*, *24*, 219-225.

Wen, W., Zhu, W., He, Y., Kochan, N.A., Reppermund, S., Slavin, M.J., Brodaty, H., et al. (2011). Discrete neuroanatomical networks are associated with specific cognitive abilities in old age. *The Journal of Neuroscience*, *31*(4), 1204 -1212.

Whalley, H.C., Simonotto, E., Flett, S., Marshall, I., Ebmeier, K.P., Owens, D.G.C., Goddard, N.H., et al. (2004). fMRI correlates of state and trait effects in subjects at genetically enhanced risk of schizophrenia. *Brain*, *127*, 478-490. doi:10.1093/brain/awh070

Whalley, H.C., Simonotto, E., Marshall, I., Owens, D.G.C., Goddard, N.H., Johnstone, E.C., & Lawrie, S.M. (2005). Functional disconnectivity in subjects at high genetic risk of schizophrenia. *Brain*, *128*, 2097-2108. doi: 10.1093/brain/awh556

Whalley, H.C., Simonotto, E., Moorhead, W., McIntosh, A., Marshall, I., Ebmeier, K.P., Owens, D.G.C., et al. (2006). Functional imaging as a predictor of schizophrenia. *Biological Psychiatry*, *60*(5), 454-462. doi:10.1016/j.biopsych.2005.11.013

White, T., Andreasen, N.C., Nopoulos, P., & Magnotta, V. (2003). Gyrification abnormalities in childhood- and adolescent-onset schizophrenia. *Biological Psychiatry*, *54*, 418-426.

Whitfield-Gabrieli, S., Thermenos, H.W., Milanovic, S., Tsuang, M.T., Faraone, S.V., McCarley, R.W, Shenton, M.E, et al. (2009). Hyperactivity and hyperconnectivity of the default network in schizophrenia and in first-degree relatives of persons with schizophrenia. *Proceedings of the National Academy of Sciences of the United States of America*, *106*(4), 1279-1284.

Whitlow, C.T., Casanova, R., & Maldjian, J.A. (2011). Effect of resting-state functional MR imaging duration on stability of graph theory metrics of brain network connectivity. *Neuroradiology*, *259*(2), 516-524.

Wiegand, L.C., Warfield, S.K., Levitt, J.J., Hirayasu, Y., Salisbury, D.F., Heckers, S., et al. (2005). An in vivo MRI study of prefrontal cortical complexity in first-episode psychosis. *American Journal of Psychiatry*, *162*, 65-70.

Wig, G.S., Schlaggar, B.L., & Petersen, S.E. (2011). Concepts and principles in the analysis of brain networks. *Annals of the New York Academy of Sciences*, *1224*, 126-146.

Wilke, M., Kaufmann, C., Grabner, A., Pütz, B., Wetter, T. C., & Auer, D.P. (2001). Gray matter-changes and correlates of disease severity in schizophrenia: A statistical parametric mapping study. *NeuroImage*, *13*, 814 - 824.

Witkin, A. P. (1987). Scale-space filtering. *Readings in computer vision: issues, problems, principles, and paradigms*, 329–332. San Francisco: Morgan Kaufmann.

Wood, S.J, Velakoulis, D, Smith, D.J., Bond, D., Stuart, G.W., McGorry, P.D., Brewer, W.J., et al. (2001). A longitudinal study of hippocampal volume in first episode psychosis and chronic schizophrenia. *Schizophrenia Research*, *52*, 37-46.

Wright, I.C., Ellison, Z.R., Sharma, T, Friston, K.J., Murray, R.M., & McGuire, P.K. (1999). Mapping of grey matter changes in schizophrenia. *Schizophrenia Research*, *35*(1), 1-14.

Wright, I.C., McGuire, P.K., Poline, J.B., Travere, J.M., Murray, R.M., Frith, C.D., Frackowiak, R.S.J., et al. (1995). A voxel-based method for the statistical analysis of gray and white matter density applied to schizophrenia. *NeuroImage*, *2*(4), 244-252.

Wright, I.C., Rabe-Hesketh, S., Woodruff, P.W., David, A.S., Murray, R.M., & Bullmore, E.T. (2000). Meta-analysis of regional brain volumes in schizophrenia. *The American Journal of Psychiatry*, *157*(1), 16-25.

Wu, K., Taki, Y., Sato, K., Kinomura, S., Goto, R., Okada, K., Kawashima, R., et al. (2011). Age-related changes in topological organization of structural brain networks in healthy individuals. *Human Brain Mapping*. doi:10.1002/hbm.21232

Wu, K., Taki, Y., Sato, K., Sassa, Y., Inoue, K., Goto, R., Okada, K., et al. (2011). The overlapping community structure of structural brain network in young healthy individuals. *PLoS One*, *6*(5), e19608:1-14. doi:10.1371/journal.pone.0019608

Wässle, H., Peichl, L., & Boycott, B.B. (1981). Morphology and topography of on- and off-alpha cells in the cat retina. *Proceedings of the Royal Society of London. Series B, Biological Sciences*, *212*(1187), 157-175. Retrieved from http://www.ncbi.nlm.nih.gov/pubmed/6166012

Xue, Z., Shen, D., & Davatzikos, C. (2004). Determining Correspondence in 3-D MR Brain Images Using Attribute Vectors as Morphological Signatures of Voxels. *IEEE Transactions on medical imaging*, *23*, 1276–1291.

Yan, C., Gong, G., Wang, J., Wang, D., Liu, D., Zhu, C., Chen, Z.J., et al. (2011). Sex- and brain size-related small-world structural cortical networks in young adults: A DTI tractography study. *Cerebral Cortex*, *21*(2), 449-458. doi:10.1093/cercor/bhq111

Yao, Z., Zhang, Y., Lin, L., Zhou, Y., Xu, C., Jiang, T., & the Alzheimer's Disease Initiative (ADNI). (2010). Abnormal cortical networks in mild cognitive impairment and Alzheimer's disease. *PLoS Computational Biology*, *6*(11), e1001006:1-11. doi:10.1371/journal.pcbi.1001006

Yu, Q., Sui, J., Rachakonda, S., He, H., Pearlson, G., & Calhoun, V.D. (2011). Altered small-world brain networks in temporal lobe in patients with schizophrenia performing an auditory oddball task. *Frontiers in Systems Neuroscience*, *5*, 7:1-13.

Yuan, K., Qin, W., Liu, J., Guo, Q., Dong, M., Sun, J., Zhang, Y., et al. (2010). Altered small-world brain functional networks and duration of heroin use in male abstinent heroin-dependent individuals. *Neuroscience Letters*, *477*(1), 37-42.

Zalesky, A., Fornito, A., Harding, I.H., Cocchi, L., Yücel, M., Pantelis, C., & Bullmore, E.T. (2010). Whole-brain anatomical networks: Does the choice of nodes matter? *NeuroImage*, *50*(3), 970-983.

Zalesky, A., Fornito, A., Seal, M.L., Cocchi, L., Westin, C.-F., Bullmore, E.T., Egan, G.F., et al. (2011). Disrupted axonal fiber connectivity in schizophrenia. *Biological Psychiatry*, *69*(1), 80-89.

Zemanova, L., Zhou, C., & Kurths, J. (2006). Structural and functional clusters of complex brain networks. *Physica D*, *224*, 202-212.

Zhang, F., Jiang, L., Chen, C., Dong, Q., & Yun, L. (2009). Brain functional networks involved in finger movement. *Conference on Biomedical Engineering and Informatics* (pp. 1-4). Tianjin, China. Retrieved from http://ieeexplore.ieee.org/xpls/abs_all.jsp?arnumber=5302335

Zhang, F., Chen, C., & Jiang, L. (2010). Brain functional networks analysis and comparison. *3rd International Conference on Biomedical Engineering and Informatics* (pp. 1151-1155).

Zhang, J., Cai, S.-M., Fu, Z.-Q., & Zhou, P.-L. (2010). Topological variations of large-scale brain functional networks based on mutual information. *International Conference on Bioinformatics and Biomedical Engineering* (pp. 1-4). Chengdu.

Zhang, T., Wang, J., Yang, Y., Wu, Q., Li, B., Chen, L., Yue, Q., et al. (2011). Abnormal small-world architecture of top – down control networks in obsessive – compulsive disorder. *Journal of Psychiatry & Neuroscience*, *36*(1), 23-31.

Zhang, Y., Jiang, J., Lin, L., Shi, F., Zhou, Y., Yu, C., Li, K., et al. (2008). A surface-based fractal information dimension method for cortical complexity analysis. *MIAR '08 Proceedings of the 4th international workshop on Medical Imaging and Augmented Reality* (pp. 133-141). Berlin, Heidelberg, Germany.: Springer-Verlag.

Zhou, L., Wang, Y., Li, Y., Yap, P.-T., Shen, D., & the Alzheimer's. Disease Neuroimaging Initiative (ADNI). (2011). Hierarchical anatomical brain networks for MCI prediction: Revisiting volumetric measures. *PLoS One*, *6* (7), e21935:1-14. doi:10.1371/journal.pone.0021935

Zhu, H., Li, Y., Ibrahim, J.G., Lin, W., & Shen, D. (2009). MARM: Multiscale adaptive regression models for neuroimaging data. *Information Processing in Medical Imaging*, *21*, 314-325.

Zhu, W., Wen, W., He, Y., Xia, A., & Anstey, K.J. (2010). Changing topological patterns in normal aging using large-scale structural networks. *Neurobiology of Aging*, *in press*. doi:10.1016/j.neurobiolaging.2010.06.022

Zilles, K., Armstrong, E., Schleicher, A., & Kretschmann, H.J. (1988). The human pattern of gyrification in the cerebral cortex. *Anatomy and Embryology*, *179* (2), 173-179.